MANITOBA GEOLOGICAL SURVEY
MGS
1928

GR2016-1

GEOSCIENTIFIC REPORT

Geology of the Paint and Phillips lakes area, Thompson nickel belt, central Manitoba (parts of NTS 63O1, 8, 9, 63P5, 12)

By
C.G. Couëslan

Manitoba

Geoscientific Report GR2016-1

Geology of the Paint and Phillips lakes area, Thompson nickel belt, central Manitoba (parts of NTS 63O1, 8, 9, 63P5, 12)

by C.G. Couëslan

Winnipeg, 2016

Growth, Enterprise and Trade

Hon. Cliff Cullen
Minister

James Wilson
Deputy Minister

Tim Friesen
Assistant Deputy Minister

Manitoba Geological Survey

Christian Böhm
A/Director

Manitoba

Couëslan, C.G. 2016: Geology of the Paint and Phillips lakes area, Thompson nickel belt, central Manitoba (parts of NTS 63O1, 8, 9, 63P5, 12); Manitoba Growth, Enterprise and Trade, Manitoba Geological Survey, Geoscientific Report GR2016-1, 44 p. and 1 colour map at 1:50 000 scale.

NTS grid: 63O1, 8, 9, 63P5, 12

Keywords: carbonatite; Manitoba; Ospwagan group; Paint Lake; Paint sequence; Thompson nickel belt; Trans-Hudson orogen; ultrapotassic syenite

Published by:

Manitoba Growth, Enterprise and Trade
Manitoba Geological Survey
360–1395 Ellice Avenue
Winnipeg, Manitoba
R3G 3P2 Canada

Telephone: 1-800-223-5215 (General Enquiry)
204-945-6569 (Publication Sales)
Fax: 204-945-8427

E-mail: minesinfo@gov.mb.ca

Website: manitoba.ca/minerals

ISBN No.: 978-0-7711-1577-6

This publication is available to download free of charge at manitoba.ca/minerals

Cover illustration: Gossan-stained outcrops of Paint sequence wacke in central Paint Lake, Manitoba.

Abstract

This report presents the results of bedrock mapping in the Paint and Phillips lakes area. Mapping was initiated with an aim to identify map units in the Archean basement of the Thompson nickel belt. From this work, twelve map units were defined, including both Archean and Paleoproterozoic rocks. Three units recognized as Archean include an amphibolitic gneiss suite, multicomponent gneiss consisting largely of tonalitic orthogneiss, and siliceous gneiss. Three units of unconstrained age include an enderbite gneiss suite, ubiquitous bands and boudins of plagioclase amphibolite, and small granodiorite intrusions. Six Paleoproterozoic units include metasedimentary rocks of the newly defined Paint sequence and the Ospwagan group, and intrusive rocks including pyroxenite, melasyenite, pegmatite and carbonatite.

Whole-rock lithogeochemistry of the amphibolitic gneiss suite suggests an arc affinity for these rocks, which may consist, at least in part, of metavolcanic rocks and contain evidence for local hydrothermal alteration. The melasyenite shares many geochemical characteristics with ultrapotassic rocks, being enriched in both incompatible large-ion lithophile elements (K, Sr, Ba, LREE) and compatible (Mg, Cr, Ni) elements. Strongly negative ε_{Nd} values indicate derivation from modified lithospheric mantle. Trace-element and Sm-Nd isotope geochemistry of Paint sequence wacke suggests that this sequence is distinct from the Ospwagan group and does not represent a laterally equivalent depositional facies.

Uranium-lead dating of igneous zircon from the melasyenite yields a magmatic age of ca. 1883 Ma, contemporaneous with the timing of mafic and ultramafic magmatism related to the Molson dike swarm. It is possible that this mafic magmatism provided the thermal input required for partial melting of the modified lithospheric mantle and generation of ultrapotassic magmas. A limited dataset of detrital zircon U-Pb ages from Paint sequence wacke yields two age modes centred at ca. 2670–2644 Ma and 2436 Ma, suggesting deposition during the Paleoproterozoic. Metamorphic zircon U-Pb ages from Paint sequence wacke suggest prograde (likely medium-grade) metamorphism at ca. 1797 Ma, followed by leucosome crystallization (cooling from high-grade metamorphic conditions) by ca. 1766 Ma.

Sulphidic horizons in the Ospwagan group are believed to be the sulphide source for nickel deposits hosted by ultramafic bodies in the Thompson nickel belt. Although unrelated to the Ospwagan group, disseminated sedimentary sulphide is common in Paint sequence wacke, as are sulphide-enriched lenses of iron formation. A mineralized ultramafic body at Phillips Lake appears to be hosted in Paint sequence rocks, suggesting that there is potential for the Paint sequence to host magmatic nickel deposits in the Thompson nickel belt.

TABLE OF CONTENTS

Page

TABLES

FIGURES

MAP

Introduction

Paint Lake is located approximately 20 km south of the city of Thompson, Manitoba, within the prolific Thompson nickel belt (TNB). A historical resource for Vale's mining operations in the Thompson area (Thompson, Birchtree and Pipe deposits) is 150 Mt at 2.32% Ni and 0.16% Cu (Layton-Matthews et al., 2007), and total reserves for the Thompson operation as of 2011 were 27.5 Mt at 1.75% Ni (Vale S.A., 2012). Nickel mineralization in the belt is associated with ultramafic intrusions in sulphidic sedimentary rocks of the Paleoproterozoic Ospwagan group.

This report documents the lithology, geochemistry and geochronology of Archean and Paleoproterozoic rocks in the Paint Lake area. Initiated in 2008, the objective of this project was to subdivide the migmatitic gneiss of the Archean basement, and to identify metasedimentary rocks that could be correlative with Ospwagan group stratigraphy (see Couëslan, 2008a, 2009a, 2012; Couëslan and Martins, 2010). During the course of mapping, a new metasedimentary sequence was identified, as were two varieties of intrusive alkaline rocks. Additional work was carried out on a mafic gneiss suite.

Previous work

The earliest geological investigations in the Paint Lake area were conducted by J.B. Tyrrell, who crossed the lake in 1896 while following a route from Sipiwesk Lake to Nelson House (Tyrrell, 1903). His report gives a brief description of the landscape and geology of the area. He was followed in the summer of 1930 by J.F. Wright, who travelled the Grass River from Wekusko Lake to Thicket Portage (Wright, 1938). Wright (1938) briefly described the rocks of the Paint Lake area and was the first to recognize the presence of garnet-bearing metasedimentary gneiss.

Dawson (1952) produced the first geological map of the area centred around Partridge Crop Lake and including Paint Lake, which was published at a scale of 1:126 720 (1 inch to 2 miles). Four belts of metasedimentary gneiss were recognized in the Paint Lake area during mapping, striking northeast for 30–32 km through the lake. Godard (1966) described several varieties of gneiss in the Paint Lake area based on fieldwork in the summers of 1962 and 1963. Macek and Russell (1978) mapped a 14 km by 4 km strip through central Paint Lake and classified most rocks according to their migmatitic textures, as outlined by Mehnert (1968). Charbonneau et al. (1979) completing the mapping of the lake and integrated the data of Macek and Russell (1978) with their own to produce two preliminary maps at a scale of 1:25 000 (Charbonneau and Sutherland, 1979a, b). Mapping at this time was based on descriptive petrography, with the result that the majority of rocks underlying Paint Lake were described as one of several varieties of migmatitic or enderbitic gneiss, or part of a layered metagabbro suite. Russell (1980, 1981) described the geology of the Paint Lake area, including a detailed study of the metamorphism and structures. Additional detailed structural studies were carried by Feuten et al. (1986) and Feuten and Robin (1989). Macek (1985) conducted 1:20 000 scale mapping in the Phillips Lake area and recognized several units similar to those at Paint Lake.

More recently, Schneider et al. (2007), Heaman et al. (2009) and Machado et al. (2011a) conducted regional geochronology studies involving rocks from the Paint Lake area. Couëslan and Pattison (2012) and Couëslan et al. (2013) studied the nature and timing of metamorphism of the Paint Lake area as part of a regional study.

Methods and scope

The purpose of this project was to subdivide the migmatitic gneiss of the Archean basement to the Ospwagan group into discrete units, and to identify metasedimentary rocks that could be correlative with Ospwagan group stratigraphy. This was accomplished by using regional mapping combined with petrographic microscopy and modern geochemical methods. Regional mapping in the Paint and Phillips lakes areas was conducted at a scale of 1:20 000 by the author during the 2008, 2009, 2010 and 2012 field seasons (Couëslan, 2008a, 2009a, 2012; Couëslan and Martins, 2010). Preliminary maps of the Paint Lake area were released after the 2008 and 2009 field seasons (Couëslan, 2008b, 2009b), and a revised and expanded version of the map, including the 2010 mapping results, is included herein as Map GR2016-1-1. The map area is largely confined to the shoreline and islands of Paint Lake, owing to poor bedrock exposure away from the lake. Satellite imagery and hand-held GPS were used for plotting station locations and navigation.

Samples were collected during mapping for thin-section and petrographic analysis. A representative selection of 52 rock samples was submitted to Activation Laboratories (Ancaster, Ontario) for major- and trace-element analyses by lithium metaborate/tetraborate fusion, inductively coupled plasma–emission spectrometry (ICP-ES) and mass spectrometry (ICP-MS). Three samples of wacke and one sample of melasyenite were submitted to R.A. Creaser at the University of Alberta Radiogenic Isotope Facility (Edmonton, Alberta) for Sm-Nd isotope analysis. A sample of the melasyenite was also submitted to L.M. Heaman at the University of Alberta Radiogenic Isotope Facility for U-Pb dating of zircon by isotope dilution–thermal ionization mass spectrometry (ID-TIMS). Seven thin sections of wacke with in situ or in-source, orthopyroxene-bearing leucosome were submitted for in situ analyses of zircon and monazite by laser ablation–multicollector–inductively coupled plasma–mass spectrometry (LA-MC-ICP-MS). The original intention was to date the timing of leucosome generation; however, the analyses also included inherited/detrital cores of zircon and this information is included in this report. Geochemical and isotopic data can be found in Data Repository Item DRI2016001[1], as well as in tables throughout the report.

[1] MGS Data Repository Item DRI2016001, containing the data or other information sources used to compile this report, is available to download free of charge at http://www2.gov.mb.ca/itm-cat/web/freedownloads.html, or on request from minesinfo@gov.mb.ca or Mineral Resources Library, Manitoba Growth, Enterprise and Trade, 360–1395 Ellice Avenue, Winnipeg, Manitoba R3G 3P2, Canada.

Regional geological framework

Paint Lake is located along the eastern margin of the TNB, which, along with the Assean Lake crustal complex, Split Lake block and Fox River belt, makes up the exposed portion of the Superior boundary zone of Manitoba (Figure 1; Bell, 1971; Barager and Scoates, 1981; Weber, 1990; Böhm et al., 2003). The Superior boundary zone represents the Superior craton margin, which was metamorphosed and deformed during the Trans-Hudson orogeny. The TNB is flanked to the northwest by the Kisseynew domain of the Trans-Hudson orogen, and to the southeast by the Pikwitonei granulite domain (PGD) of the northwestern Superior craton. The TNB is largely underlain by reworked Archean gneiss of the Superior craton (Figure 2). The gneiss is typically quartzofeldspathic with enclaves of mafic to ultramafic rock. It is commonly migmatitic and characterized by complex internal structures that are the result of multiple generations of Archean and Paleoproterozoic deformation and metamorphism. Clearly recognizable paragneiss is rare. The gneiss is interpreted to be derived from the adjacent PGD, which was subjected to amphibolite- to granulite-facies metamorphic conditions from ca. 2720 to 2640 Ma (Hubregtse, 1980; Russell, 1981; Mezger et al., 1990; Heaman et al., 2011). The granulites of the PGD were exhumed and unconformably overlain by the Paleoproterozoic supracrustal rocks of the Ospwagan group prior to ca. 1880 Ma (Scoates et al., 1977; Bleeker, 1990; Zwanzig et al., 2007).

Ospwagan group

The following summary of the Ospwagan group is largely sourced from Bleeker (1990) and Zwanzig et al. (2007). The lowermost unit of the Ospwagan group is the Manasan formation, which consists of two members: the lower M1 member, consisting of layered to laminated metasandstone with local metaconglomerate layers near the base; and the overlying M2 member, consisting of semipelitic rock (Figure 3). The Manasan formation is interpreted as a transgressive, fining-upward sequence deposited along a passive margin. This siliciclastic system grades into the overlying calcareous sedimentary rocks of the Thompson formation.

The Thompson formation consists of three members: the T1 member comprises a variety of calcareous–siliceous rocks including chert, calcsilicate and impure marble; the T2 member is a semipelitic, calcareous gneiss that is only rarely present; and the T3 member consists of impure dolomitic marble with local horizons of calcsilicate. The Thompson formation represents a transition from a siliciclastic-dominated to a carbonate-dominated system. Lower units of the Ospwagan group (Manasan and Thompson formations) are exposed in western Paint Lake.

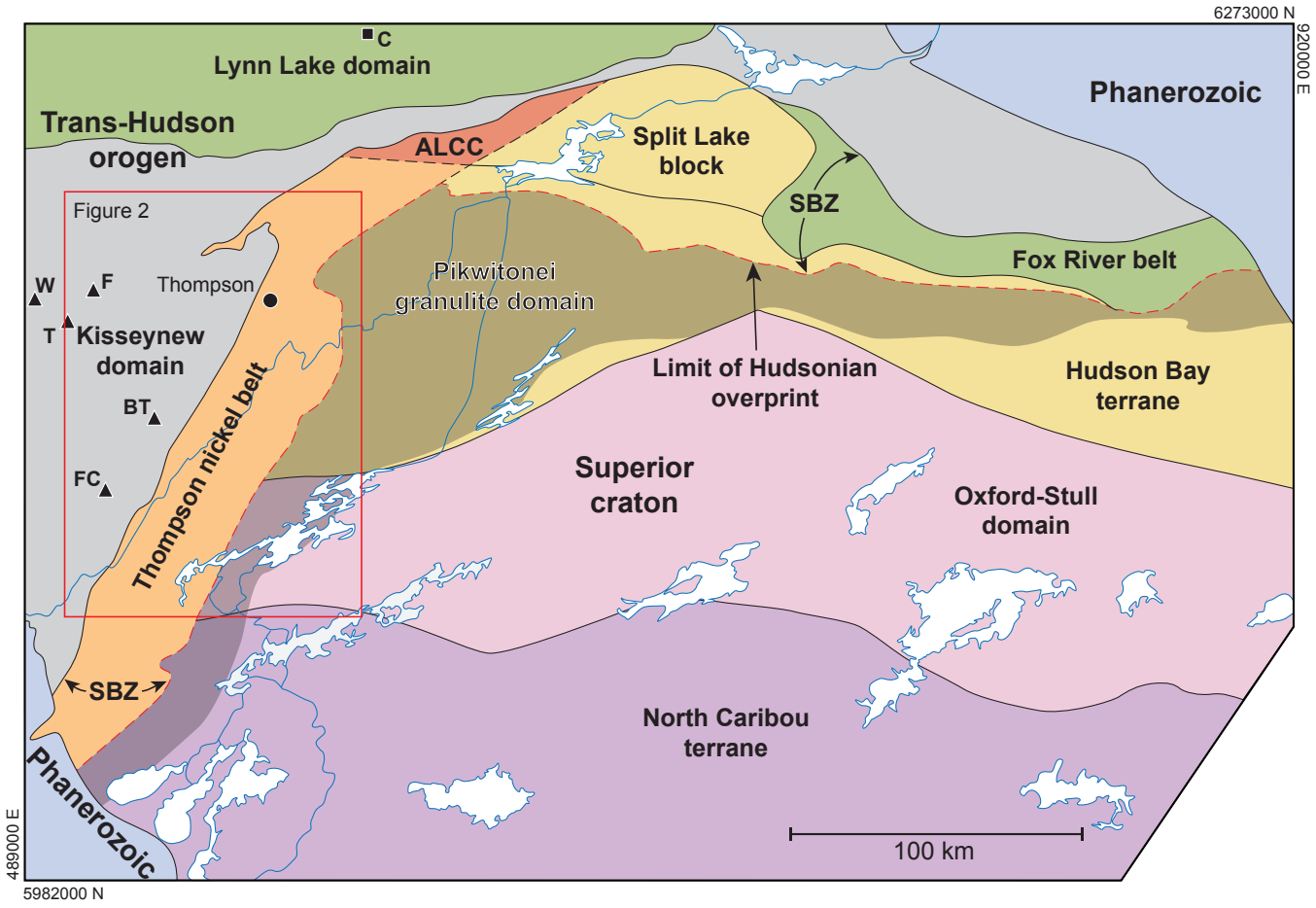

Figure 1: *Tectonic-elements of the northwestern Superior craton and adjacent Trans-Hudson orogen of Manitoba (modified from Weber, 1990). Black triangles indicate intrusions of the Footprint Lake plutonic suite: BT, Bison–Tullibee lakes; F, Footprint Lake; FC, Ferguson Creek; T, Threepoint Lake; W, Wapisu Lake. Black square indicates the location of Campbell Lake. Other abbreviations: ALCC, Assean Lake crustal complex; SBZ, Superior boundary zone.*

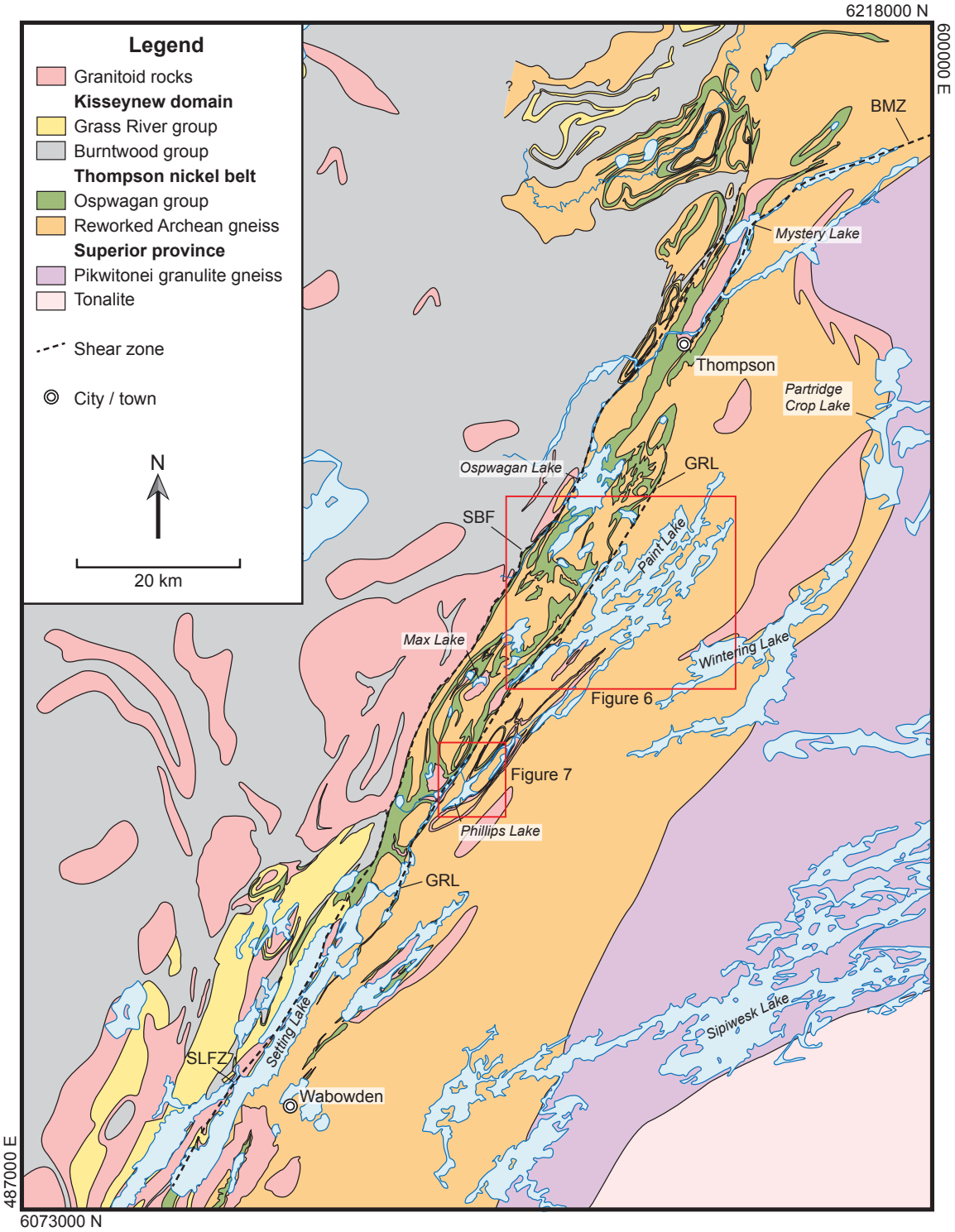

Figure 2: *Lithology of the Thompson nickel belt and adjacent portions of the Kisseynew domain and Superior craton (modified from Macek et al., 2006). Abbreviations: BMZ, Burntwood mylonite zone; GRL, Grass River lineament; SBF, Superior boundary fault; SLFZ, Setting Lake fault zone.*

The Pipe formation is subdivided into three members. The P1 member consists of a graphite-rich, sulphide-facies iron formation at the base (the locus of the Pipe II and Birchtree orebodies), overlain by a silicate-facies iron formation. The top of the P1 member consists of a reddish, laminated, siliceous rock. The P1 member grades into the overlying metapelitic rocks of the P2 member. The base of the P3 member is marked by a sulphide-facies iron formation (the locus of the Thompson orebody). The P3 member consists of a wide variety of rock types, including laminated, siliceous metasedimentary rocks; silicate-, carbonate- and local oxide-facies iron formations; semipelitic rocks, calcsilicate and a local horizon of relatively pure dolomitic marble. It is suggested that the Pipe formation was deposited in an open-marine setting dominated by a mix of

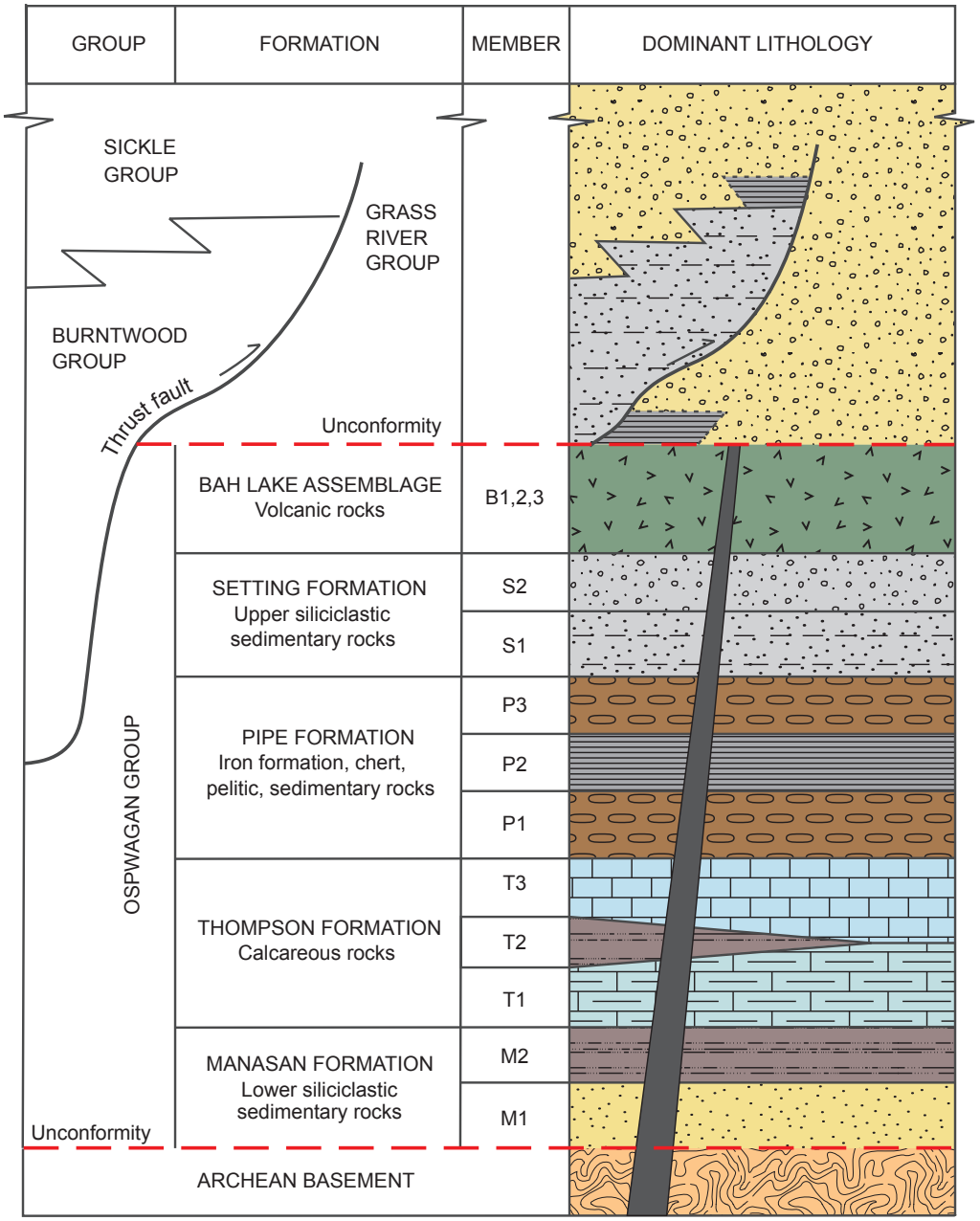

Figure 3: *Schematic tectonostratigraphic and lithostratigraphic section of the Ospwagan group and siliciclastic units of the adjoining Kisseynew domain (adapted from Bleeker, 1990; Zwanzig et al., 2007).*

chemical-sediment deposition and fine to very fine siliciclastic deposition.

The Setting formation is divided into two members and is defined to include all siliciclastic rocks above the iron formation of the uppermost P3 member. The S1 member consists of rhythmically interbedded quartzite and pelitic schist with local calcareous concretions, which are very characteristic of the S1 member. The S2 member consists of thickly layered greywacke, with local horizons grading from conglomeratic at the base to pelitic at the top. No contact has been observed between the S1 and S2 members. It is possible that they represent a lateral facies change as opposed to a vertical succession. The S2 member appears to be missing altogether in the Pipe mine area, where contacts between the S1 member and the overlying Bah Lake assemblage are clearly exposed. The Setting formation is interpreted to have been deposited by turbidity currents in a relatively deep marine environment. The coarse clastic material and thick turbidite bedding of the S2 member may represent the onset of active tectonism, or a lateral sedimentary facies change possibly to a submarine-channel or upper-fan environment.

At the top of the Ospwagan group is the metavolcanic Bah Lake assemblage, which consists of mafic to ultramafic volcanogenic rocks dominated by massive to pillowed metabasalt flows with local metapicrite and minor synvolcanic intrusions. The Bah Lake assemblage is dominated by a high-Mg suite (similar to N-MORB) that occurs throughout much of the main TNB, and an incompatible-element–enriched suite (similar to E-MORB) that occurs in the northwestern Setting Lake area and along the margin of the Kisseynew domain (Zwanzig, 2005). The enriched suite is interpreted to overlie the high-Mg

suite; however, it is uncertain if this represents a stratigraphic or tectonic relationship. The Bah Lake assemblage may suggest the onset of active rifting in the TNB.

The clastic material that formed the Ospwagan group was sourced almost entirely from erosion of the Superior craton. Whole-rock Nd-model ages for the Ospwagan group range from ca. 3.2 to 2.8 Ga, which is only slightly younger than the ages determined for the underlying Archean gneiss (ca. 3.5–3.2 Ga; Böhm et al., 2007). Hundreds of Archean detrital zircon grains have been dated from the Ospwagan group (Bleeker and Hamilton, 2001; Rayner et al., 2006; Burnham et al., 2009; Machado et al., 2011b); however, a single zircon from the Setting formation yielded an age of ca. 1974 Ma (Bleeker and Hamilton, 2001). The main section of the Bah Lake assemblage metavolcanic rocks on Setting Lake is intruded by a ca. 1891 Ma calcalkaline pluton (Percival et al., 2004, 2005). This effectively brackets the deposition of the top of the Ospwagan group sequence to between ca. 1891 and 1974 Ma. The Ospwagan group rocks were subjected to multiple generations of deformation and metamorphic conditions as high as lower-granulite facies during the Trans-Hudson orogeny.

Mafic–ultramafic magmatism and associated nickel deposits

Most ultramafic bodies in the TNB occur as discrete boudins characterized by tectonized contacts with the enclosing country rock. Larger, less deformed bodies commonly exhibit a thin pyroxenitic basal zone and a thicker lower zone of chromite-bearing olivine peridotite or dunite that grades upward into a thinner pyroxenitic upper zone. This asymmetric variation in cumulate olivine and whole-rock MgO content is consistent with the younging direction of the Ospwagan group country rocks (Bleeker, 1990; Layton-Matthews et al., 2007). This correlation between magmatic zonation and younging direction suggests the ultramafic intrusions were emplaced as concordant to semiconcordant sill-like bodies. Although ultramafic intrusions also occur in Archean gneiss, most economic deposits occur where the ultramafic sills intrude the Ospwagan group cover sequence (Bleeker, 1990; Layton-Matthews et al., 2007; Zwanzig et al., 2007). These deposit-hosting ultramafic bodies occur along two horizons within the Pipe formation characterized by high concentrations of sedimentary sulphides (sulphide-facies iron formations; Bleeker, 1990; Zwanzig et al., 2007). Mixing calculations based on Se/S ratios of nickel ores indicate that 70–100% of the sulphide mass was derived through the assimilation of country-rock sulphide (Bleeker and Macek, 1996). Uranium-lead ages of ca. 1880–1877 Ma have been determined for ultramafic bodies at the Pipe II mine, Setting Lake and Paint Lake (Hulbert et al., 2005; Heaman et al., 2009; Scoates et al., 2010). These ages are identical to the potentially comagmatic mafic to ultramafic intrusions of the Molson dike swarm (ca. 1880 Ma; Scoates and Macek, 1978; Heaman et al., 1986, 2009).

Deformation

The Archean deformation history of the TNB is largely obscured by Paleoproterozoic deformation related to the Trans-Hudson orogeny. The Ospwagan group was affected by four main phases of deformation (Bleeker, 1990; Burnham et al., 2009). Early deformation (D_1) predates the ca. 1880 Ma Molson dikes; however, this early deformation is also largely obscured by later deformation. The F_1 generation of folds has only been identified at the Pipe II mine where mafic dikes of the Molson swarm crosscut folded Pipe formation rocks. Although Bleeker (1990) interpreted this deformation as the main nappe-forming event, it is now recognized that Kisseynew domain rocks belonging to the ca. 1845–1830 Ma Burntwood and Grass River groups are infolded into the westernmost nappe structures, so these structures must postdate the ca. 1880 Ma magmatic event (Percival et al., 2005; Zwanzig et al., 2007). The D_1 deformation phase is now tentatively interpreted to have produced relatively upright folds, which may indicate that the sedimentary pile was detached from the basement (Burnham et al., 2009).

The dominant phase of penetrative deformation is D_2, which affected both the Ospwagan group and ca. 1880 Ma magmatic rocks (Figure 4a). Kisseynew basin sedimentary rocks were thrust onto the Superior craton margin along early D_2 thrust faults. Thrust faulting was followed by the formation of F_2 nappe structures, which incorporated the underlying Archean gneiss. The nappe structures have been interpreted as either east verging (Bleeker, 1990; White et al., 2002) or southwest verging (Zwanzig et al., 2007; Burnham et al., 2009). The recumbent folds are associated with regionally penetrative S_2 fabrics. The D_2 phase of deformation is interpreted to be the result of convergence between the Superior craton margin and the Reindeer zone of the Trans-Hudson orogen from ca. 1830 to 1800 Ma.

The D_3 phase of deformation resulted in isoclinal folds with vertical to steeply southeast-dipping axial planes (Figure 4b; Bleeker, 1990; Burnham et al., 2009). Axial-planar S_3 fabrics are locally observed in the noses of regional and minor F_3 folds but are coplanar with S_2 along the fold limbs, forming a composite S_2–S_3 fabric. Mylonite zones with subvertical stretching lineations parallel many of the regional F_3 folds (Bleeker, 1990; Burnham et al., 2009). Tightening of D_3 structures continued during D_4, marked by localized retrograde greenschist metamorphism along mylonitic and brittle cataclastic, northeast-striking shear zones that commonly indicate southeast-side-up sinistral movement (Bleeker, 1990; Burnham et al., 2009). The D_3–D_4 structures are the result of a transition to transpressional tectonics following the collision of the Superior craton with the Reindeer zone, and may be the consequence of far-field stresses generated by tectonic events to the south (e.g., Yavapi orogeny). The D_3–D_4 structures exert a first-order control on the present-day distribution of metamorphic zones within the TNB (Couëslan and Pattison, 2012).

Metamorphism

Similar to the deformation history, Archean metamorphic assemblages and textures were largely destroyed by Hudsonian metamorphism. The TNB can be divided into three regional, nested metamorphic zones—middle-amphibolite facies, upper-amphibolite facies and granulite facies—which are arranged subparallel to the strike of the belt and the regional D_3–D_4 structures (Figure 5; Couëslan and Pattison, 2012). Peak metamorphic assemblages decrease to middle-amphibolite facies along

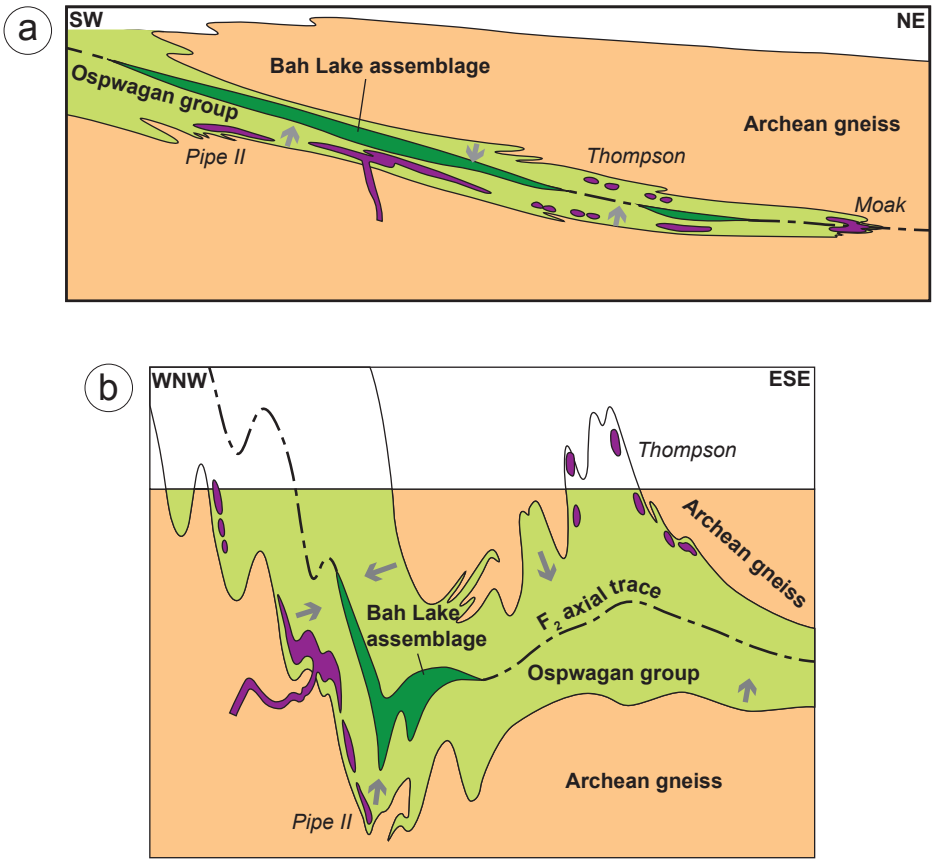

Figure 4: *Schematic cross-sections through regional fold structures in the Thompson nickel belt:* ***a)*** *northeast longitudinal cross-section through a regional F_2 nappe structure; upright F_3 folds are omitted from this schematic section to illustrate the original geometry of the F_2 nappe;* ***b)*** *schematic west-northwest cross-section through the nappe structure of (a), which is refolded by F_3 (Bleeker, 1990).*

the eastern margin of the TNB. The TNB is characterized by relatively low-pressure and high-temperature peak metamorphic assemblages, and broadly clockwise P-T-t paths (Couëslan and Pattison, 2012). Relatively steep geothermal gradients occur across the strike of the metamorphic-facies zones. Peak metamorphic conditions in each of these metamorphic zones are estimated to have been 550–620°C and 3–5 kbar in the central middle amphibolite–facies zones, 640–755°C and 3–6 kbar in the upper amphibolite–facies zone, 775–830°C and 5–7 kbar in the granulite-facies zones, and 645–700°C and 6.5–7.7 kbar in the eastern middle amphibolite–facies zone (Couëslan and Pattison, 2012). Paint and Phillips lakes lie within the easternmost zone of granulite-facies rocks. The structural control on the distribution of metamorphic-facies zones suggests that peak metamorphism and associated metamorphic isograds were established prior to late D_3–D_4.

Metamorphic mineral assemblages suggest a northward increase in pressure from the Pipe mine area toward the Moak Lake area. This indicates greater postmetamorphic uplift toward the north. Tectonic studies by White et al. (1999, 2002) and Kuiper et al. (2011) suggest that the Thompson promontory may have acted as an indenter into the Reindeer zone toward the northwest or west-northwest, coinciding with greater burial depths and higher pressures.

Metamorphic monazite grains ranging in age from ca. 1835 to 1770 Ma record prograde to near-peak metamorphic conditions in the TNB (Couëslan et al., 2013; Couëslan, unpublished data, 2015). Couëslan et al. (2013) interpreted monazite growth to be largely syn-D_2, based on microstructural observations; however, the coplanar relationship between S_2 and S_3, and the generally accepted timing of terminal collision between the Reindeer zone and Superior craton (ca. 1830–1800 Ma; Ansdell, 2005; Burnham et al., 2009; Corrigan et al., 2009), suggest that this period of prograde metamorphism likely continued during D_3. Peak metamorphism was likely syn-D_3 and occurred diachronously across the various metamorphic-facies zones during metamorphic relaxation. Cooling and crystallization of leucosome in the granulite-facies zones is recorded by ca. 1750 Ma monazite (Couëslan et al., 2013) and is similar to $^{40}Ar/^{39}Ar$ ages of hornblende from the upper amphibolite–facies zone (ca. 1745 Ma) and biotite from the central middle amphibolite–facies zone (ca. 1755 Ma; Schneider et al., 2007), indicating cooling across the TNB at this time. Cooling was likely coincident with differential uplift along D_3–D_4 structures, with $^{40}Ar/^{39}Ar$ biotite ages indicating continued cooling until at least ca. 1700 Ma (Schneider et al., 2007; Couëslan et al., 2013).

An alternative tectonic model promotes long-lived transpressional tectonics from ca. 1850 to 1750 Ma, and possibly as late as 1720 Ma (Gapais et al., 2005; Burnham et al., 2009; Machado et al., 2011b). However, the recent metamorphic and geochronology studies of Couëslan and Pattison (2012) and Couëslan et al. (2013), and the delineation of belt-parallel

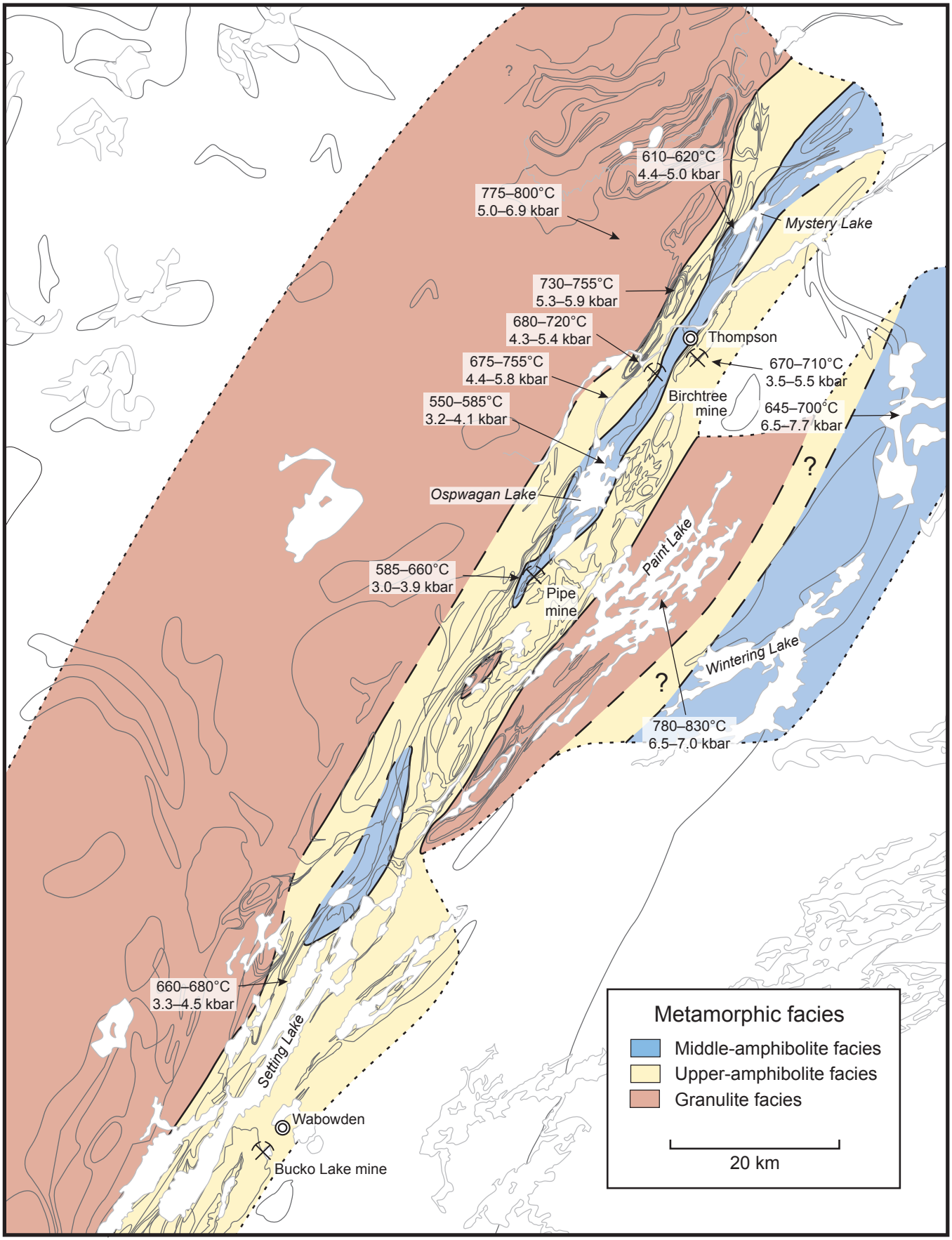

Figure 5: *Metamorphic facies of the Thompson nickel belt and adjacent Kisseynew domain (Couëslan and Pattison, 2012). Solid black lines define indicated facies-zone boundaries, dashed black lines define inferred boundaries, and dotted black lines indicate the limits of data. Solid grey lines indicate lithological boundaries from Figure 2.*

metamorphic-facies zones, are in strong agreement with the nappe-tectonics model of Bleeker (1990), whereas the transpressional model predicts nonsystematic variations in metamorphic grade throughout the belt (Machado et al., 2011b).

Local geology

The Paint and Phillips lakes area is underlain by dominantly Archean gneissic rocks that have been intruded by Paleoproterozoic plutonic rocks and plutonic rocks of uncertain age. Three northeast-striking belts of metasedimentary rocks occur in the Paint Lake area (Figure 6) and have been informally termed the Paint sequence. Rocks belonging to the same metasedimentary package are also present at Phillips Lake (Figure 7; Couëslan, 2012). A single northeast-striking belt of Ospwagan group rocks is recognized along the western shore of Paint Lake (Map 2016-1-1). Rocks in the area are typically high strain: minor isoclinal folds are abundant, straight gneiss is relatively common and rootless folds are locally present. Mineral assemblages indicate lower granulite–facies metamorphism over most of the area; however, the western shore of Paint Lake in the vicinity of the Grass River lineament (Figure 2) is characterized by upper amphibolite–facies metamorphic assemblages. Amphibolite-facies retrogression of granulite-facies assemblages is relatively common, and greenschist-facies retrogression is locally associated with shear zones. Although the majority of units have been metamorphosed, the 'meta-' prefix is not utilized in the descriptions below.

Archean rocks

Three units interpreted to be Archean are present in the Paint and Phillips lakes area: amphibolitic gneiss (unit 1), multicomponent gneiss (unit 2) and siliceous gneiss (unit 3). No geochronological data are available; however, similar rocks of known Archean age have been traced from the PGD into the TNB, suggesting an Archean age for these units (Couëslan, 2013, 2014a). In addition, U-Pb zircon ages ranging from ca. 3038 to 2655 Ma have been obtained from samples of multicomponent gneiss elsewhere in the TNB (Machado et al., 1990). Although the order of these units is listed somewhat arbitrarily, mafic gneiss similar to unit 1 is considered to be the oldest unit in the adjacent PGD (Hubregtse, 1980).

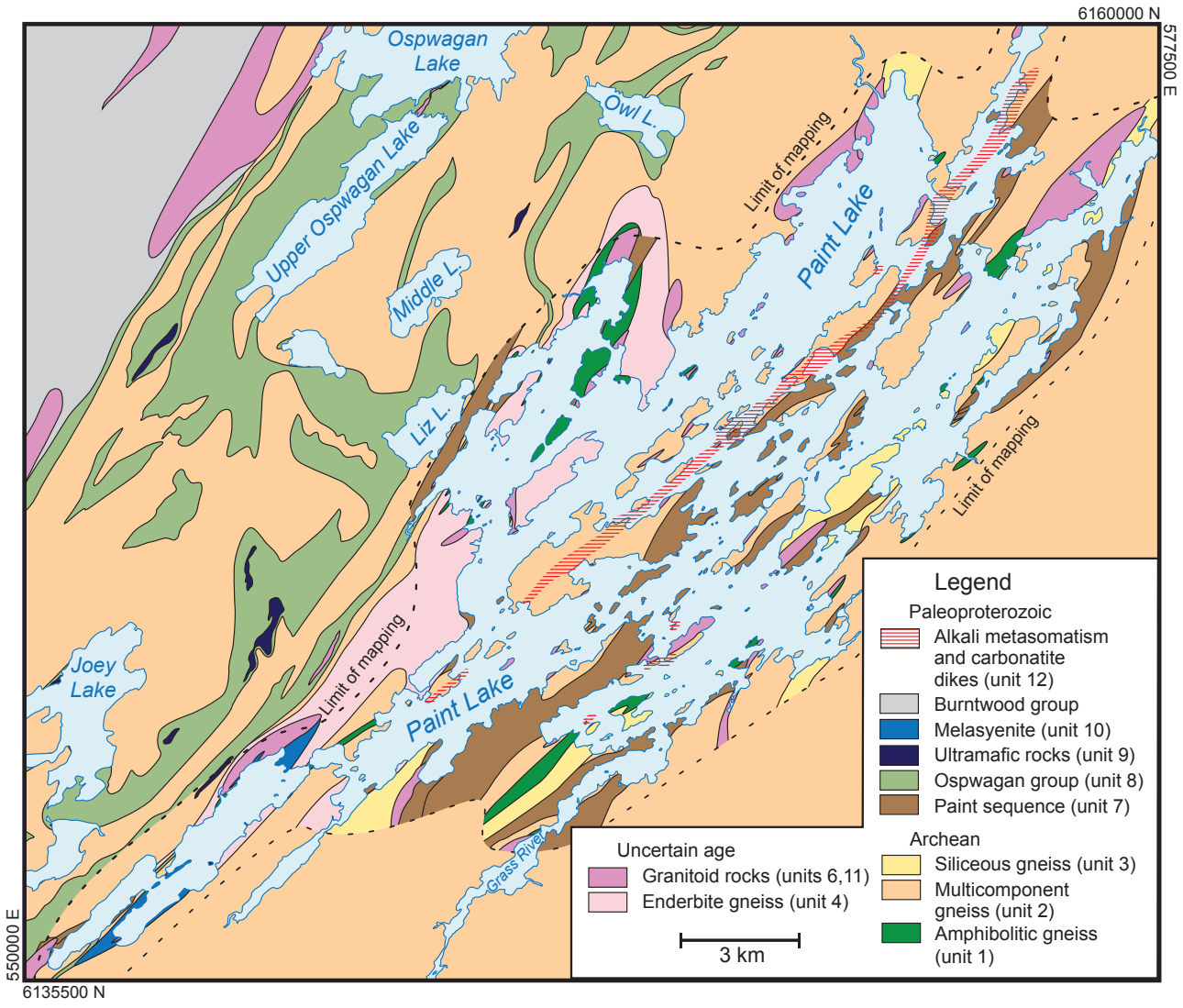

Figure 6: *Simplified lithology of the Paint Lake area. Geology outside the limit of mapping is from Macek et al. (2006). No attempt has been made to merge the two datasets.*

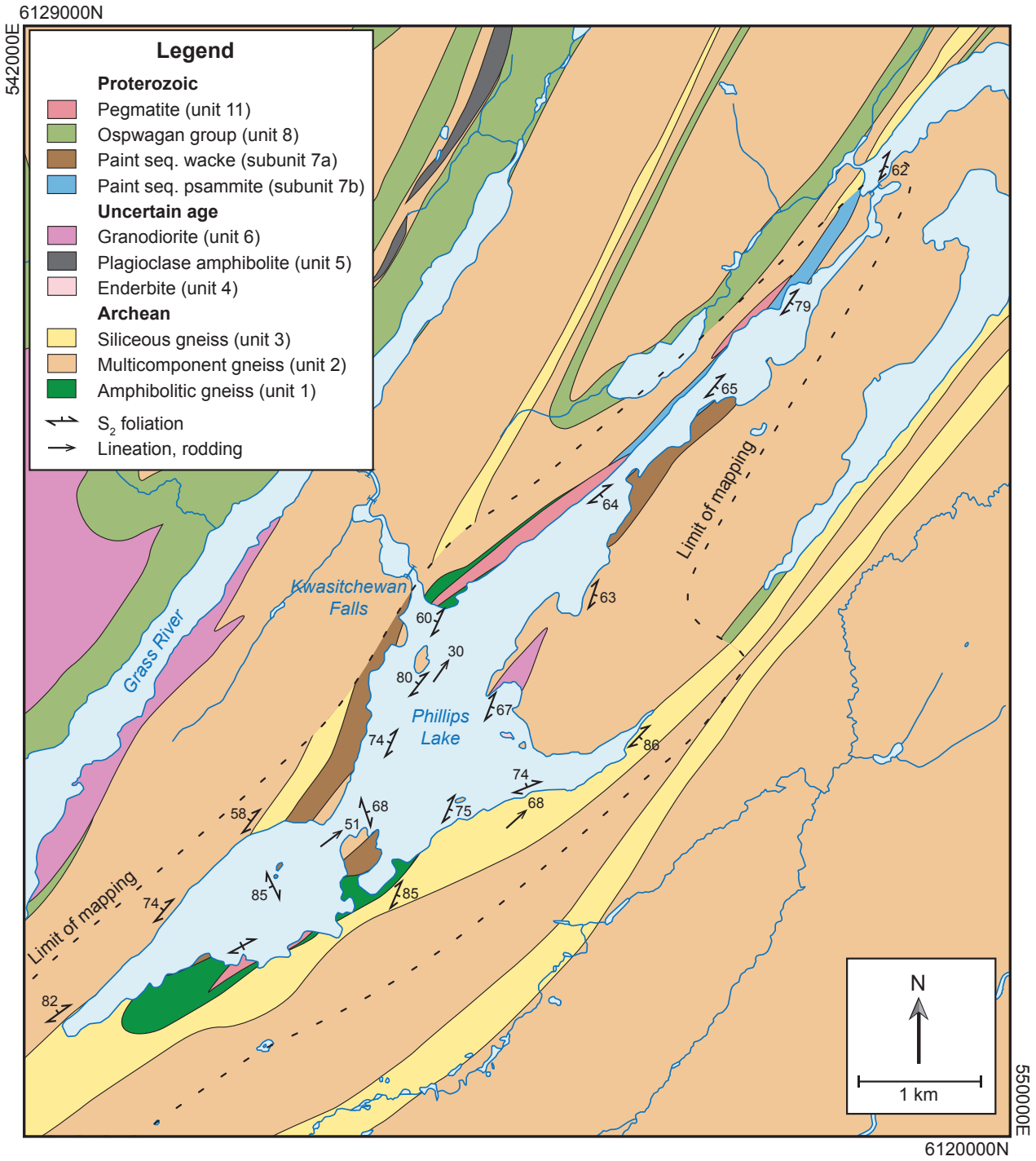

Figure 7: *Geology of the Phillips Lake area (modified from Couëslan, 2012). Geology outside the limit of mapping is from Macek et al. (2006). No attempt has been made to merge the two datasets.*

Amphibolitic gneiss (unit 1)

Amphibolitic gneiss occurs throughout the Paint and Phillips lakes area; however, a large body (approximately 1.5 km by 6 km) occurs in the west-central portion of Paint Lake. The amphibolitic gneiss consists of three subunits: mafic amphibolitic gneiss (subunit 1a), felsic amphibolitic gneiss (subunit 1b) and high-Mg amphibolitic gneiss (subunit 1c). The mafic amphibolitic gneiss (subunit 1a) is greenish black to dark grey, medium to very coarse grained, and foliated to strongly foliated (Figure 8a). It is compositionally and texturally heterogeneous, and layered on a centimetre to decimetre scale. It contains varying proportions of clinopyroxene, orthopyroxene, garnet, hornblende and plagioclase, along with minor biotite and quartz. Mafic minerals typically make up >40% of the rock and are dominated by hornblende. Leucosome, developed during peak metamorphism, locally contains porphyroblasts of orthopyroxene and also forms haloes around porphyroblasts of garnet (Figure 8a). In zones affected by amphibolite-facies retrogression, poikiloblastic garnet that encloses orthopyroxene may, in turn, be rimmed by quartz and plagioclase. At some

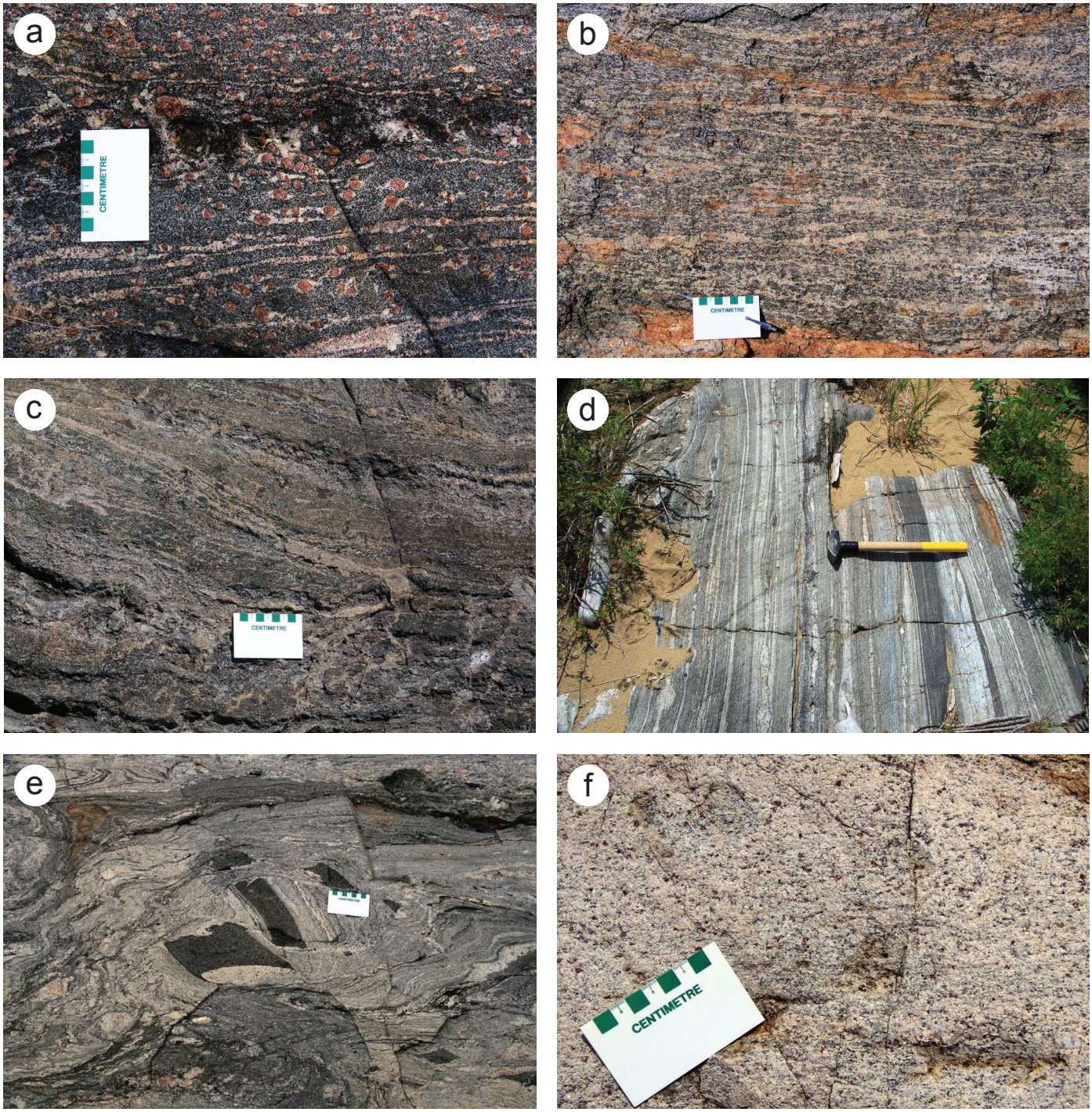

Figure 8: *Outcrop photographs of Archean units in the Paint Lake area:* ***a)*** *mafic amphibolitic gneiss (subunit 1a);* ***b)*** *felsic amphibolitic gneiss (subunit 1b);* ***c)*** *high-Mg amphibolitic gneiss (subunit 1c);* ***d)*** *typical multicomponent gneiss, consisting of hornblende gneiss interbanded with amphibolite and granodiorite (unit 2), with an ultramafic boudin in the upper left corner;* ***e)*** *multicomponent gneiss more typical of the Archean basement to the TNB (unit 2);* ***f)*** *homogeneous siliceous gneiss (unit 3), the mafic minerals consisting dominantly of garnet and magnetite.*

locations, garnet porphyroblasts have been entirely consumed and replaced by knots of plagioclase and quartz, imparting a speckled appearance to the outcrop.

A zone of cordierite-bearing gneiss up to 6 m wide is hosted by mafic amphibolitic gneiss (subunit 1a) in southwestern Paint Lake and was also described by Goddard (1966) and Charbonneau et al. (1979). The cordierite-bearing gneiss consists dominantly of orthopyroxene, cordierite, garnet, quartz and biotite, with lesser amounts of plagioclase and retrograde anthophyllite. The zone is conformable with the regional gneissosity and is relatively heterogeneous, with cordierite-rich bands up to 30 cm thick that typically alternate with more garnet-rich bands. Gneiss containing significant cordierite, garnet and orthopyroxene indicates a relatively aluminous and magnesian bulk composition, analogous to cordierite-anthophyllite/gedrite rocks of the amphibolite facies. Such bulk compositions have a fairly

restricted petrogenesis and typically originate as either unusually magnesian pelite (Drüppel et al., 2013) or chloritic, hydrothermally altered rock (Roberts et al., 2003; Peck and Smith, 2005; Bonnet and Corriveau, 2007). A hydrothermal origin is the preferred interpretation, based on geochemical similarities to the mafic amphibolitic gneiss (subunit 1a).

Although previously interpreted to represent a layered mafic intrusion (Macek and Russell, 1978; Charbonneau et al., 1979), similar mafic gneiss in the PGD is locally associated with metasedimentary rocks, suggesting that at least some of the amphibolitic gneiss occurrences could represent metavolcanic rocks (Couëslan et al., 2012; Couëslan, 2013, 2014a). A volcanic to hypabyssal origin for the mafic gneiss is also supported by the cordierite-bearing rock of southwestern Paint Lake, which could represent a zone of premetamorphic, hydrothermal chloritic alteration.

The felsic amphibolitic gneiss (subunit 1b) is typically light grey on weathered surfaces and dark honey brown on fresh surfaces (Figure 8b). Similar to the mafic gneiss, it is medium to very coarse grained, foliated and compositionally heterogeneous, and contains variable proportions of orthopyroxene, garnet, hornblende, plagioclase and quartz, with minor clinopyroxene and magnetite. The mafic mineral content of the felsic gneiss is <30% and can be as low as 5% in discrete layers. Local bands consist almost exclusively of garnet and quartz. The felsic amphibolitic gneiss was previously interpreted as a layered anorthositic gabbro (Macek and Russell, 1978; Charbonneau et al., 1979). However, the locally quartz-rich (up to 47 vol. %) nature of the rock could suggest a felsic volcanic or siliciclastic protolith, although metamorphic processes such as migmatization and amphibolitization could result in elevated or heterogeneous quartz distribution. Subunits 1a and 1b of the amphibolitic gneiss are commonly spatially associated, and a compositional gradation appears to exist between the two end-members. A compositional gradation may also exist between the felsic amphibolitic gneiss and the siliceous gneiss (unit 3), which is found in close spatial association in the southeastern portions of Paint and Phillips lakes.

A second variety of mafic gneiss, the high-Mg amphibolitic gneiss (subunit 1c), is present in the southwesternmost corner of Paint Lake and on Phillips Lake, where it is spatially associated with subunits 1a and b. Although texturally very similar to the other, more common variety of mafic amphibolitic gneiss (subunit 1a), this second variety is typically green to dark green and contains little to no garnet (Figure 8c). The colour of the gneiss is caused by an abundance of green clinopyroxene and amphibole. Other minerals present include orthopyroxene, plagioclase and minor biotite and quartz. The absence of garnet in subunit 1c is likely a function of the bulk-rock composition, which is more magnesian than the garnet-bearing rocks of subunit 1a.

Multicomponent gneiss (unit 2)

The dominant lithology in the Paint Lake area is multicomponent gneiss (unit 2). It consists of varying proportions of hornblende- and/or biotite-bearing granodioritic to tonalitic gneiss, along with variable but typically subordinate amounts of plagioclase amphibolite (unit 5), granodiorite (unit 6), aplite, pegmatite (unit 11) and assorted ultramafic blocks and boudins. Rare bands of siliceous gneiss (unit 3), enderbite gneiss (unit 4), amphibolitic gneiss (unit 1) and iron formation (subunit 7c) can also be present. These rock types occur as intermixed and highly attenuated, centimetre- to metre-scale bands (Figure 8d). Hornblende-bearing granodioritic to tonalitic gneiss typically forms the dominant component of the unit. It varies from pinkish grey to light grey, and is medium to coarse grained and strongly foliated. It contains 10–30% hornblende but may also contain up to 2% garnet and 7% biotite. It rarely contains up to 5% clinopyroxene and 15% orthopyroxene. It varies from crudely banded to well banded on a millimetre to centimetre scale and is locally highly strained and intensely folded. Rarely the gneiss contains orthopyroxene- or hornblende-bearing leucosome. The biotite-bearing gneiss is generally less abundant than the hornblende variety; however, it is more common in the west portion of the lake. It is texturally and compositionally similar but contains 10–30% biotite, with 2–5% hornblende. It can locally contain trace amounts of garnet, 3–5% orthopyroxene and up to 20% K-feldspar. The hornblende- and biotite-bearing gneisses are likely derived from the various tonalitic to granodioritic granulite gneisses of the adjacent PGD, which are generally considered to be intrusive into the mafic gneiss units (Hubregtse, 1980).

The ultramafic rocks generally constitute less than 2% of a given outcrop but may occur as blocks or boudins up to 5 m across. They include clinopyroxenite, pyroxenite, ultramafic amphibolite and ultramafic schist. The most abundant type of ultramafic rock is clinopyroxenite, which commonly forms boudins or discontinuous layers less than 15 cm thick. The clinopyroxenite can contain variable but minor amounts of biotite, plagioclase, garnet, hornblende, quartz and carbonate. Individual boudins typically have selvages of hornblende up to 1 cm thick. Locally, the clinopyroxenite contains up to 30% apatite as segregations or discontinuous layers. The apatite-bearing clinopyroxenite may be genetically related to the suite of carbonatitic rocks as either disaggregated metasomatic veins or fragments of a magmatic ultramafic phase.

The character of the multicomponent gneiss changes where it is associated with large volumes of pegmatite and toward the western edge of the map area, especially where it is spatially associated with Ospwagan group rocks (unit 8). The migmatite retains a strong gneissosity and is intensely folded; however, the individual components of the gneiss become increasingly difficult to identify, the mafic content is reduced, and hornblende and plagioclase generally become subordinate to biotite and K-feldspar, respectively (Figure 8e). Gneiss of this type is more typical of the Archean basement gneiss of the TNB.

Siliceous gneiss (unit 3)

The siliceous gneiss (unit 3) occurs as centimetre- to metre-scale bands within the multicomponent gneiss and as larger bodies along the east side of Paint Lake and in the Phillips Lake area (up to 900 m wide and possibly continuous over a strike length of >23 km). The siliceous gneiss is white to light grey, medium to coarse grained, foliated and moderately magnetic. It is tonalitic, with 40–50% quartz and <12% mafic minerals (Figure 8f). Garnet and magnetite are ubiquitous, and

varying proportions of biotite and hornblende can also be present. Diffuse centimetre-scale patches contain up to 80% quartz. Millimetre- to centimetre-scale gneissic banding varies from well defined to diffuse, and extensive homogeneous zones are also present. The quartz-rich character of the gneiss, combined with local well-defined banding, is reminiscent of metapsammite; however, extensive homogeneous zones suggest an igneous plutonic protolith, with zones of gneissic banding likely developed due to heterogeneous strain. The quartz-rich nature of the rock could, in part, be related to metamorphic processes such as migmatization and the growth of metamorphic garnet and magnetite. The siliceous gneiss is commonly intruded by pegmatite dikes (unit 11). More mafic and banded portions of the siliceous gneiss are compositionally similar to the felsic amphibolitic gneiss (subunit 1b), and it is possible the two units are gradational.

Rocks of uncertain age

The age of three map units, enderbite gneiss (unit 4), plagioclase amphibolite (unit 5) and granodiorite (unit 6), remains unconstrained. All three units display Hudsonian fabrics, thus providing a minimum Paleoproterozoic age; however, no maximum age constraint is defined. The units are listed in an arbitrary order; however, it should be noted that the plagioclase amphibolite (unit 5) likely consists of rocks that vary in age from Archean to Paleoproterozoic.

Enderbite gneiss (unit 4)

The enderbite gneiss (unit 4) underlies much of the western portion of Paint Lake, forming a body measuring at least 2.5 km by 10.5 km. Two varieties are recognized, a biotite-rich variety (subunit 4a) and a hornblende-bearing variety (subunit 4b). Both varieties are relatively siliceous, with 30–40% quartz, and contain pods of K-feldspar–bearing and orthopyroxene- or hornblende-bearing leucosome. The biotite enderbite makes up the largest volume of this unit, with the hornblende enderbite occurring along the periphery, perhaps reflecting a compositional zonation in the original igneous body. The biotite enderbite (subunit 4a) is honey brown to greenish grey on fresh surfaces and brown-grey on weathered surfaces (Figure 9a). It is medium to coarse grained and foliated to strongly foliated. It typically contains 20–30% mafic minerals as varying proportions of biotite and orthopyroxene. In general, there is an inverse relationship between the biotite and orthopyroxene content. Orthopyroxene is locally enclosed by leucosome, suggesting it is the product of a melt-producing reaction, such as the incongruent breakdown of biotite (Figure 9a). Local hornblende, clinopyroxene and garnet occur in minor amounts. The biotite enderbite locally contains sheet-like or nebulous mafic-enriched zones that locally characterize entire outcrops. These zones typically contain around 40% mafic minerals as roughly equal proportions of biotite and orthopyroxene, and up to 10% clinopyroxene. It is unclear if these zones represent large-scale cognate inclusions or discontinuous zonation within the enderbite body. The hornblende enderbite (subunit 4b) is light grey, medium to coarse grained and foliated (Figure 9b). It contains 20–30% mafic minerals as varying proportions of hornblende, biotite and orthopyroxene.

The enderbite gneiss (unit 4) is compositionally and texturally distinct from the multicomponent gneiss (unit 2), which is interpreted to be derived from retrogressed enderbitic gneiss of the PGD. This suggests a less complex history and possibly a younger overall age. The presence of S_2–S_3–concordant, weakly foliated to massive, orthopyroxene-bearing leucosome suggests that the enderbitic gneiss was subjected to Paleoproterozoic granulite-facies metamorphic conditions and that it may represent a metatonalite intrusion rather than a true igneous enderbite (tonalite derived from anhydrous melt). This is supported by the inverse relationship between biotite and orthopyroxene content, and the presence of what appears to be peritectic orthopyroxene porphyroblasts enclosed by leucosome (Figure 9a). The enderbite gneiss (unit 4) is commonly intruded by pegmatitic dikes (unit 11). Where pegmatitic intrusions are abundant, the gneiss is typically retrogressed and orthopyroxene is scarce to absent.

Plagioclase amphibolite (unit 5)

Large masses, discontinuous bands and boudins of plagioclase amphibolite are ubiquitous in the Paint Lake area, occurring in the majority of outcrops. This rock is dark green-grey, fine to medium grained and foliated. It generally contains

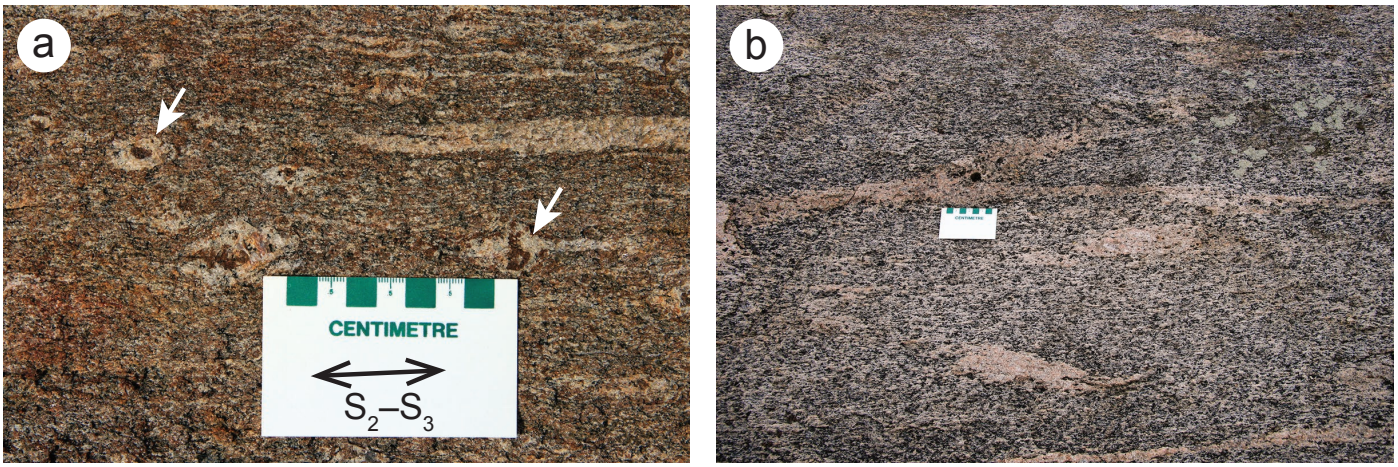

Figure 9: *Outcrop photographs of rock types in unit 4, western Paint Lake:* ***a)*** *biotite enderbite (subunit 4a), arrows indicating orthopyroxene porphyroblasts enclosed by leucosome;* ***b)*** *hornblende enderbite (subunit 4b).*

50–70% hornblende and plagioclase with or without minor quartz. Minor amounts of clinopyroxene and garnet may be present, and orthopyroxene locally accounts for up to 15% of the rock. The amphibolite bodies vary from centimetres to tens of metres in size and range from relatively massive to strongly gneissic. They are likely derived from mafic rocks of various ages, from Archean to Paleoproterozoic, including ca. 1880 Ma Molson dikes (Heaman et al., 2009). Bands of plagioclase amphibolite are cut by pegmatite dikes (unit 11) and are metasomatized where spatially associated with carbonatite dikes (unit 12).

Granodiorite (unit 6)

Bodies of granodiorite (6) occur throughout the map area, ranging from centimetre-thick dikes to large bodies up to 400 m by 2600 m that are elongate parallel to the regional foliation. The granodiorite is light grey to pinkish grey, medium to coarse grained and foliated. The mafic mineral content is typically 10–15% and consists of hornblende and/or biotite. Up to 2% magnetite and 2% garnet may also be present. Diffuse centimetre-scale gneissosity is common and the rock is locally porphyritic, with K-feldspar phenocrysts up to 2 cm long. The phenocrysts are commonly rounded and are locally aligned with the regional lineation. The granodiorite (unit 6) is commonly intruded by pegmatite dikes (unit 11) and locally intruded by carbonatite dikes (unit 12).

Paleoproterozoic rocks

Units 7–12 are interpreted to be Paleoproterozoic and are listed in approximate order of age. The placement of Paint sequence rocks (unit 7) before Ospwagan group rocks (unit 8) is arbitrary, as the age relationship between these two units is not constrained. Ultramafic (unit 9) and syenite (unit 10) intrusions were likely roughly contemporaneous, based on published ages for ultramafic intrusions in the TNB (ca. 1880 Ma; Hulbert et al., 2005; Heaman et al., 2009; Scoates et al., 2010) and U-Pb zircon dating of the melasyenite (unit 10, this study).

Paint sequence (unit 7)

Three northeast-striking belts of supracrustal rocks occur in the Paint Lake area and have been informally termed the Paint sequence (unit 7). They outcrop along the eastern shore, through the central islands and along the western shore. Similar rocks have also been recognized along strike on Phillips Lake, and along the western margin of the TNB at Manasan Falls (Couëslan, 2011, 2012). The stratigraphy of the Paint sequence is unconstrained, so the subunits are listed in order of decreasing abundance. The Paint sequence consists dominantly of wacke (subunit 7a) and psammite (subunit 7b), with subordinate iron formation (subunit 7c) and pelite (subunit 7d), and rare boudins of calcsilicate. The wacke (subunit 7a) is light grey to light brownish grey, medium to coarse grained, foliated and compositionally layered at millimetre to centimetre scale (Figure 10a). It contains 5–15% garnet, 5–20% orthopyroxene, 10–30% biotite, 30–50% quartz, and plagioclase. In general, the amount of orthopyroxene is inversely proportional to the amount of garnet present. This inverse relationship could be related to variations in bulk composition; however, orthopyroxene is typically less abundant in the westernmost occurrences of wacke, suggesting the abundance of orthopyroxene could also be related to variations in metamorphic grade. The wacke typically contains minor pyrrhotite and locally minor graphite, magnetite, hornblende and K-feldspar. Centimetre- to decimetre-thick bands of psammite and iron formation are common. Centimetre- to decimetre-scale pods of leucosome are locally orthopyroxene bearing. The leucosome is commonly concordant with S_2–S_3 and locally pools in D_2–D_3 boudin necks, suggesting a Paleoproterozoic age for leucosome formation. Outcrops of this unit are characterized by rusty weathered surfaces because of minor but ubiquitous pyrrhotite. The compositions of the wacke (subunit 7a) and psammite (subunit 7b) are gradational into one another and they are typically interbedded. Rare lenses of molybdenite, up to 3 cm long, occur in both wacke and psammite, and may correspond to occurrences of molybdenite described by Dawson (1952) and Charbonneau et al. (1979). No associated alteration or patterns of distribution were identified with the molybdenite occurrences.

The psammite (subunit 7b) is white to light grey, medium to coarse grained, foliated to mylonitic and compositionally layered on a centimetre scale (Figure 10b). It contains trace to 7% garnet, 2–5% orthopyroxene, 2–10% biotite, 30–70% quartz and 20–60% plagioclase. Minor amounts of pyrrhotite and graphite are locally present. The psammite is typically interlayered with centimetre- to metre-thick layers of wacke. The psammite can contain garnet-bearing concretions up to several centimetres thick (Figure 10c). The concretions are composed of 7–10% garnet and quartz with minor carbonate, and are typically restricted to rare exposures of interbedded psammite and pelite (subunit 7d). The pelite occurs as lenses and layers up to 30 cm thick, interlayered with psammite (Figure 10d). Rare, metre-scale layers of pelite also occur, interlayered with psammite layers up to 10 cm thick. The pelite is typically coarse grained and strongly foliated. It contains 5–20% sillimanite, 5–30% garnet, 10–20% K-feldspar, 20–40% biotite, and quartz and plagioclase. Cordierite is locally present and can constitute up to 10% of the rock.

The Paint sequence iron formation (subunit 7c) is rarely the dominant phase in an outcrop, but rather occurs as discontinuous bands and lenses up to 3 m thick within the wacke (Figure 10e). It is dark greenish grey to brownish red, fine to coarse grained, foliated and locally strongly magnetic. The composition is generally that of silicate-facies iron formation with varying proportions of biotite, pyrrhotite, Ca-amphibole, magnetite, orthopyroxene, garnet and quartz. Oxide-facies iron formation with quartz and up to 30% magnetite is rare. Exposures are characterized by alternating, millimetre- to centimetre-scale siliceous and ferruginous layers, and intense gossan on weathered surfaces. Iron formation locally occurs as layers up 10 m thick hosted by the multicomponent gneiss (unit 2), indicating that some occurrences of iron formation are likely Archean.

A Paleoproterozoic age for the Paint sequence is suggested by a limited dataset of U-Pb ages from detrital zircons recovered from the wacke (see ‘Geochronology’ section). Paint sequence rocks are locally intruded by relatively straight-walled mafic

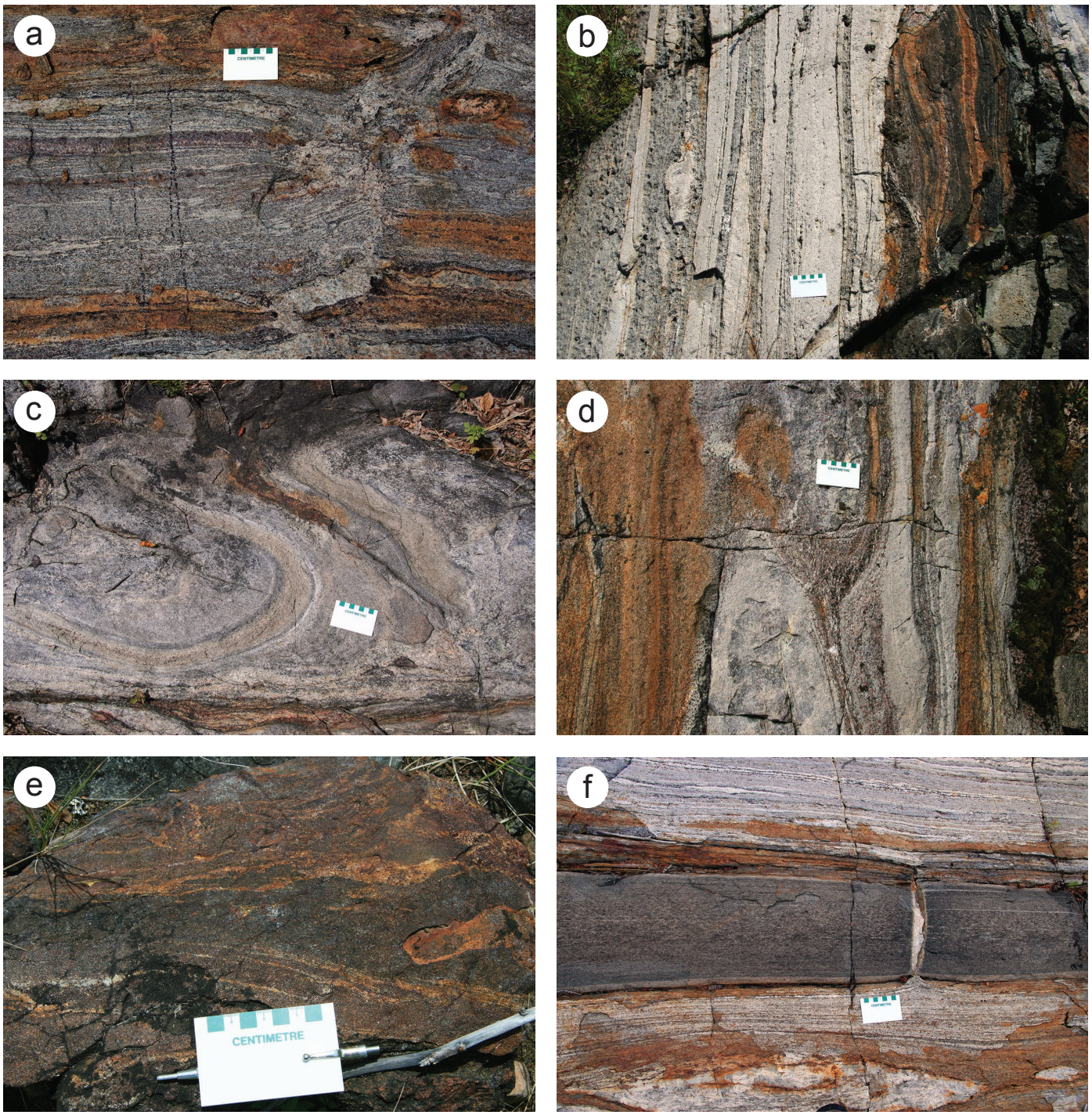

Figure 10: *Outcrop photographs of unit 7:* ***a)*** *Paint sequence wacke (subunit 7a);* ***b)*** *Paint sequence psammite (subunit 7b, underlying scale card) interbedded with wacke (subunit 7a) and containing a lens of iron formation (subunit 7c, right side of image);* ***c)*** *garnet-bearing concretions (left and above scale card) in Paint sequence psammite; note thin wispy lens of pelite at bottom of photo;* ***d)*** *Paint sequence pelite (subunit 7d) interbedded with psammite/quartzite;* ***e)*** *Paint sequence iron formation (subunit 7c);* ***f)*** *mafic dike intruding Paint sequence wacke; the dike is interpreted to be Paleoproterozoic and possibly related to the ca. 1880 Ma Molson dikes (Heaman et al., 2009).*

dikes, which are tentatively interpreted to be part of the Paleoproterozoic Molson dike swarm (Figure 10f), suggesting a minimum age of ca. 1880 Ma for the sequence. Paint sequence rocks are also intruded by pegmatite (unit 11) and carbonatite dikes (unit 12).

A discrete banded gneiss (unit 7e) was identified at two locations along a 3 km strike length in east-central Paint Lake. The banded gneiss is spatially associated with wacke (subunit 7a) and psammite (subunit 7b) of the Paint sequence and consists of gradational, alternating mafic, intermediate and felsic bands that are laterally continuous and of a uniform thickness at outcrop scale (Figure 11a). The unit is tentatively interpreted as a volcaniclastic rock; however, it could also represent a recrystallized zone of Archean straight gneiss.

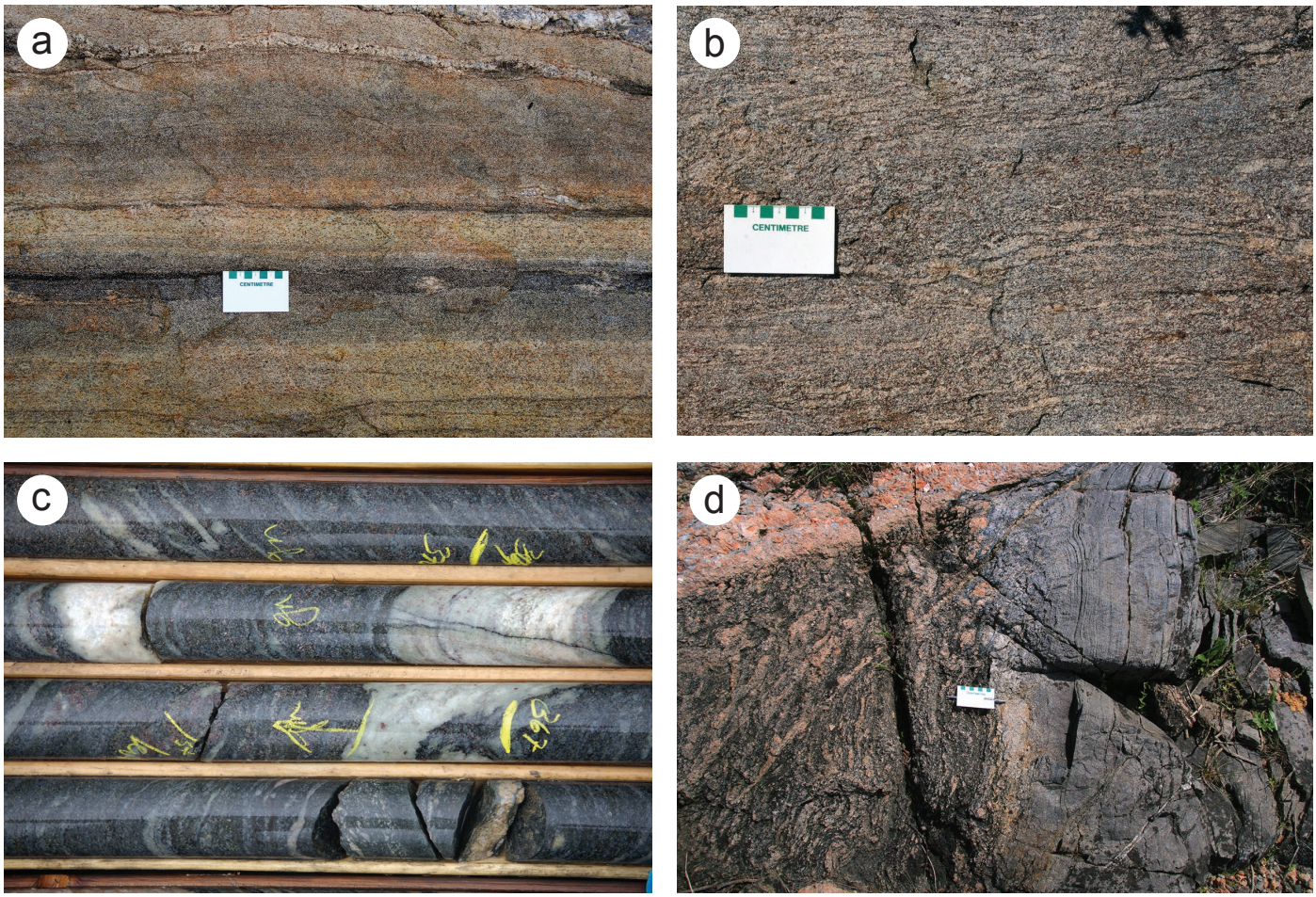

Figure 11: *Outcrop photographs of supracrustal rocks from the Paint and Phillips lakes area:* ***a)*** *banded gneiss unit closely associated with Paint sequence sedimentary rocks in east-central Paint Lake and tentatively interpreted as a volcaniclastic rock (subunit 7e);* ***b)*** *Paint sequence wacke along the west shore of Phillips Lake;* ***c)*** *Paint sequence wacke in diamond-drill core from Phillips Lake (PL96-22);* ***d)*** *contact between Manasan formation M1 member quartzite (right of scale card) and M2 member semipelite (left of scale card) of the Ospwagan group (unit 8), cut by discordant pegmatite dike (unit 11; upper left), southwestern Paint Lake.*

Wacke and local psammite occur along the east and west shores, and central islands, of Phillips Lake. The sedimentary rocks are texturally, mineralogically and geochemically similar to the Paint sequence rocks (Figure 11b), occur along strike with occurrences on Paint Lake and are believed to be part of the same sequence. A re-evaluation of Falconbridge and Inco diamond-drill core from the Phillips Lake area suggests the presence of a relatively thick package of Paint sequence rocks consisting dominantly of wacke with centimetre- to metre-scale intercalations of psammite, iron formation and local calcareous rocks (Figure 11c). The sedimentary rocks contain local bands of plagioclase amphibolite, interpreted as diabase dikes, and host bodies of serpentinized ultramafic rock, the latter having implications for nickel exploration in the belt (see 'Economic considerations' section).

Ospwagan group (unit 8)

A narrow band of Ospwagan group sedimentary rocks (unit 8) occurs along the western side of Paint Lake. Outcrops consist of Manasan formation quartzite (M1 member) and semipelite (M2 member; Figure 11d) and local Thompson formation calcareous rocks. The remainder of the Ospwagan group stratigraphy has either been truncated or is not exposed. The sedimentary rocks are steeply dipping to vertical and the stratigraphic younging direction is toward the east. The M1 quartzite is beige to grey, fine grained and massive to laminated, and contains 2–3% biotite and local garnet. The M2 semipelite forms a pinkish-grey, coarse-grained and strongly foliated diatexite. The diatexite is K-feldspar and quartz rich, with 20–30% biotite and local garnet. Minor layers and boudins of calcsilicate are locally present within the M2 member, indicating a transition to carbonate deposition and proximity to the basal contact of the Thompson formation (Zwanzig et al., 2007). Thompson formation marble is exposed during low-water periods at the Paint Lake marina, adjacent to the restaurant and lounge. The marble is grey, medium to coarse grained and strongly foliated. Mafic minerals consist of variable amounts of tremolite, chloritized phlogopite and serpentinized olivine. Ospwagan group rocks are commonly intruded by pegmatite dikes (unit 11).

Pyroxenite (unit 9)

A single exposure of pyroxenite (unit 9) occurs in the southwest corner of the Paint Lake area. It is dark green, coarse grained and weakly foliated. It contains trace to minor amounts

of phlogopite, 7–10% quartz, 10–15% Ca-amphibole, and orthopyroxene. The rock appears relatively homogeneous with the exception of pockets bearing up to 12% quartz and plagioclase. The quartz is, at least in part, a byproduct of amphibolitization of the pyroxene. The pyroxenite is compositionally and texturally similar to nickel-bearing ultramafic bodies elsewhere in the TNB and is assumed to be of the same age (ca. 1880 Ma; Hulbert et al., 2005; Heaman et al., 2009; Scoates et al., 2010).

Melasyenite (unit 10)

An elongate body of melasyenite (10) is present in the southwest corner of the Paint Lake area (Figure 6). It is up to 700 m thick and greater than 7 km long. The syenite is characterized by phenocrysts of K-feldspar hosted in a groundmass rich in mafic minerals. The majority of melasyenite exposures were subjected to some degree of metasomatism/recrystallization and contain alkali-feldspar granite dikes. Unmetasomatized outcrops are rare and are dark brown to black, weakly foliated to foliated, and characterized by dark grey to black K-feldspar phenocrysts up to 3 cm long in a medium- to coarse-grained matrix of reddish-brown biotite, amphibole and honey-brown K-feldspar (Figure 12a). Potassium-feldspar phenocrysts commonly display Carlsbad twinning and locally have pale yellow cores. Dark brownish-green clinoamphibole forms less abundant phenocrysts up to 2 cm across.

Point counts (n = 2567) on four thin sections yielded a modal analysis of 59.1% K-feldspar, 23.0% clinoamphibole, 9.5% biotite, 3.6% orthopyroxene, 3.1% quartz, 1.2% apatite, 0.2% zircon and 0.1% each of rutile and unidentified opaque minerals. Both the K-feldspar and clinoamphibole phenocrysts

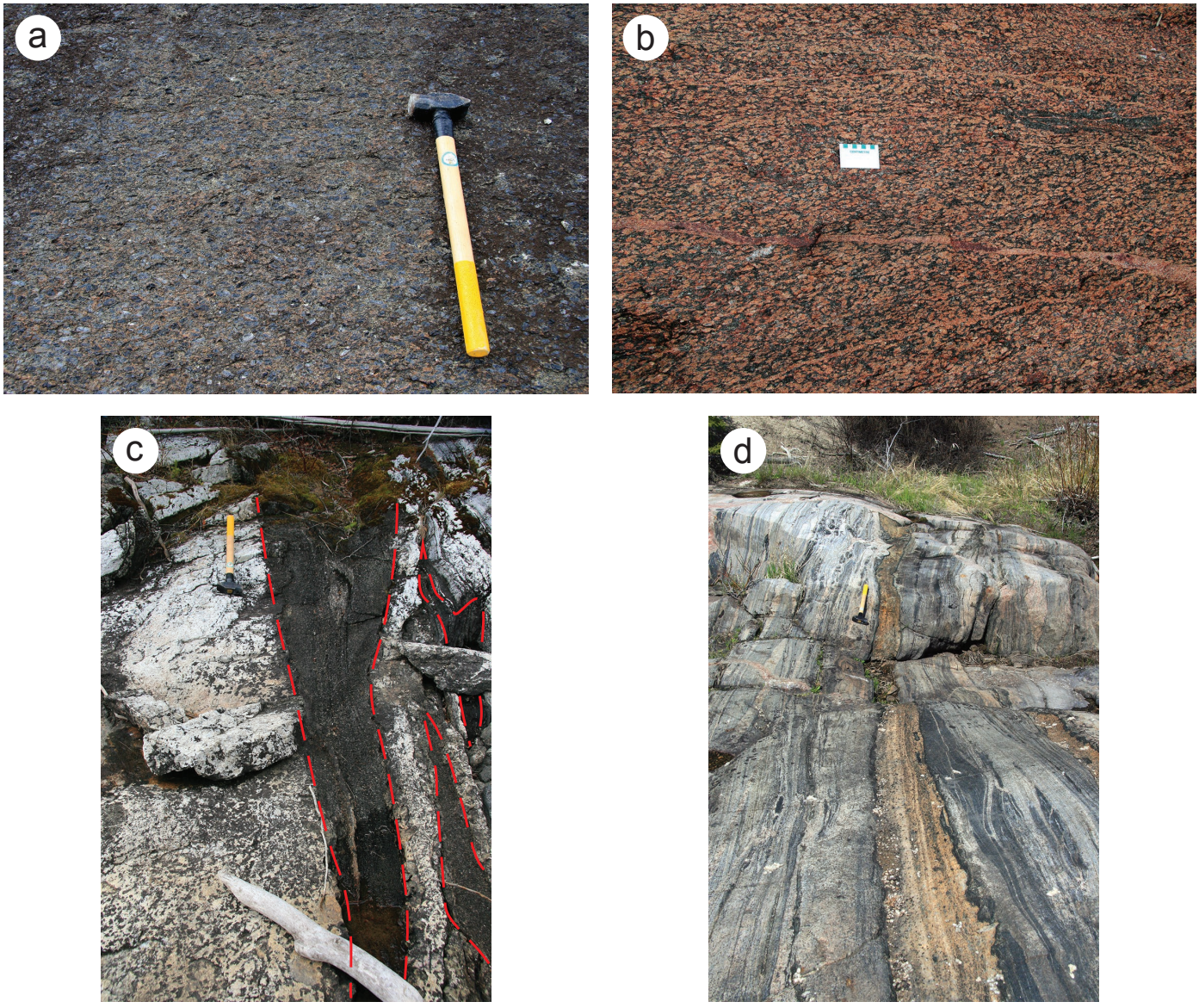

Figure 12: *Outcrop photographs of Paleoproterozoic alkaline rocks in the Paint Lake area:* ***a)*** *unmetasomatized melasyenite (unit 10), much of the rock consisting of black K-feldspar phenocrysts;* ***b)*** *metasomatized/recrystallized melasyenite (unit 10); note the brick-red colour of the K-feldspar phenocrysts;* ***c)*** *dolomite-carbonatite (subunit 12a; outlined in red) covered by black lichen and hosted in metasomatized pegmatite; note the bleached white appearance of the pegmatite;* ***d)*** *calcite-carbonatite (subunit 12b; chalky yellow band down centre of photo).*

contain abundant micro-inclusions of biotite, apatite, rutile and unidentified opaque minerals. The phenocrysts typically display thin, inclusion-free rims. Rare, round inclusions of green clinopyroxene occur in K-feldspar phenocrysts. The margins of K-feldspar phenocrysts are commonly recrystallized to form thin polycrystalline rims. These polycrystalline rims, as well as K-feldspar in the groundmass, are inclusion free and commonly display perthitic intergrowth, which is absent in the phenocrysts. Groundmass clinoamphibole is also largely inclusion free. The amphibole displays pleochroism ranging from pale yellow-green to bright grassy green to purplish brown. Amphibole grains commonly contain thin intergrowths of biotite along cleavage traces. Quartz occurs only in the groundmass. Orthopyroxene is typically uralitized and occurs in the groundmass. Zircon locally forms clusters or glomerocrysts of anhedral grains that locally display prominent overgrowths.

In the vicinity of alkali-feldspar granite dikes, the melasyenite becomes variably metasomatized. The colour can vary from dark purplish grey to brick red, and the rocks become strongly foliated to mylonitic (Figure 12b). Potassium-feldspar phenocrysts become rounded, and the dark grey to black colouration becomes progressively replaced by pink to red. The groundmass of metasomatized syenite consists of trace amounts of apatite, up to 10% quartz and variable amounts of biotite and amphibole. Alkali-feldspar granite dikes are up to 1 m thick. The dikes are reddish pink to orangey pink, medium to coarse grained and foliated. The granite generally contains minor clinopyroxene or clinoamphibole and locally up to 3% titanite. Larger dikes commonly show gradations toward more syenitic compositions with only 5% quartz. The alkali-feldspar granite dikes are assumed to be cogenetic with the melasyenite.

Granitic pegmatite (unit 11)

Pink pegmatite dikes (unit 11) are present in almost every outcrop in the Paint Lake area. Dikes are typically centimetre to metre scale; however, elongate plugs up to several hundred metres thick and >2 km long are also present. Foliated to protomylonitic dikes are most common and generally trend subparallel to the regional foliation. Massive dikes are less common and typically cut across the regional foliation at a high angle. Aplitic dikes are locally present and can be frequently traced into more pegmatitic units. The pegmatite is typically K-feldspar rich, with 10–30% plagioclase and 20–30% quartz. Biotite is common and may constitute up to 12% of the rock. Up to 3% garnet may be present, especially in proximity to sedimentary rocks or mafic amphibolitic gneiss. Three to five percent magnetite occurs as rare iridescent blue grains. Pegmatite dikes locally contain up to 10% allanite. The allanite is metamict and forms subhedral to euhedral prismatic grains up to 1 cm across. The allanite appears to be associated with late, anastomosed fractures.

Carbonatite (unit 12)

A swarm of thin carbonatite dikes (unit 12) is present through the central islands of Paint Lake over a strike length of at least 23 km. Individual dikes are typically <1 m thick and occur within a zone up to 500 m wide characterized by pervasive Na-Ca metasomatism. Two varieties of carbonatite are present: a more primitive, grey dolomite-carbonatite (subunit 12a); and a more evolved, pink calcite-carbonatite (subunit 12b; Chakhmouradian et al., 2009). They are foliated and strike subparallel to regional fabrics (trending 040°). The dikes are interpreted to be Proterozoic because they crosscut all but the latest, discordant and massive pegmatite dikes (unit 11). The carbonatite dikes are interpreted to be of postorogenic affinity based on their geochemical, petrographic and structural characteristics (Chakhmouradian et al., 2009).

Dikes of dolomite-carbonatite (subunit 12a) up to 3 m thick only occur within the middle 9 km of the swarm's exposed strike length. They are light grey, medium to coarse grained, foliated and moderately to strongly magnetic. Weathered surfaces are typically covered by black lichen (Figure 12c). They typically contain trace to minor amounts of phlogopite, clinopyroxene, magnetite, titanite and apatite, with 20–30% serpentinized olivine, and white to grey carbonate. Apatite locally forms up to 15% of the rock. Veinlets of chrysotile and magnetite are common. Rare green spinel is observed in thin section.

Dikes of calcite-carbonatite (subunit 12b) occur along the entire exposed strike length of the swarm. They are pink, fine to coarse grained, foliated and strongly magnetic in places. The dikes typically have an earthy yellow-orange coating on weathered surfaces and are up to 2.8 m thick (Figure 12d). The calcite-carbonatite contains trace to minor amounts of sulphide, magnetite, biotite, titanite, scapolite and allanite, and up to 25% apatite, 30% green clinopyroxene and/or amphibole, and pink to white carbonate. The dikes locally contain up to 25% magnetite as elongate clots up to 3 cm long. Xenoliths of metasomatized country rock are common. A more detailed description of the calcite-carbonatite can be found in Chakhmouradian et al. (2009).

The carbonatite dikes typically have selvages enriched in amphibole and apatite in roughly equal proportions and containing variable amounts of scapolite and 3–5% titanite. Metasomatized country rock adjacent to carbonatite dikes is characterized by a bleached appearance. The normally grey multicomponent gneiss (unit 2) is white to pale pink due to replacement of metamorphic plagioclase by metasomatic feldspar, and replacement of dark metamorphic amphibole and biotite by metasomatic light green actinolite and locally clinopyroxene. Quartz is typically less abundant in metasomatized rocks. Pegmatite dikes in the vicinity of carbonatite occurrences are commonly white and contain 5–10% clinopyroxene and/or amphibole, and <15% quartz.

Lithogeochemistry and Sm-Nd isotope geochemistry

In order to establish the composition of rocks in the Paint Lake area, a suite of representative samples, including most of the principal map units, was collected for lithogeochemical analysis; however, for the purpose of this report, the descriptions of geochemical attributes will be restricted to the amphibolitic gneiss (unit 1), Paint sequence wacke (subunit 7a) and melasyenite (unit 10). In addition, Sm-Nd isotope geochemistry was obtained for samples of the Paint sequence wacke (subunit 7a) and the melasyenite (unit 10). Results of the lithogeochemical

and Sm-Nd isotope analyses are provided in Data Repository Item DRI2016001[2].

Sampling and analytical methods

Representative samples (>1.5 kg) were collected from most of the principal map units for geochemical analysis. Due to the high metamorphic grade of rocks in the Paint Lake area, many of the units have been subjected to anatexis of varying intensity. In rock types that underwent minimal partial melting, care was taken to sample material with little to no leucosome. In rock types subjected to intense partial melting, samples were selected that appeared to be representative of the bulk composition in terms of proportion of leucosome to melanosome or mesosome, and care was taken to avoid what appeared to be injected leucosome in favour of material that appeared to consist of in situ or in-source leucosome. Material displaying evidence of alteration was avoided. Weathered surfaces were either removed on the outcrop at the time of sampling or cut off with a saw at the Manitoba Geological Survey's Midland Sample and Core Library prior to crushing. Samples were crushed to <5 mm at the Midland Sample and Core Library using a steel jaw-crusher. Pulps were produced in a steel swing mill and were homogenized by rolling and then splitting to approximately 55 g of analytical material. A minimum of one internal standard and one blind duplicate was inserted for every twenty samples submitted for analysis.

Samples were analyzed at Activation Laboratories Ltd. (Ancaster, Ontario) using the '4Litho' analytical package, which employs a lithium metaborate/tetraborate fusion technique, followed by nitric-acid digestion and analysis by inductively coupled plasma–emission spectrometry (ICP-ES) for the major elements and selected trace elements (Ba, Be, Sc, Sr, V, Y, Zr), ion-specific electrode (ISE) for F (in selected samples) and inductively coupled plasma–mass spectrometry (ICP-MS) for the remainder of the trace elements and rare-earth elements. Samples suspected of containing appreciable carbonate were analyzed for total C, sometimes bundled with analysis of total S, by combusting the sample in an induction furnace and measuring the release of CO_2 and SO_2 by infrared spectrometry. Some samples of Paint sequence rocks suspected of containing sedimentary sulphide were analyzed by total-digestion ICP-ES for selected trace elements (Ag, Cd, Cu, Ni, Pb, Zn) and sulphur contained within sulphides. Three samples of Paint sequence rocks were also analyzed for ferrous iron by titration.

Four samples of Paint sequence wacke and one sample of melasyenite were submitted for Sm-Nd isotope geochemical analysis to the University of Alberta Radiogenic Isotope Facility (Edmonton, Alberta). The rock-sampling and initial-processing procedures followed were the same as those for lithogeochemistry samples. The samples were processed and analyzed for Sm-Nd isotopes following the chromatographic and mass-spectrometry methods outlined by Unterschutz et al. (2002) and Schmidberger et al. (2007). Samarium and neodymium isotopic compositions were determined by multicollector (MC)-ICP-MS, for which an in-house Nd isotope standard was used (Schmidberger et al., 2007). Chemical processing blanks were <200 pg for Nd and Sm. The Nd data are presented relative to a $^{143}Nd/^{144}Nd$ value of 0.511850 for the La Jolla standard, and crustal residence model ages (T_{CR}) were calculated based on the model of Goldstein et al. (1984), which assumes a linear evolution of isotopic ratios in the depleted mantle, using present-day depleted-mantle values of $^{143}Nd/^{144}Nd = 0.513160$ and $^{147}Sm/^{144}Nd = 0.2141$.

The majority of samples were collected by the author during fieldwork in 2008, 2009 and 2010 on Paint Lake and in 2012 on Phillips Lake. Sample 108-PL96-22-11 was collected by the author in 2007 from diamond–drill core from the Phillips Lake area (drillhole PL96-22; Assessment File 94497, Manitoba Growth, Enterprise and Trade, Winnipeg). Samples with 108-13- and 108-15- prefixes were collected by the author in 2013 and 2015, respectively. Samples 12-03-4198-1 and 12-03-4201-1 were collected by H. Zwanzig in 2003 from a syenite intrusion southwest of the study area at Max Lake. Samples with a 38-03- prefix were collected by J.J. Macek in 2003 at Paint Lake. Of these samples, the data for 38-03-90-1 and 38-03-90-2 were previously published in Böhm et al. (2007) and Zwanzig et al. (2008). Universal Transverse Mercator (UTM) co-ordinates (Zone 4, NAD83) are provided for all samples in DRI2016001.

Amphibolitic gneiss (unit 1)

Attempts were made to sample the amphibolitic gneiss from relatively homogeneous bands; however, due to the coarse grain-size and heterogeneity of the gneiss, it was difficult to ascertain what represented a meaningful bulk composition. Fluid-soluble, large-ion lithophile elements (LILE; e.g., K, Rb, Ba, Sr) were generally not utilized in describing the geochemistry of the amphibolitic gneiss because of their mobility under high-grade metamorphic conditions. Plots utilizing trace elements are therefore restricted to the less mobile elements, including high-field-strength elements (HFSE; Ti, Hf, Zr, Nb), rare-earth elements (REE) and Th.

On the basis of discrimination diagrams, the mafic amphibolitic gneiss (unit 1a) varies in composition from basalt to andesite, whereas the high-Mg amphibolitic gneiss (unit 1c) varies from high-Mg tholeiite to basaltic andesite to andesite (Figure 13a–c). The felsic amphibolitic gneiss (subunit 1b) plots as dacite and rhyolite on the total alkali–silica diagram of Le Maitre (2002) and cation diagram of Jensen and Pyke (1982); however, it plots in the andesite field on the Zr/Ti–Nb/Y diagram of Pearce (1996). The mafic and felsic amphibolitic gneisses (subunits 1a, b) are characterized by Mg# (100*Mg/Fe^T+Mg) <50 (with the exception of the cordierite-bearing rock discussed below), while the high-Mg amphibolitic gneiss (subunit 1c) is characterized by Mg# >50. Use of the term 'high-Mg' to describe subunit 1c is meant to reflect the relatively higher Mg# of this subunit, and is not used in the classical sense (>8 wt. % MgO). The high concentration of MgO (19.5 wt. %) in sample 108-12-022B (subunit 1c) is suggestive of either a cumulate origin, or magma of boninitic or komatiitic

[2] MGS Data Repository Item DRI2016001, containing the data or other information sources used to compile this report, is available to download free of charge at http://www2.gov.mb.ca/itm-cat/web/freedownloads.html, or on request from minesinfo@gov.mb.ca or Mineral Resources Library, Manitoba Growth, Enterprise and Trade, 360–1395 Ellice Avenue, Winnipeg, Manitoba R3G 3P2, Canada.

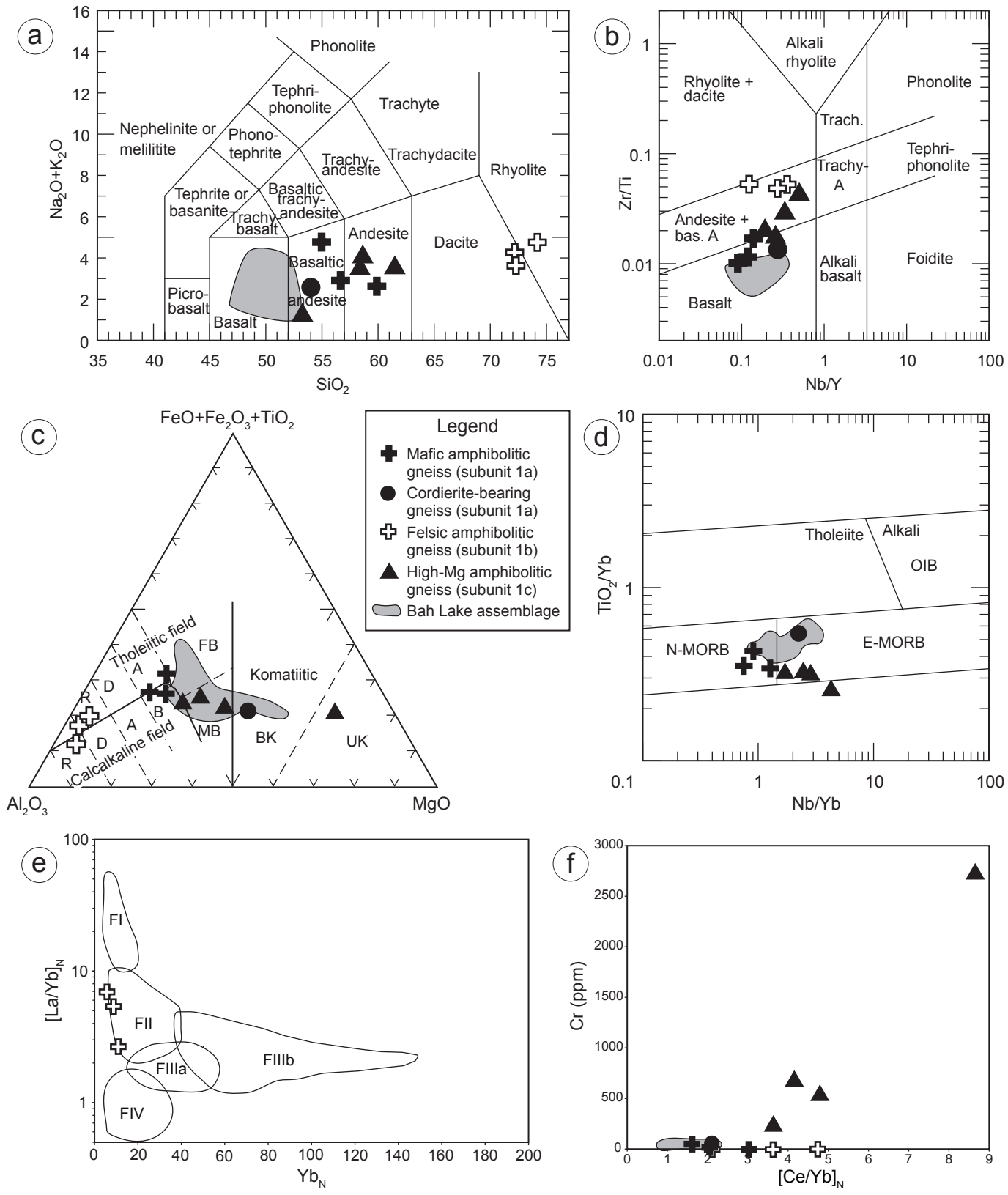

Figure 13: *Geochemical discrimination diagrams for amphibolitic gneiss (unit 1):* ***a)*** *total alkali vs. silica (TAS) diagram (after Le Maitre, 2002);* ***b)*** *Nb/Y–Zr/Ti diagram (after Pearce 1996);* ***c)*** *Al_2O_3–FeO+Fe_2O_3+TiO_2–MgO diagram (after Jensen and Pyke, 1982);* ***d)*** *TiO_2/Yb–Nb/Yb diagram (after Pearce 2008);* ***e)*** *$[Yb]_N$–$[La/Yb]_N$ diagram outlining the fields for FI–FIV rhyolite (after Hart et al., 2004);* ***f)*** *$[Ce/Yb]_N$–Cr diagram. The composition of Bah Lake assemblage rocks (n = 36) is from Zwanzig (2005). Abbreviations: A, andesite; B, basalt; bas., basaltic; BK, basaltic komatiite; D, dacite; E-MORB, enriched mid-ocean-ridge basalt; FB, high-Fe tholeiitic basalt; MB, high-Mg tholeiitic basalt; N-MORB, normal mid-ocean-ridge basalt; OIB, oceanic-island basalt; R, rhyolite; Trach., trachyite; UK, ultramafic komatiite.*

affinity (Figure 13c). In addition to Mg#, the high-Mg gneiss (subunit 1c) is typically more enriched in compatible elements (e.g., Cr, Ni) compared to the mafic gneiss (subunit 1a).

Chondrite-normalized rare-earth element (REE) profiles of the mafic amphibolitic gneiss (subunit 1a) are slightly concave upward with shallow to moderate negative slopes for light rare-earth elements (LREE) and very slight positive slopes for heavy rare-earth elements (HREE; Figure 14a). The felsic amphibolitic gneiss (subunit 1b) is characterized by similar concave-upward normalized REE profiles (Figure 14c), with a slightly more fractionated LREE profile. The normalized REE profiles for the high-Mg amphibolitic gneiss (subunit 1c) typically have shallower negative slopes for LREE and steeper slopes for middle rare-earth elements (MREE) than subunits 1a and b; HREE display a slight positive slope; and some samples display a positive Eu anomaly, which could indicate the presence of cumulate plagioclase (Figure 14e). The consistent positive HREE profile for all three subunits suggests a relatively shallow magmatic source in the mantle, above the stability field of garnet (Hanson, 1980). All mafic samples (subunits 1a, c) lie within the MORB field on the TiO_2/Yb–Nb/Yb diagram of Pearce (2008), which supports magma generation at shallow levels in the mantle (Figure 13d). The felsic amphibolitic gneiss (subunit 1b) is compositionally similar to FII felsic rocks, which are interpreted to form in Archean rift environments from the partial melting of hydrated basaltic crust at midcrustal levels (Figure 13e; Hart et al., 2004; Piercey, 2011).

Multi-element diagrams normalized to primitive mantle display negative anomalies of Nb and Ti for all varieties of amphibolitic gneiss, suggesting arc affinity (Figure 14b, d, f). Profiles for the high-Mg amphibolitic gneiss (subunit 1c; Figure 14f) are less enriched in Th than the mafic and felsic varieties of amphibolitic gneiss (subunits 1a, b; Figure 14b, d). This could indicate less interaction with sialic crust, although depletion of Th during partial melting is a possibility. The relatively shallow negative slopes of the profiles for the mafic and high-Mg amphibolitic gneiss (subunits 1a, c) are more typical of tholeiitic basalt than calcalkaline basalt. Although there is minor to moderate overlap between the compositions of the amphibolitic gneiss (unit 1) and Bah Lake assemblage at the top of the Ospwagan group in Figure 13, the relatively flat normalized trace-element profiles for the Bah Lake assemblage are typical for N-MORB to E-MORB compositions (Figure 14g, h; Zwanzig, 2005).

The cordierite-bearing gneiss hosted within the mafic amphibolitic gneiss (subunit 1a) yields an Mg# of 68, similar to values for the high-Mg amphibolitic gneiss (subunit 1c); however, the elevated concentrations of MgO could result from premetamorphic chlorite alteration. The Cr content of the cordierite-bearing rock (60 ppm) is more similar to that of the mafic amphibolitic gneiss (subunit 1a) that hosts it, and Cr is generally considered to be immobile in hydrothermal systems. The normalized REE and multi-element profiles of the cordierite-bearing gneiss are also most similar to those of the mafic gneiss, with an arc-type trace-element signature and a relatively shallow, negative REE profile (Figure 14a, b). Because of the difference in normalized REE profiles of subunits 1a and c, and the difference in Cr content, the two subunits can be distinguished by plotting $[Ce/Yb]_N$ vs. Cr (Figure 13f). On this diagram, the cordierite-bearing rock shows a greater resemblance to the mafic amphibolitic gneiss (subunit 1a; Figure 13f).

The cordierite-bearing gneiss is enriched in both Mg (Mg# = 68) and Al (ASI = 2.9), which can be indicative of a metamorphosed hydrothermal alteration. Alteration indices were calculated for the amphibolitic gneiss using the NORMAT approach of Piché and Jébrak (2004). The technique uses a normative mineral approach to calculate the overall intensity of alteration (IFRAIS), as well as specific normative-mineral alteration indices for paragonite (IPARA), sericite (ISER), chlorite (ICHLO) and pyrophyllite (IPYRO). The majority of mafic gneiss and high-Mg gneiss (subunits 1a, c) yielded IFRAIS values close to 100, indicating a fresh, unaltered protolith (Table 1). In contrast, the cordierite-bearing rock yielded an IFRAIS value of 8, suggesting an intensely altered protolith. Alteration appears to have been dominantly chloritic (ICHLO = 45), accompanied by lesser paragonitic and sericitic alteration (IPARA = 28, ISER = 19). This style of alteration could indicate relatively shallow-level (volcanic to subvolcanic) hydrothermal activity. The NORMAT calculations also point toward weak to moderate alteration of the felsic amphibolitic gneiss (subunit 1b; Table 1), dominated by paragonitic alteration.

Melasyenite (unit 10)

Because of a lack of exposure, only one sample of fresh, nonmetasomatized melasyenite (unit 10) was collected and analyzed for lithogeochemistry; however, data for two samples of brick-red, metasomatized syenite, collected by J.J. Macek in 2003, show little variation from the nonmetasomatized sample. The melasyenite is characterized by an unusual chemical composition. Samples are intermediate based on SiO_2 content (59–61 wt. %), yet are enriched in K_2O (7–8 wt. %; K_2O/Na_2O = 4.2–5.2) and relatively primitive in terms of MgO (6–8 wt. %; Mg# 55–56). The composition meets the chemical criteria of ultrapotassic rocks as defined by Foley et al. (1987; K_2O/Na_2O >2; K_2O >3 wt. %; MgO >3 wt. %). The fresh melasyenite plots as weakly peralkaline on the alumina saturation–index diagram, while metasomatized syenite plots as weakly metaluminous (Figure 15a). Samples of a similar syenite intrusion from nearby Max Lake also plot as weakly metaluminous (Zwanzig, unpublished data, 2004). The syenite plots within the group I field of ultrapotassic rocks in the major-element diagrams of Foley et al. (1987; Figure 15b–d) and is most similar to group I rocks from orogenic zones. Normalized multi-element profiles are also similar to group I ultrapotassic rocks of Foley et al. (1987; Figure 15e), which are members of the lamproite clan. Although the melasyenite cannot be classified as a lamproite, the similar geochemical characteristics may point toward an analogous magmatic source.

Chondrite-normalized REE profiles for the melasyenite have steep negative slopes (Figure 16a), and primitive mantle–normalized multi-element profiles display enrichments in LILE and relative depletions in HFSE, suggestive of subduction zone–related processes (Figure 16b). Although enriched in LILE and LREE (211–220 ppm Rb, 1220–1479 ppm Sr, 4558–5370 ppm Ba, $[Ce/Yb]_N$ = 59–66), the melasyenite is also

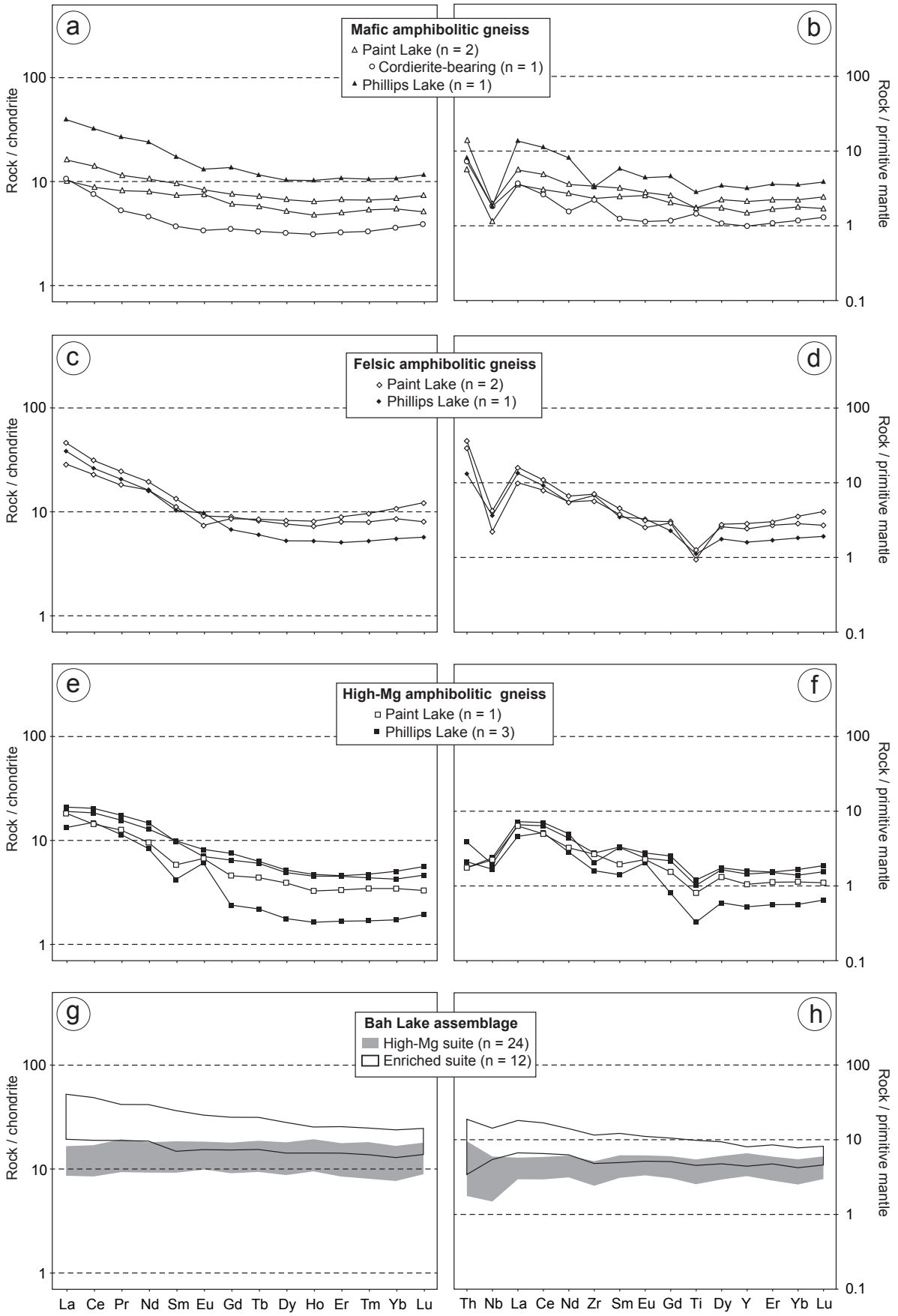

Figure 14: *Chondrite-normalized REE profiles (left column) and primitive mantle–normalized multi-element profiles (right column) for amphibolitic gneiss (unit 1) and the Bah Lake assemblage of the Ospwagan group (n = 36; Zwanzig, 2005). Normalizing values for chondrite are from McDonough and Sun (1995) and normalizing values for primitive mantle are from Sun and McDonough (1989).*

Table 1: Normative mineral alteration indices calculated for samples of amphibolitic gneiss (unit 1) using the NORMAT method of Piché and Jébrak (2004).

Sample	Unit	Map unit	Location	IFRAIS[1]	IPARA[2]	ISER[3]	ICHLO[4]	IPYRO[5]
108-08-093A	Mafic amphibolitic gneiss	1a	Paint Lake	100.00	0.00	0.00	0.00	0.00
108-08-247A	Mafic amphibolitic gneiss	1a	Paint Lake	97.20	2.31	0.49	0.00	0.00
108-12-037C	Mafic amphibolitic gneiss	1a	Phillips Lake	100.00	0.00	0.00	0.00	0.00
108-15-PT01	Cordierite-bearing amphibolitic gneiss	1a	Paint Lake	8.09	27.98	19.23	44.70	0.00
108-08-055	Felsic amphibolitic gneiss	1b	Paint Lake	85.54	13.59	0.87	0.00	0.00
108-08-241B	Felsic amphibolitic gneiss	1b	Paint Lake	72.57	25.17	2.26	0.00	0.00
108-12-037A	Felsic amphibolitic gneiss	1b	Phillips Lake	96.16	3.43	0.41	0.00	0.00
108-13-PT02	High-Mg amphibolitic gneiss	1c	Paint Lake	100.00	0.00	0.00	0.00	0.00
108-12-022A	High-Mg amphibolitic gneiss	1c	Phillips Lake	100.00	0.00	0.00	0.00	0.00
108-12-022B	High-Mg amphibolitic gneiss	1c	Phillips Lake	100.00	0.00	0.00	0.00	0.00
108-12-022C	High-Mg amphibolitic gneiss	1c	Phillips Lake	100.00	0.00	0.00	0.00	0.00

[1] index of alkali-element depletion; lower numbers indicate increase intensity of depletion
[2] index of paragonitization; higher numbers indicate increasing intensity
[3] index of sericitization; higher numbers indicate increasing intensity
[4] index of chloritization; higher numbers indicate increasing intensity
[5] index of pyrophyllitization; higher numbers indicate increasing intensity

enriched in trace elements characteristic of primitive magmas (e.g., 252 ppm Ni, 396 ppm Cr). An initial ε_{Nd} value of –15.0 (at 1.88 Ga; see 'U-Pb geochronology' section) for the fresh melasyenite is similar to the value of –14.4 obtained for the Max Lake syenite and suggests interaction with evolved crustal material or modified lithospheric mantle (Table 2).

Although the chemical characteristics of the melasyenite (unit 10) are similar to sanukitoid rocks (Stern et al., 1989), there are some distinct differences. Sanukitoid suites typically consist of dioritic, monzodioritic and granodioritic rocks (containing essential plagioclase), whereas the melasyenite contains no plagioclase. Enrichment of LREE, Ba and Rb is also considerably higher in the melasyenite than would be considered typical for a sanukitoid ($[Ce/Yb]_N$ = 7–47, ~1000 ppm Ba, Rb/Sr <0.1; Stern et al., 1989). In addition, initial ε_{Nd} values for sanukitoid rocks are invariably juvenile (+1 to +2.5; Stern et al., 1989), in contrast to the strongly negative values of the Paint Lake melasyenite.

Paint sequence (unit 7)

The wacke (subunit 7a) was the most intensively sampled unit of the Paint sequence. Whole-rock geochemical data for the wacke were normalized to the average pelite of the P2 member of the Pipe formation and plotted on multi-element diagrams in order to compare the Paint sequence rocks to other recognized metasedimentary sequences in the TNB, as outlined in Zwanzig et al. (2007). The Paint sequence wacke (subunit 7a) appears to be geochemically distinct from Ospwagan group rocks of similar bulk composition (Figure 17b–d). The wacke is typically less enriched in Rb, Th, Nb, K and Zr than semipelitic to pelitic rocks of the Manasan formation M2 member and Pipe formation P2 member. As well, the wacke is characterized by more pronounced enrichment in Sr and P compared to the M2 and P2 members, as well as wacke and mudstone from the Setting formation. Normalized multi-element patterns for the Paint sequence wacke are fairly similar to patterns exhibited by the Burntwood, Grass River and Sickle groups; however, the Paint sequence rocks show a slightly more fractionated REE pattern (Figure 17e, f). The trace-element content of the Paint sequence wacke also bears a strong resemblance to samples of TNB Archean basement characterized by low La/Yb ratios (Figure 17g; Zwanzig et al., 2007). Similarities in multi-element patterns suggest the Paint sequence wacke could be largely derived from the underlying Archean basement of the TNB, or possibly from arc-related sources, similar to the detritus source for the Burntwood, Grass River and Sickle groups.

Böhm et al. (2007) demonstrated the use of crustal-residence Nd-model ages for distinguishing between the Ospwagan group (T_{CR} = 3.22–2.82 Ga), Archean basement gneiss (T_{CR} = 3.70–3.14 Ga) and more juvenile metasedimentary rocks of the Burntwood, Sickle and Grass River groups (T_{CR} = 2.62–2.02 Ga, Figure 18). Crustal-residence Nd-model ages obtained for the Paint sequence wacke range from 3.57 to 3.23 Ga (Figure 18, Table 3), suggesting older crustal sources for detritus in the Paint sequence than is typical for the Ospwagan group, and differing significantly from the juvenile source for the Burntwood, Grass River and Sickle groups. The Nd-model ages are similar to those for the Archean basement to the TNB, suggesting an Archean age for the sedimentary sequence; however, detrital zircon U-Pb ages suggest a Paleoproterozoic age of deposition (see 'Discussion' and 'Economic considerations' sections). Published Nd-model ages for the Archean basement to the TNB are almost exclusively from samples collected in the northern half of the belt, and are similar to model ages for Hudson Bay terrane of the Superior craton immediately to the east (ca. 4.15–3.09 Ga; Böhm et al., 2000, 2003, unpublished data, 2005; Couëslan, unpublished data, 2014, 2015; Figure 1). This suggests that much of the TNB Archean basement is derived from the adjacent Hudson Bay terrane, and that the Paint sequence could be derived from either or both of these

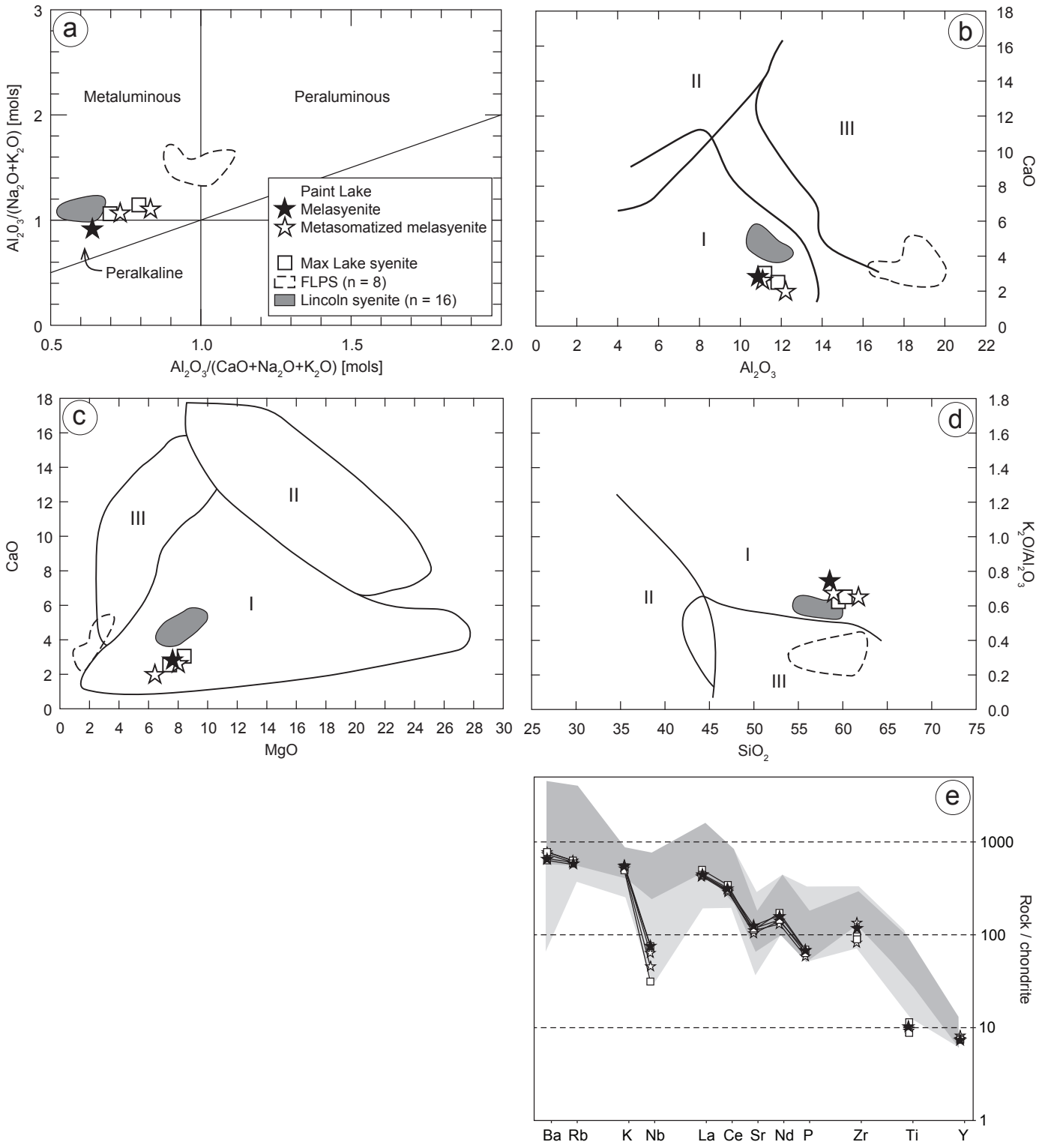

Figure 15: *Geochemical diagrams for the melasyenite (unit 10):* ***a)*** *alumina saturation–index diagram of Maniar and Piccoli (1989);* ***b)*** *Al_2O_3 vs. CaO diagram for ultrapotassic rocks (Foley et al., 1987);* ***c)*** *MgO vs. CaO diagram for ultrapotassic rocks (Foley et al., 1987);* ***d)*** *SiO_2 vs. K_2O/Al_2O_3 diagram for ultrapotassic rocks (Foley et al., 1987);* ***e)*** *chondrite-normalized values for the melasyenite plotted on Figure 8 from Foley et al. (1987), showing the range of compositions for group I ultrapotassic rocks, with the range for standard members indicated by darker shading; chondrite normalizing values are from Thompson (1982). Group I ultrapotassic rocks in (b) to (d) refers to lamproites; group II ultrapotassic rocks are commonly referred to as kamafugites but also include olivine melilitites and some ultrabasic lamprophyres; Group III ultrapotassic rocks are typical of 'Roman province–type' lavas. Abbreviation: FLPS, Footprint Lake plutonic suite.*

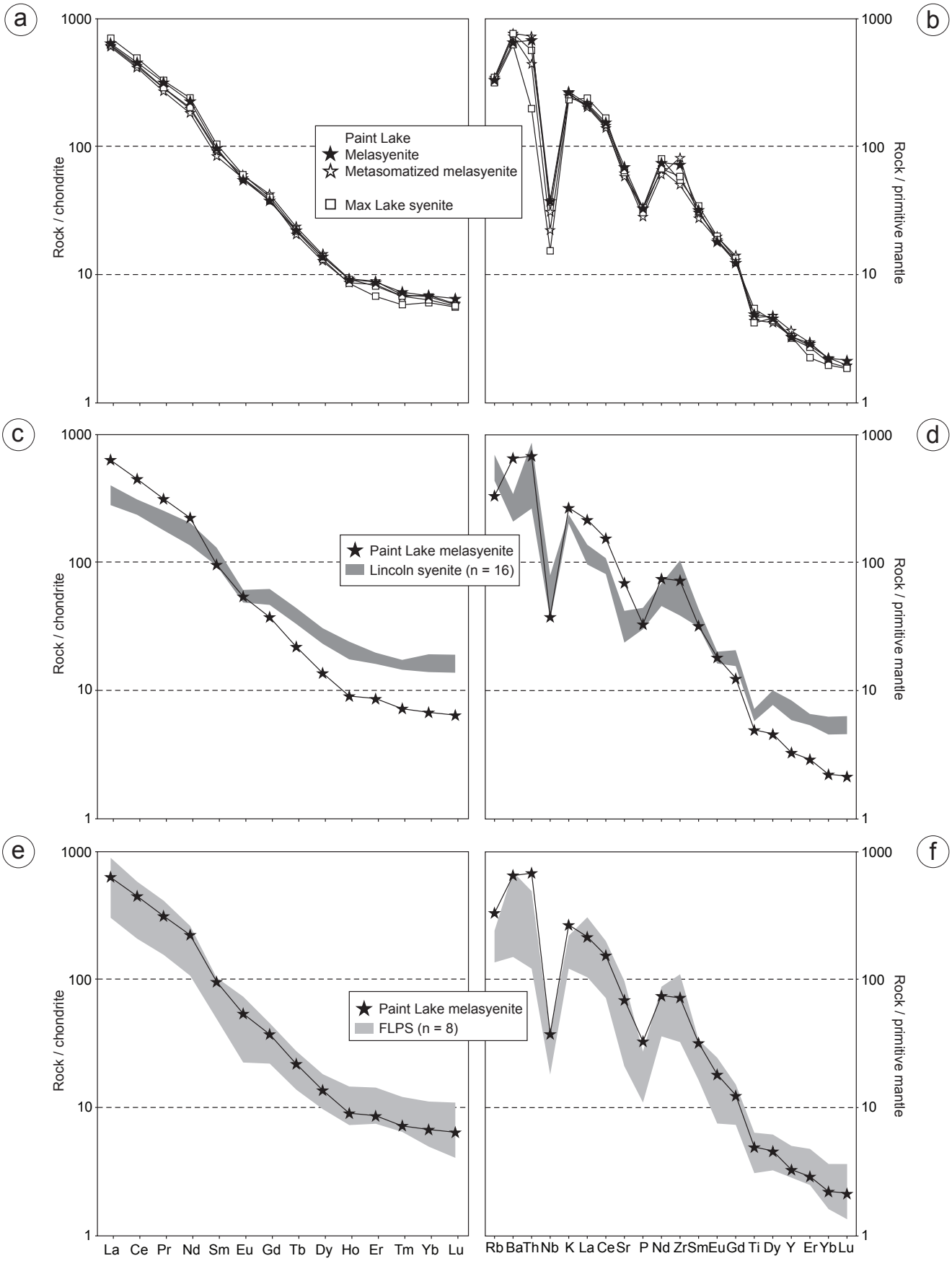

Figure 16: *Chondrite-normalized REE plots (left column) and primitive mantle–normalized multi-element plots (right column) for* ***a)*** *and* ***b)*** *melasyenite (unit 10) in the Paint Lake area;* ***c)*** *and* ***d)*** *the Lincoln syenite (West et al., 2007); and* **e)** *and* **f)** *the Footprint Lake plutonic suite (Whalen et al., 2008). Normalizing values for chondrite are from McDonough and Sun (1995), and normalizing values for primitive mantle are from Sun and McDonough (1989). Abbreviation: FLPS, Footprint Lake plutonic suite.*

Table 2: Sm-Nd isotopic data for the Paint Lake melasyenite and Max Lake syenite.

Sample number	Rock type	Map unit	Sm (ppm)	Nd (ppm)	$^{147}Sm/^{144}Nd$[1]	$^{143}Nd/^{144}Nd$[2]	ε_{Nd}[3] (1.88 Ga)	T_{CR}[4] (Ga)
108-09-350	Melasyenite	10	16.36	119.67	0.083	0.510461(5)	-15.0	3.12
12-03-4198-1[5]	Max Lake syenite		14.11	102.18	0.084	0.510504(6)	-14.4	3.09

[1] estimated error is better than 0.5%
[2] presented relative to $^{143}Nd/^{144}Nd = 0.511850$ for the La Jolla standard; numbers in parentheses are the 2σ uncertainties x10^{-6}
[3] ε_{Nd} values at 1.88 Ga calculated using present-day chondritic ratios of $^{143}Nd/^{144}Nd = 0.512638$ and $^{147}Sm/^{144}Nd = 0.1967$
[4] crustal residence Nd model ages (T_{CR}) calculated according to the linear model of Goldstein et al. (1984)
[5] Zwanzig (unpublished)

sources (Figure 18). Conversely, the North Caribou terrane, with model ages ranging from ca. 3.28 to 2.97 Ga (Anderson, unpublished data, 2013; Beaumont-Smith, unpublished data, 2004; Corkery, unpublished data, 2006; Couëslan, unpublished data, 2013) may be the main source of detritus for the Ospwagan group (Figure 18).

U-Pb geochronology

Several thin sections of Paint sequence wacke were submitted for in situ U-Pb dating of monazite in order to constrain the timing of metamorphism in the Paint Lake area. The findings were published in Couëslan et al. (2013). Zircon was also analyzed, the results of which can be found in DRI2016001 and are used to constrain the timing of both metamorphism and sedimentation of the Paint sequence. In addition, a sample of the melasyenite was submitted for U-Pb dating of zircon to constrain the age of emplacement.

Sampling and analytical methods

All samples for U-Pb dating were collected using a diamond-bladed channel saw. Samples were cut, washed and allowed to dry on the outcrop prior to be being bagged and placed in a plastic sample pail. A 4–5 kg sample of homogeneous, nonmetasomatized melasyenite was submitted to the University of Alberta Radiogenic Isotope Facility (Edmonton, Alberta) for mineral separation, processing and analysis.

The zircon separated from the melasyenite underwent conventional U-Pb dating by isotope dilution–thermal ionization mass spectrometry (ID-TIMS), which generally followed the procedures of Heaman et al. (2002). All analyses were performed on a VG354 mass spectrometer operated in single Faraday or Daly (analogue) collector peak-hopping mode, and were corrected for mass discrimination based on replicate measurement of the MBS981 and U500 standards. All measurements obtained with the Daly photomultiplier detector were adjusted for detector bias. The isotopic composition of common Pb in excess of analytical blank (5 pg of Pb) was calculated using the two-stage model of Stacey and Kramers (1975). The resulting U-Pb isotopic data are listed in Table 4 and plotted in the concordia diagram of Figure 19. All errors reported in the table are quoted at 1σ and were calculated by numerical propagation of all known sources of uncertainty. The concordia diagram was generated using the Isoplot version 3.0 application of Ludwig (2003), with the error ellipses shown at the 2σ level.

Seven polished thin sections of Paint sequence wacke sample 108-08-226 were made at the Manitoba Geological Survey`s Midland Sample and Core Library. Because the primary intent was to date metamorphism, portions of the sample were selected that consisted of neosome or neosome and discrete leucosome. Zircon was located using reflected light microscopy. The thin sections were then shipped to the University of Alberta Radiogenic Isotope Facility (Edmonton, Alberta) for backscattered electron (BSE) and cathodoluminescence (CL) imaging and U-Pb analysis.

Zircon was analyzed in situ using a Nu Plasma multiple collector (MC) ICP-MS coupled to a New Wave Research UP213 Nd:YAG laser-ablation system. Ion-counting detectors were used to measure ^{207}Pb, ^{206}Pb and ^{204}Pb, whereas U was measured on Faraday collectors. Instrument parameters and measurement protocols are outlined in Simonetti et al. (2005, 2006). Corrections for laser-induced element fractionation and instrument drift/bias were achieved by analysis of an external zircon standard (OG1) after the analysis of every 10–12 unknowns. A beam diameter of 30 μm was used for all samples. The U-Pb data can be found in DRI2016001, with all errors reported at 2σ and being a quadratic combination of the standard internal measurement error and external reproducibility of the zircon standard. Concordia diagrams, binned histograms and probability-density distribution curves, and $^{207}Pb/^{206}Pb$ ages were calculated using the Isoplot version 3.0 application of Ludwig (2003), with the error ellipses shown at 2σ. Reflected light photomicrographs were taken after analysis so that ablation pits could be accurately located on CL and BSE images.

Results

Sample 108-09-350, melasyenite (unit 10)

Sample 108-09-350 consists of dark brown to black, nonmetasomatized melasyenite. The sample was collected from the island in the channel between the two southwesternmost bays of Paint Lake. The melasyenite consists of twinned, black K-feldspar and local brownish-green amphibole phenocrysts set in a groundmass of honey-brown K-feldspar and reddish-brown biotite.

The sample yielded colourless to brown-tinted zircon fragments. Four single-crystal fragments, with high Th/U ratios (3.18–9.57) and ranging in weight from 3.3 to 10.9 μg, were selected for analysis. The four zircon fragments yielded one near-concordant (0.6%) analysis with a $^{207}Pb/^{206}Pb$ age of 1854

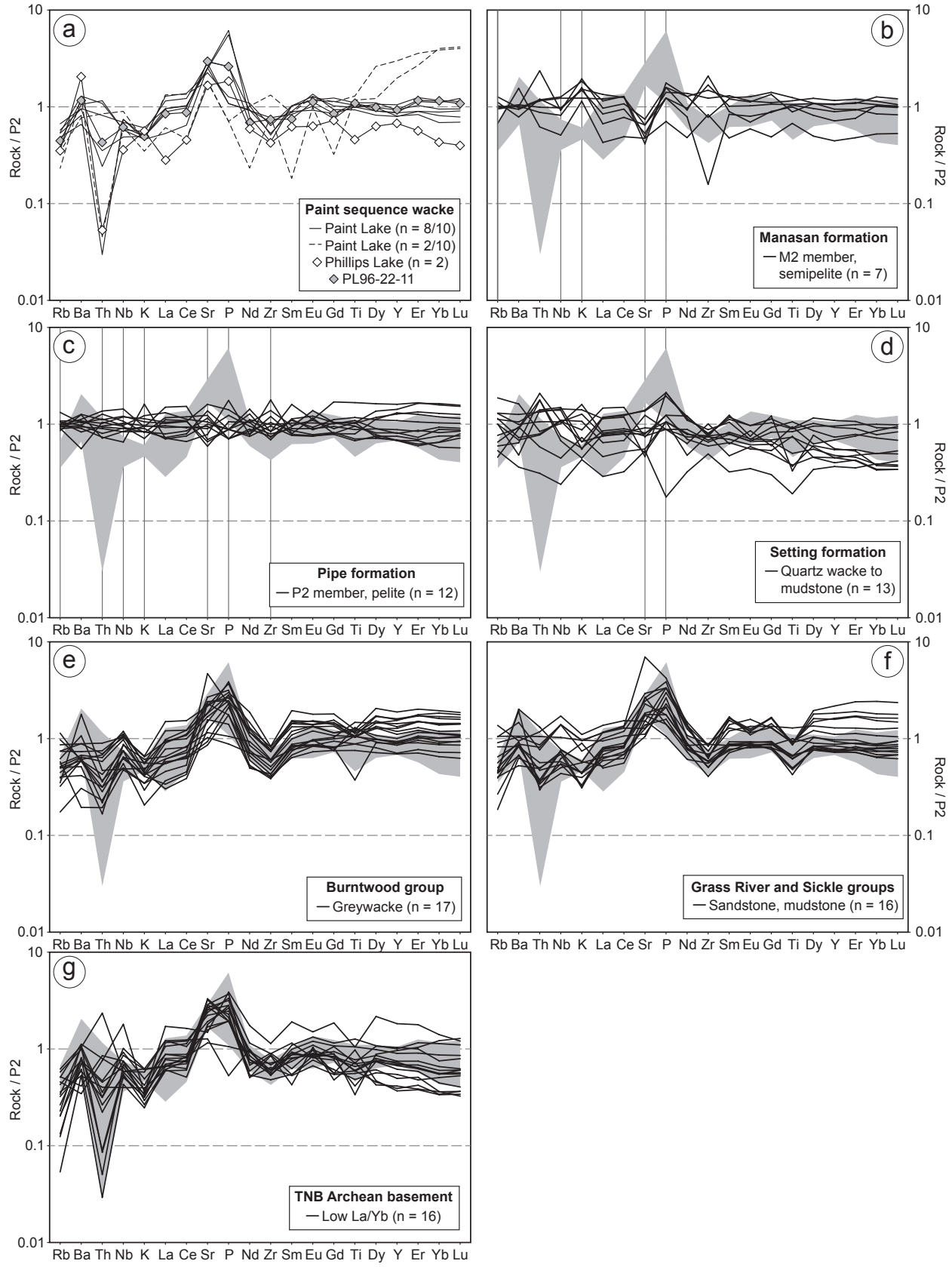

Figure 17: *Multi-element diagrams normalized to average P2 of Zwanzig et al. (2007):* ***a)*** *Paint sequence wacke from Paint and Phillips lakes; Paint Lake profiles with dashed lines are considered to be atypical;* ***b)*** *Manasan formation M2 member;* ***c)*** *Pipe formation P2 member;* ***d)*** *Setting formation quartz wacke to mudstone;* ***e)*** *Burntwood group greywacke;* ***f)*** *Grass River and Sickle groups sandstone and mudstone; and* ***g)*** *TNB Archean basement with low La/Yb ratios. The grey fields in (b) to (g) denote typical Paint sequence wacke. Compositions for TNB Archean basement and rocks of the Ospwagan, Burntwood, Grass River and Sickle groups are from Zwanzig et al. (2007).*

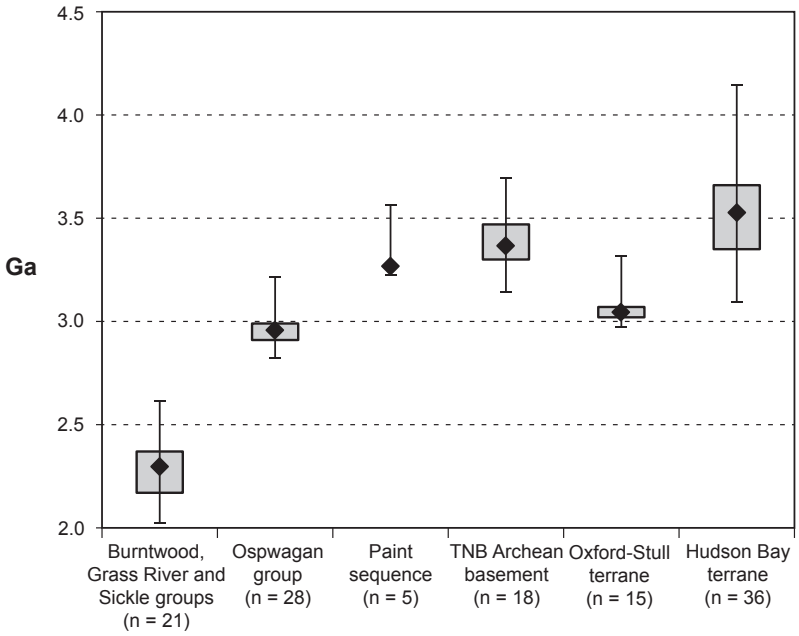

Figure 18: *Crustal-residence Nd-model ages for rocks in the TNB and adjacent Reindeer zone and Superior craton. Black lines indicate the minimum and maximum ages for each population, grey boxes the interquartile range (the middle 50% of the data from the 25th to the 75th percentile) and black diamonds the median ages. Data sources: Grass River, Sickle and Burntwood groups, Böhm et al. (2007), Couëslan (unpublished data, 2013); Ospwagan group and TNB Archean basement, Böhm et al. (2007); Paint sequence, Böhm et al. (2007, samples 38-03-90-1 and 38-03-90-2), this study; Oxford-Stull terrane, Anderson (unpublished data, 2013), Beaumont-Smith (unpublished data, 2004), Corkery (unpublished data, 2006), Couëslan (unpublished data, 2014, 2015); Hudson Bay terrane, Böhm et al. (2000, 2003, unpublished data, 1997), Couëslan (unpublished data, 2013).*

Table 3: Sm-Nd isotopic data for Paint sequence wacke.

Sample number	Rock type	Map unit	Sm (ppm)	Nd (ppm)	$^{147}Sm/^{144}Nd$[1]	$^{143}Nd/^{144}Nd$[2]	2σ abs. uncert.	T_{CR}[3] (Ga)
108-08-226A	wacke	7a	4.017	18.67	0.1301	0.511190	0.000009	3.57
108-09-422	wacke	7a	0.67	5.35	0.0757	0.510216	0.000011	3.23
108-09-453	wacke	7a	2.89	15.22	0.1148	0.511027	0.000007	3.27

[1] estimated error is better than 0.5%
[2] presented relative to $^{143}Nd/^{144}Nd$ = 0.512076 for the La Jolla standard
[3] crustal residence Nd model ages (T_{CR}) calculated according to the linear model of Goldstein et al. (1984)
Abbreviation: abs. uncert., absolute uncertainty

Table 4: U-Pb isotope dilution–thermal ionization mass spectrometry (ID-TIMS) analytical data for igneous zircon from melasyenite sample 108-09-350 (unit 10).

Sample/ fraction	Description[1]	Weight (µg)	U (ppm)	Th (ppm)	Pb (ppm)	Model Th/U	^{204}Pb (pg)	$^{206}Pb/^{204}Pb$	Isotopic ratios[2]			Age[2] (Ma)			Disc. (%)
									$^{206}Pb/^{238}U$	$^{207}Pb/^{235}U$	$^{207}Pb/^{206}Pb$	$^{206}Pb/^{238}U$	$^{207}Pb/^{235}U$	$^{207}Pb/^{206}Pb$	
1z	s col frag	3.3	358	1444	244	4.03	23	1101	0.33182 ±0.00049	5.2450 ±0.0131	0.11464 ±0.00022	1842.7 ±2.4	1860.0 ±2.1	1874.3 ±3.5	1.7
2z	s col frag	9.4	257	816	154	3.18	28	1814	0.33144 ±0.00037	5.1819 ±0.0068	0.11339 ±0.00007	1845.4 ±1.8	1849.6 ±1.0	1854.4 ±1.1	0.6
3z	l col to bwn frag	10.9	249	2378	281	9.57	48	1155	0.32459 ±0.00040	5.1157 ±0.0073	0.11430 ±0.00010	1812.1 ±1.9	1838.7 ±1.2	1868.9 ±1.6	3.5
4z	l col frag Fe st	9.9	417	2218	327	5.33	18	4791	0.33504 ±0.00045	5.3097 ±0.0082	0.11494 ±0.00009	1862.7 ±2.2	1870.4 ±1.3	1879.0 ±1.5	1.0

[1] Analyses of single grain fractions
[2] Isotopic ratios and ages are corrected for fractionation, blank, spike and initial common Pb (Stacy and Kramers, 1975); all uncertainties are reported at 1σ level
Abbreviations: bwn, brown tint; col, colourless; Disc., discordance; Fe st, iron staining; frag, fragment; l, large; s, small

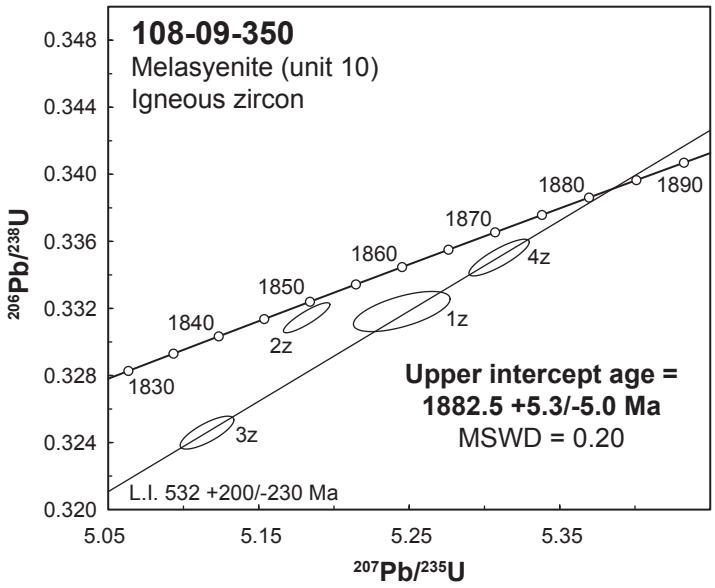

Figure 19: *U-Pb concordia diagram for igneous zircon from melasyenite sample 108-09-350 (unit 10). Abbreviations: L.I., lower intercept; MSWD, mean square of weighted deviates.*

±1.1 Ma (2z; Table 4; Figure 19). The other three fragments yielded slightly discordant analyses with $^{207}Pb/^{206}Pb$ ages of 1874 ±3.5 Ma (1z; 1.7% discordant), 1869 ±1.6 Ma (3z, 3.5% discordant) and 1879 ±1.5 Ma (4z, 1.0% discordant). A linear regression of the three discordant analyses yielded an upper intercept age of 1883 ±5 Ma (Figure 19), which is interpreted as the best estimate of the age of crystallization of the melasyenite.

Sample 108-08-226, Paint sequence wacke (subunit 7a)

Sample 108-09-226 was collected from a small island in central Paint Lake. The outcrop consists of Paint sequence wacke with local interbeds of psammite up to 5 m thick and rare bands of amphibolite up to 15 cm thick. The wacke contains leucosome at all scales, including small in situ segregations (<5 cm), larger pods interpreted to be in source (typically <20 cm) and both concordant and discordant injections. Leucosome interpreted to be in situ and in source is characterized by wispy diffuse contacts with the surrounding wacke (Figure 20a). Thin sections were cut to transect these contacts and include material from both the leucosome and neosome/residuum.

Seven thin sections (108-08-226A–G) contain zircon of variable size and morphology. The majority of grains consist of subequant, rounded detrital cores with equant to prismatic overgrowths. Photomicrographs of analyzed zircon grains were overlain on BSE and CL images to precisely locate ablation pits relative to zoning (Figure 20b, c). One hundred and thirty-seven analyses were made of 56 grains. Of these analyses, 66 are interpreted to have sampled multiple zones—both metamorphic overgrowths and detrital cores—and were rejected on this basis (e.g., Figure 20b, analyses F7A and F7C). A limited dataset of 23 analyses is interpreted to consist solely of detrital cores of zircon grains (e.g., Figure 20b, analysis F7B; Figure 20c, analysis G2C). The $^{207}Pb/^{206}Pb$ ages of these analyses range from 2870 to 2060 Ma and are presented in Table 5. Of these analyses, five were rejected because of significant discordance (>10%), and the three youngest ages were rejected because of higher analytical uncertainty (2σ >40 Ma). The remaining data define two distinct clusters centred at 2436 Ma (n = 5) and 2670–2645 Ma (n = 9), with a single analysis at 2850 Ma (n = 1; Figure 21).

Forty-eight analyses are interpreted to represent metamorphic zircon grains and metamorphic overgrowths on detrital cores (e.g., Figure 20c, analyses G2A and G2B), with one analysis being rejected on the basis of significant discordance (>10%; Table 6, analysis D6B). Three distinct styles of zoning were identified in these grains. The most common is relatively homogeneous to diffusely zoned zircon as discrete grains or overgrowths around detrital cores (Figure 20c). The homogeneous zircon occurs as prismatic to rounded equant grains in the neosome/residuum and leucosome. Grains of the homogeneous zircon are locally elongate parallel to S_2–S_3 and enclosed by S_2–S_3 biotite in the neosome/residuum, and more rarely occur as inclusions in S_2–S_3 biotite of the neosome and as inclusions in subhedral, poikiloblastic orthopyroxene (likely peritectic) of the leucosome. Zircon grains A4, A6 and G9 are prismatic to equant and characterized by concentric, oscillatory growth-zoning around detrital cores. Zircon A4 is an inclusion in a granoblastic plagioclase grain within leucosome, whereas zircon G9 is enclosed by granoblastic plagioclase grains within the leucosome and zircon A6 is associated with schlieric biotite and plagioclase at the leucosome margin. A single sector-zoned grain (zircon G7) is equant and euhedral, and enclosed by granoblastic quartz and plagioclase in leucosome.

A $^{207}Pb/^{206}Pb$ age-probability curve for these analyses displays a prominent peak centred at ca. 1798 Ma, with two smaller 'bumps' toward younger ages (Figure 22a). The prominent peak corresponds to the 38 analyses of homogeneous zircon. This type of zircon yielded slightly discordant analyses (Figure 22b) with a weighted mean $^{207}Pb/^{206}Pb$ age of 1797 ±3 Ma (n = 38),

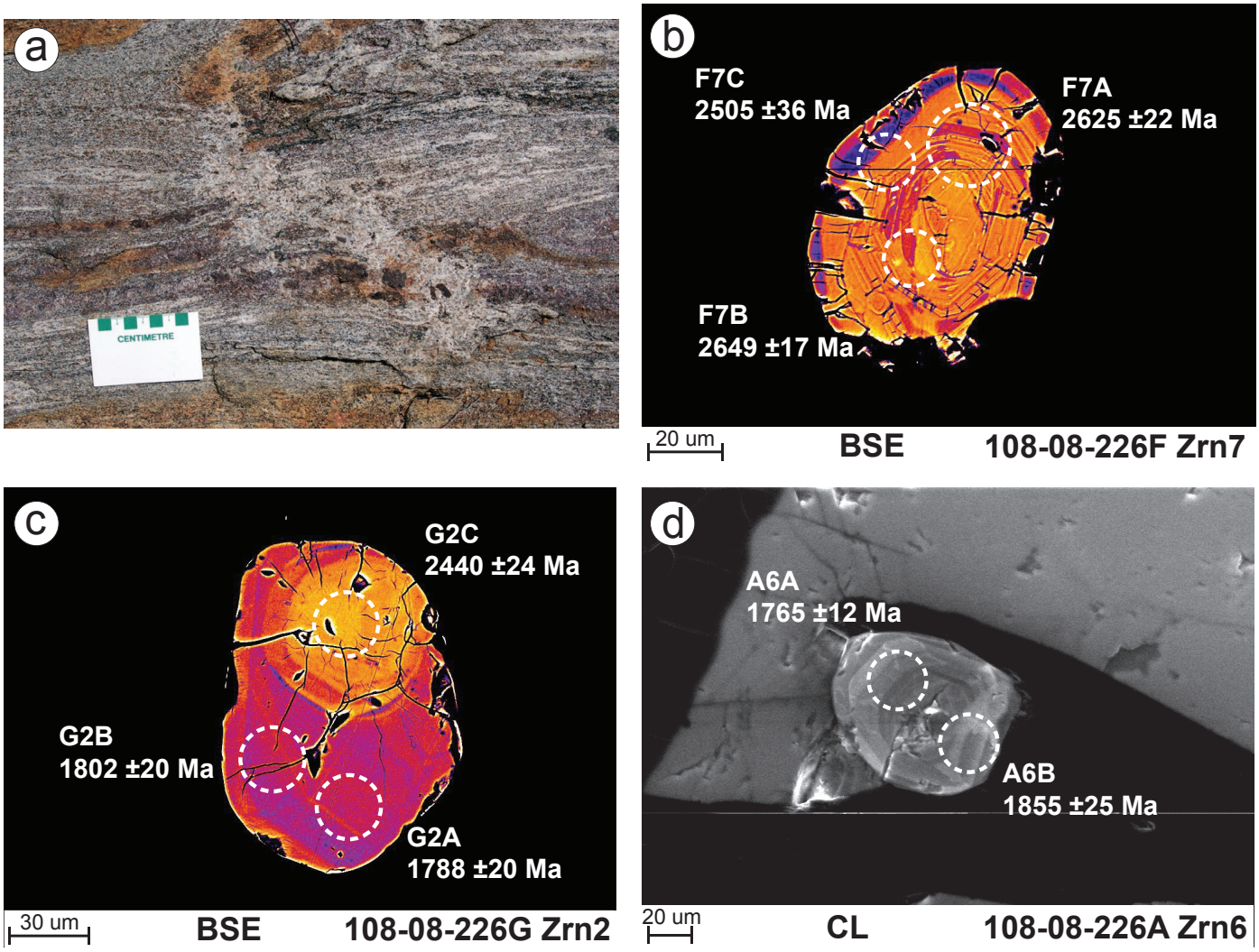

Figure 20: *Outcrop photograph at the sampling site for 108-08-226, showing in-source leucosome with diffuse margins* ***(a)****; false-colour backscattered electron (BSE) images of zircon (Zrn) grains F7* ***(b)*** *and G2* ***(c)****; and grey-scale cathololuminescence (CL) image of zircon A6* ***(d)****, showing the locations of ablation pits and their corresponding* $^{207}Pb/^{206}Pb$ *ages. Uncertainties are reported at 2σ.*

which is considered to be the best estimate of the age of crystallization. A probability plot of the remaining analyses suggests two $^{207}Pb/^{206}Pb$ age peaks: a prominent narrow peak centred at ca. 1765 Ma and a broader peak centred at ca. 1743 Ma, plus a single analysis at ca. 1805 Ma (Figure 23a). The narrow peak corresponds to three concentrically zoned grains (A4, A6, G9), the analyses of which yielded a concordant age of 1766 ±8 Ma (n = 3) with an identical weighted mean $^{207}Pb/^{206}Pb$ age (Figure 23b). A single analysis from concentrically zoned grain G9 (G9B) yielded a $^{207}Pb/^{206}Pb$ age of 1805 ±20 Ma, which is identical within error to the prominent peak of the homogeneous zircon and could indicate a relict age domain corresponding to that period of zircon growth (Hoskin and Black, 2000). An age of ca. 1766 Ma is therefore considered to be the best estimate for the crystallization of concentrically zoned zircon. The younger, broad age peak corresponds to five analyses of a sector-zoned zircon (G7). These analyses yielded a nearly concordant age of 1738 ±10 Ma (Figure 23c) and a weighted mean $^{207}Pb/^{206}Pb$ age of 1739 ±11 Ma (n = 5), which is considered to be the best estimate of the age of crystallization.

Discussion

Melasyenite

Ultrapotassic rocks are believed to be derived from partial melting of metasomatized mantle peridotite (Nelson et al., 1986; Foley et al., 1987; Foley, 1992; Peccerillo, 1992; West et al., 2007). The metasomatism is believed to be generated by upward movement of either volatiles or small melt fractions within the mantle, and results in heterogeneous mantle material enriched in incompatible elements; in the case of ultrapotassic rocks, this is believed to consist largely of phlogopite-enriched peridotite at depths >100 km. Because metasomatic minerals have a lower melting temperature than mantle peridotite, a thermal event will initially cause partial melting of the metasomatic material followed by the surrounding mantle peridotite, resulting in an ultrapotassic magma that is enriched in incompatible elements (e.g., LILE and HFSE) and mantle-compatible elements (e.g., MgO, Cr and Ni). High concentrations of incompatible elements (including Nd and Sm) make the geochemical characteristics of ultrapotassic rocks relatively insensitive to crustal contamination.

Table 5: U-Pb laser-ablation, multicollector, inductively coupled plasma–mass spectrometry (LA-MC-ICP-MS) analytical data for detrital zircon from Paint sequence wacke sample 108-08-226.

Sample/analysis numbers	Description	^{206}Pb (cps)	^{204}Pb (cps)	Isotopic ratios						ρ	Age (Ma)						Disc. (%)
				^{207}Pb/^{206}Pb	± (2σ)	^{207}Pb/^{235}U	± (2σ)	^{206}Pb/^{238}U	± (2σ)		^{207}Pb/^{206}Pb	± (2σ)	^{207}Pb/^{235}U	± (2σ)	^{206}Pb/^{238}U	± (2σ)	
108-08-226A-1	complex core	1230054	182	0.13367	0.00833	7.19164	0.67104	0.39022	0.02709	0.744	2147	105	2135	80	2124	124	1.2
108-08-226B-1	osc core + trunc m annulus	253384	57	0.20295	0.00316	15.81291	0.66518	0.56511	0.02208	0.929	2850	25	2866	39	2888	90	-1.6
108-08-226B-3A	osc core	647821	84	0.18619	0.00272	13.07184	0.92447	0.50918	0.03523	0.978	2709	24	2685	65	2653	149	2.5
108-08-226B-5	osc core + trunc z annulus	1212875	111	0.15949	0.00303	9.46310	0.47206	0.43033	0.01985	0.925	2450	32	2384	45	2307	89	6.9
108-08-226B-8	osc core	893201	94	0.18243	0.00272	13.42613	0.61397	0.53376	0.02308	0.945	2675	24	2710	42	2757	96	-3.8
108-08-226C-1	m core	1740271	143	0.20550	0.00257	18.19892	1.05328	0.64229	0.03629	0.976	2870	20	3000	54	3198	141	-14.5
108-08-226C-1A	osc annulus	1635361	143	0.18182	0.00278	13.75430	0.76725	0.54866	0.02943	0.962	2670	25	2733	51	2820	121	-6.9
108-08-226C-2A	osc core	2079171	88	0.18538	0.00272	15.24771	0.73114	0.59653	0.02723	0.952	2702	24	2831	45	3016	109	-14.6
108-08-226C-3A	dark core	384212	100	0.18382	0.00227	15.49473	0.86655	0.61136	0.03335	0.975	2688	20	2846	52	3075	132	-18.2
108-08-226E-6A	osc core	1732554	42	0.15811	0.00213	9.30579	0.58015	0.42687	0.02598	0.976	2436	23	2369	56	2292	116	7
108-08-226E-11A	osc core	1923213	29	0.18065	0.00279	12.68153	1.00018	0.50914	0.03938	0.981	2659	25	2656	72	2653	166	0.3
108-08-226E-12C	z. core	282613	290	0.13378	0.00315	6.62995	0.42180	0.35943	0.02125	0.929	2148	41	2063	55	1979	100	9.1
108-08-226E-13B	m. core	1543186	90	0.16231	0.00218	10.29044	0.41105	0.45982	0.01730	0.942	2480	23	2461	36	2439	76	2
108-08-226F-6A	osc core + trunc annulus	611331	737	0.17943	0.00199	10.30795	0.42588	0.41665	0.01658	0.963	2648	18	2463	38	2245	75	18
108-08-226F-6B	osc core + trunc annulus	901868	279	0.17793	0.00206	11.75632	0.52256	0.47921	0.02057	0.966	2634	19	2585	41	2524	89	5
108-08-226F-7B	osc core	1886435	271	0.17954	0.00184	11.78843	0.94037	0.47619	0.03767	0.992	2649	17	2588	72	2511	162	6.3
108-08-226F-8B	osc core + trunc m annulus	1538469	257	0.18259	0.00189	13.05377	0.82272	0.51851	0.03224	0.986	2677	17	2684	58	2693	135	-0.7
108-08-226F-10A	osc core	1481680	323	0.17914	0.00177	11.57324	0.72802	0.46855	0.02911	0.988	2645	16	2571	57	2477	127	7.6
108-08-226G-1A	osc core	2101619	64	0.15505	0.00220	9.02813	0.67883	0.42231	0.03118	0.982	2402	24	2341	67	2271	140	6.5
108-08-226G-2C	m core	1848089	51	0.15852	0.00225	9.29790	0.76084	0.42541	0.03428	0.985	2440	24	2368	72	2285	153	7.5
108-08-226G-6B	m core	866903	58	0.12721	0.00567	6.10567	0.69782	0.34810	0.03663	0.921	2060	77	1991	95	1925	173	7.5
108-08-226G-10B	dark core, osc annulus	1010183	194	0.17596	0.00235	11.57051	0.87480	0.47692	0.03549	0.984	2615	22	2570	68	2514	153	4.7
108-08-226G-10C	osc annulus	2577838	207	0.18325	0.00216	11.63686	1.01212	0.46057	0.03969	0.991	2682	19	2576	78	2442	173	10.8

Abbreviations: Disc., discordance; m, massive; osc, oscillatory zoned; trunc, truncated; z, zoned

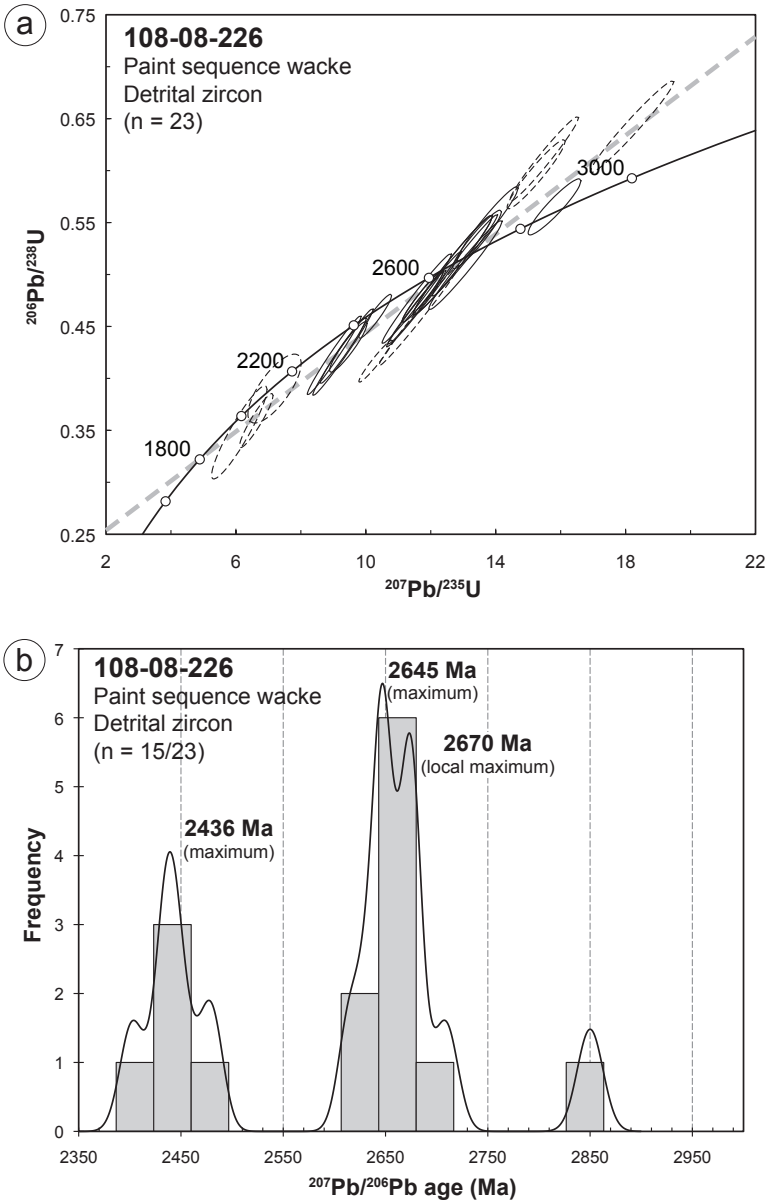

Figure 21: *Results of U-Pb laser-ablation, multicollector, inductively coupled plasma–mass spectrometry (LA-MC-ICP-MS) analyses of detrital zircon from Paint sequence wacke 108-08-226:* ***a)*** *U-Pb concordia diagram with filtered analyses shown as solid ellipses and rejected analyses as dashed ellipses; thick dashed line represents a discordia line projected through 1797 Ma and 2685 Ma (see text for details);* ***b)*** *frequency histogram and probability curve for the filtered dataset of $^{207}Pb/^{206}Pb$ ages. Error ellipses are shown at 2σ.*

The group I ultrapotassic rocks, which are geochemically most similar to the Paint Lake melasyenite, are believed to be derived from harzburgite (depleted mantle peridotite) that has been enriched in phlogopite (Foley et al., 1987; Foley, 1992; Peccerillo, 1992). Low ε_{Nd} values for these rocks suggest either metasomatic events that significantly predate the partial melting event, or involvement of metasomatizing fluids that were isotopically evolved. The arc-like signatures displayed by some group I ultrapotassic rocks can be attributed to several factors: metasomatizing fluids derived from an underlying subducting slab; continued release of fluid or melt from a fossil subduction zone; or involvement of large fragments of subducted oceanic crust and sediments with long residence times (~1 b.y.; Nelson et al., 1986; Foley et al., 1987).

West et al. (2007) described a texturally, mineralogically and geochemically similar syenite from the Appalachian orogen in Maine. The Lincoln syenite is a Late Silurian to Early Devonian intrusion of intermediate composition (55–59 wt. % SiO_2) that is enriched in LILE (Figure 16c, d) as well as compatible elements (Mg# >49, >130 ppm Ni, >400 ppm Cr). The syenite is also characterized by negative ε_{Nd} values ranging from –4.8 to –5.7 (at 418 Ma). The petrogenesis of these rocks calls for partial melting of a mantle wedge, previously metasomatized through subduction processes (West et al., 2007).

There are also many similarities between the Paint Lake melasyenite and the K-feldspar porphyritic Footprint Lake plutonic suite (FLPS) of the northeastern Kisseynew domain

Table 6: U-Pb, laser-ablation, multicollector, inductively coupled plasma–mass spectrometry (LA-MC-ICP-MS) analytical data for metamorphic zircon from Paint sequence wacke sample 108-08-226.

Sample/analysis numbers	Description	^{206}Pb (cps)	^{204}Pb (cps)	Isotopic ratios						ρ	Age (Ma)						Disc. (%)
				^{207}Pb/^{206}Pb	± (2σ)	^{207}Pb/^{235}U	± (2σ)	^{206}Pb/^{238}U	± (2σ)		^{207}Pb/^{206}Pb	± (2σ)	^{207}Pb/^{235}U	± (2σ)	^{206}Pb/^{238}U	± (2σ)	
108-08-226A-4	conc zoning	1116965	132	0.10815	0.00069	4.60232	0.19450	0.30863	0.01289	0.988	1769	12	1750	35	1734	63	2.2
108-08-226A-6	conc zoning	796078	111	0.10797	0.00070	5.01784	0.29170	0.33708	0.01947	0.994	1765	12	1822	48	1873	93	-7
108-08-226B-3	h dark overgrowth	382151	83	0.10991	0.00160	4.92813	0.22390	0.32518	0.01399	0.947	1798	26	1807	38	1815	68	-1.1
108-08-226B-5A	h dark overgrowth	347086	97	0.10977	0.00161	5.15053	0.29163	0.34029	0.01861	0.966	1796	26	1844	47	1888	89	-5.9
108-08-226B-12	diff zoning	576089	104	0.10863	0.00158	5.06169	0.25376	0.33794	0.01621	0.957	1777	26	1830	42	1877	78	-6.5
108-08-226B-12A	diff zoning	609876	113	0.10907	0.00161	4.94084	0.27735	0.32855	0.01779	0.965	1784	27	1809	46	1831	86	-3.1
108-08-226B-13	h grain	309437	96	0.10886	0.00158	4.79941	0.23873	0.31977	0.01522	0.957	1780	26	1785	41	1789	74	-0.5
108-08-226B-13A	h grain	284293	95	0.10894	0.00159	4.82380	0.25927	0.32114	0.01661	0.962	1782	26	1789	44	1795	81	-0.9
108-08-226C-6	h grain	126143	57	0.10990	0.00137	5.10535	0.25948	0.33691	0.01660	0.969	1798	23	1837	42	1872	80	-4.7
108-08-226C-6A	h grain	137335	58	0.10985	0.00139	5.01424	0.23091	0.33105	0.01466	0.962	1797	23	1822	38	1843	71	-3
108-08-226C-6B	h grain	135134	56	0.11074	0.00140	5.06236	0.24715	0.33156	0.01563	0.966	1812	23	1830	41	1846	75	-2.2
108-08-226C-6C	h grain	88639	46	0.10910	0.00144	5.19219	0.29928	0.34516	0.01937	0.974	1784	24	1851	48	1911	92	-8.2
108-08-226C-6D	h grain	114880	51	0.10907	0.00140	5.21210	0.30598	0.34657	0.01986	0.976	1784	23	1855	49	1918	94	-8.7
108-08-226C-7	diff zoning, idio og	76533	76	0.10957	0.00147	4.84251	0.22596	0.32054	0.01432	0.958	1792	24	1792	39	1792	70	0
108-08-226C-7A	diff zoning, idio og	79550	56	0.11037	0.00141	5.08956	0.25757	0.33444	0.01638	0.968	1806	23	1834	42	1860	79	-3.5
108-08-226C-7B	diff zoning, idio og	112311	56	0.11047	0.00138	4.92048	0.26560	0.32304	0.01697	0.973	1807	22	1806	45	1805	82	0.2
108-08-226C-7C	diff zoning, idio og	111368	59	0.10960	0.00145	4.87580	0.23661	0.32265	0.01506	0.962	1793	24	1798	40	1803	73	-0.6
10808226D-4A	h grain	270772	165	0.11039	0.00095	4.98157	0.35099	0.32729	0.02289	0.993	1806	16	1816	58	1825	110	-1.2
10808226D-5A	h grain	450214	192	0.11004	0.00088	5.20277	0.33147	0.34292	0.02167	0.992	1800	15	1853	53	1901	103	-6.5
10808226D-5B	h grain	350110	171	0.10986	0.00088	5.27712	0.26278	0.34837	0.01712	0.987	1797	15	1865	42	1927	81	-8.4
10808226D-6A	h annulus	335416	204	0.10957	0.00095	5.07785	0.31115	0.33611	0.02039	0.990	1792	16	1832	51	1868	98	-4.9
10808226D-6B	dark h core	254911	185	0.11034	0.00098	5.52896	0.28427	0.36341	0.01840	0.985	1805	16	1905	43	1998	86	-12.5
10808226D-6C	h annulus	296902	177	0.10978	0.00087	4.78710	0.28635	0.31626	0.01875	0.991	1796	14	1783	49	1771	91	1.5
10808226D-6D	dark h core	226389	160	0.10988	0.00089	5.26757	0.34667	0.34768	0.02271	0.992	1797	15	1864	55	1924	108	-8.1
10808226D-6E	h annulus	300456	174	0.10965	0.00088	5.05025	0.27602	0.33403	0.01806	0.989	1794	14	1828	45	1858	87	-4.1
10808226D-6F	dark h core	187054	170	0.10979	0.00091	5.04773	0.22830	0.33346	0.01483	0.983	1796	15	1827	38	1855	71	-3.8
10808226D-6G	dark h core	188641	156	0.11008	0.00093	4.84721	0.26196	0.31935	0.01705	0.988	1801	15	1793	44	1787	83	0.9

Abbreviations: conc, concentric; diff, diffuse; Disc., discordance; h, homogeneous; idio, idiomorphic; og, overgrowth

Table 6 (continued): U-Pb, laser-ablation, multicollector, inductively coupled plasma–mass spectrometry (LA-MC-ICP-MS) analytical data for metamorphic zircon from Paint sequence wacke sample 108-08-226.

Sample/analysis numbers	Description	^{206}Pb (cps)	^{204}Pb (cps)	Isotopic ratios						ρ	Age (Ma)						Disc. (%)
				$^{207}Pb/^{206}Pb$	± (2σ)	$^{207}Pb/^{235}U$	± (2σ)	$^{206}Pb/^{238}U$	± (2σ)		$^{207}Pb/^{206}Pb$	± (2σ)	$^{207}Pb/^{235}U$	± (2σ)	$^{206}Pb/^{238}U$	± (2σ)	
10808226E-2A	h grain	525948	87	0.11004	0.00124	5.24635	0.26506	0.34578	0.01703	0.975	1800	20	1860	42	1914	81	-7.3
10808226E-4A	h overgrowth	440952	96	0.11004	0.00125	5.31911	0.30880	0.35058	0.01996	0.981	1800	21	1872	48	1937	95	-8.8
10808226E-4B	h overgrowth	416601	64	0.10968	0.00125	4.75388	0.23704	0.31435	0.01526	0.974	1794	21	1777	41	1762	74	2
10808226E-4E	h overgrowth	470824	81	0.11023	0.00130	5.08180	0.30930	0.33436	0.01996	0.981	1803	21	1833	50	1859	96	-3.6
10808226E-5A	h grain	349867	56	0.10996	0.00126	4.80666	0.29603	0.31703	0.01918	0.982	1799	21	1786	50	1775	93	1.5
10808226E-5B	h grain	356145	60	0.11014	0.00125	5.12153	0.22483	0.33724	0.01430	0.966	1802	21	1840	37	1873	69	-4.6
10808226E-7A	diff zoning	282345	23	0.10978	0.00124	4.87205	0.25373	0.32186	0.01636	0.976	1796	20	1797	43	1799	79	-0.2
10808226E-7C	diff zoning	235317	20	0.10902	0.00129	4.78550	0.40841	0.31837	0.02691	0.990	1783	21	1782	69	1782	130	0.1
10808226F-3A	diff zoning	528678	109	0.11079	0.00109	4.62120	0.25707	0.30251	0.01656	0.984	1812	18	1753	45	1704	81	6.8
10808226F-4A	h overgrowth	565160	181	0.11011	0.00109	4.91423	0.28505	0.32368	0.01850	0.985	1801	18	1805	48	1808	89	-0.4
10808226F-9A	h grain	701286	210	0.11044	0.00110	4.53304	0.26193	0.29769	0.01694	0.985	1807	18	1737	47	1680	84	8
10808226F-9B	h grain	293402	238	0.10993	0.00111	4.39587	0.29633	0.29002	0.01933	0.989	1798	18	1712	54	1642	96	9.9
10808226G-2A	h overgrowth	372134	27	0.10930	0.00124	4.86845	0.40604	0.32305	0.02669	0.991	1788	20	1797	68	1805	129	-1.1
10808226G-2B	h overgrowth	296715	38	0.11015	0.00123	4.80903	0.37322	0.31664	0.02432	0.990	1802	20	1786	63	1773	118	1.8
10808226G-7A	sector zoned	177539	5	0.10676	0.00131	4.62841	0.36104	0.31443	0.02422	0.988	1745	22	1754	63	1762	118	-1.2
10808226G-7B	sector zoned	166395	16	0.10618	0.00153	4.46281	0.31956	0.30484	0.02138	0.980	1735	26	1724	58	1715	105	1.3
10808226G-7C	sector zoned	247507	2	0.10730	0.00135	4.24865	0.43992	0.28717	0.02952	0.993	1754	23	1683	82	1627	146	8.2
10808226G-7D	sector zoned	147049	12	0.10605	0.00153	4.27284	0.34679	0.29221	0.02334	0.984	1733	26	1688	65	1653	115	5.2
10808226G-7E	sector zoned	133150	16	0.10569	0.00142	4.32880	0.35059	0.29707	0.02373	0.986	1726	24	1699	65	1677	117	3.3
10808226G-9A	conc overgrowth	359491	9	0.10756	0.00124	4.36042	0.36967	0.29403	0.02470	0.991	1758	21	1705	68	1662	122	6.2
10808226G-9B	conc overgrowth	703126	149	0.11032	0.00121	4.53825	0.33276	0.29836	0.02163	0.989	1805	20	1738	59	1683	107	7.6

Abbreviations: conc, concentric; diff, diffuse; Disc., discordance; h, homogeneous; idio, idiomorphic; og, overgrowth

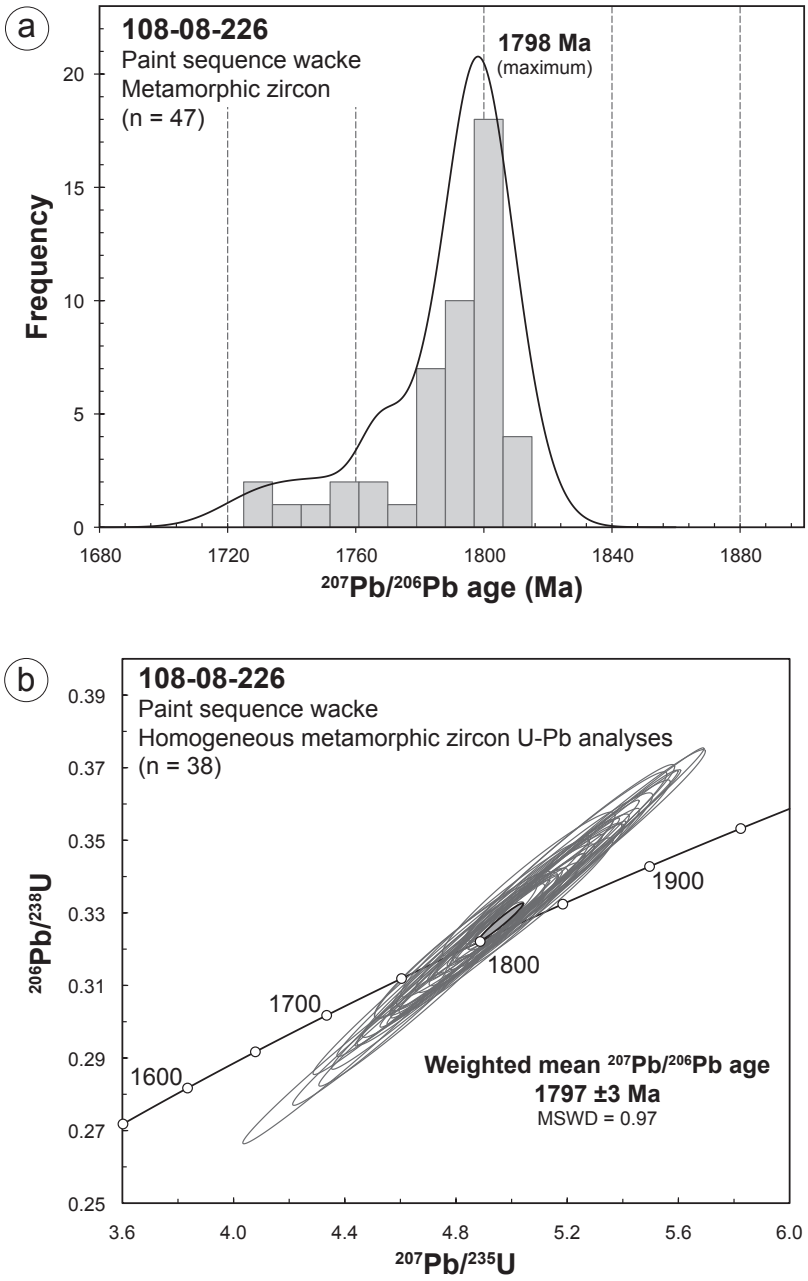

Figure 22: *Results of U-Pb analyses of metamorphic zircon from Paint sequence wacke 108-08-226:* ***a)*** *frequency histogram and probability curve for $^{207}Pb/^{206}Pb$ ages of all metamorphic zircon;* ***b)*** *U-Pb concordia diagram for homogeneous metamorphic zircon; the weighted mean $^{207}Pb/^{206}Pb$ age is considered the best estimate for timing of crystallization. Error ellipses are shown at the 2σ level, with outlined ellipses representing individual analyses and the filled ellipse representing the calculated mean age.*

(Figure 1; Whalen et al., 2008). Rare-earth element and multi-element patterns are very similar (Figure 16e, f), intrusive ages are identical within error (ca. 1879–1882 Ma; Percival et al., 2007) and ε_{Nd} values are strongly negative (from –10.9 to –9.88); however, the intrusions are metaluminous to peraluminous, have Mg# ranging from 20 to 27 and are depleted in Cr and Ni (Whalen et al., 2008; Murphy and Zwanzig, work in progress). The intrusions also commonly contain plagioclase and range in composition from syenite-monzonite to syenogranite-monzogranite. Whalen et al. (2008) interpreted the most mafic end-members of the FLPS to be derived from subcontinental lithospheric mantle that was metasomatized by subduction processes to phlogopite-bearing peridotite. In this model, more felsic end-members of the FLPS are the result of mixing of the mantle-derived melts and crust-derived minimum eutectic melts, with the trace-element signature being completely dominated by the enriched, mafic end-member. However, very low concentrations of Ni and Cr (at or below detection limits) within the mafic end-members of the FLPS argue against them being primary mantle-derived melts. This suggests that even the most mafic end-members of the FLPS have likely undergone some degree of fractionation.

Intrusions of the FLPS are closely associated with culminations of Archean, Superior-like crust in the northeastern Kisseynew domain (Percival et al., 2007; Whalen et al., 2008). Some of the intrusions occur near the domain boundary with

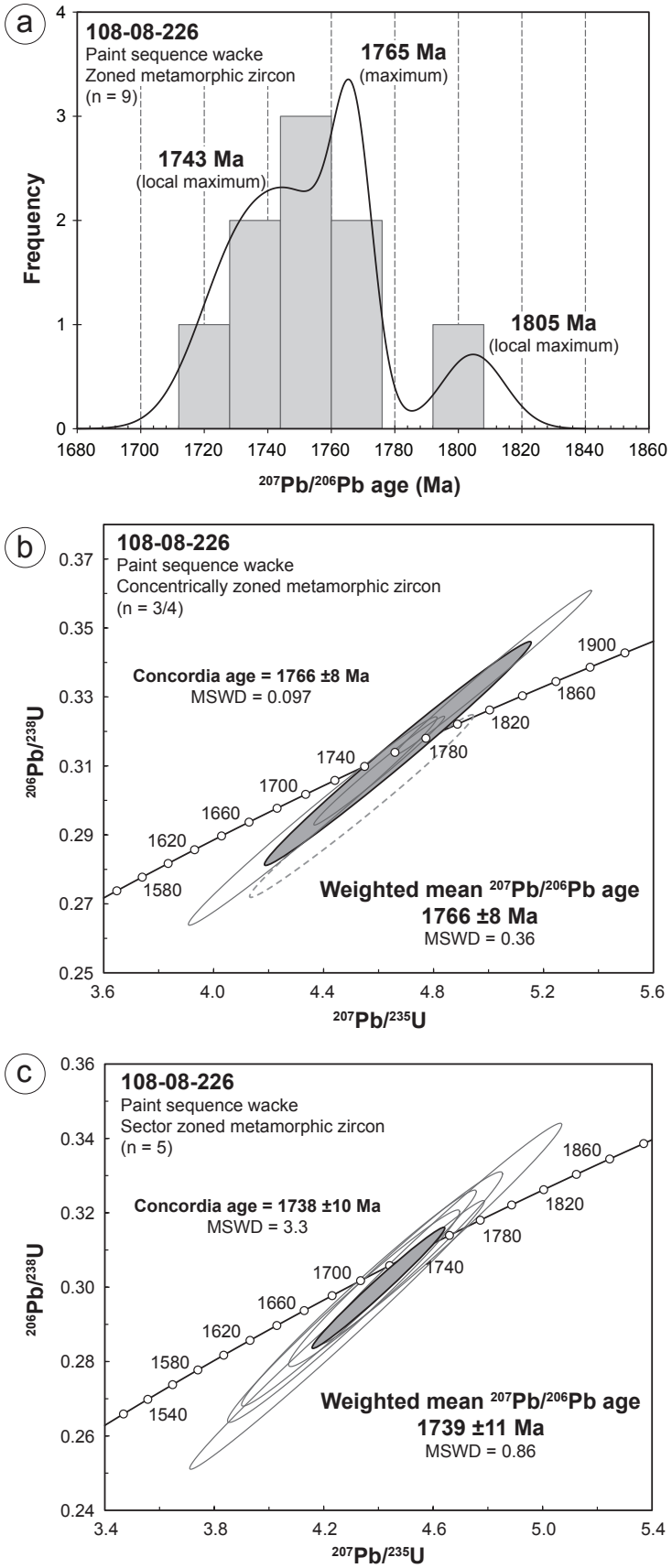

Figure 23: *Results of U-Pb analyses of zoned metamorphic zircon from Paint sequence wacke 108-08-226:* ***a)*** *frequency histogram and probability curve for $^{207}Pb/^{206}Pb$ ages;* ***b)*** *U-Pb concordia diagram for concentrically zoned zircon;* ***c)*** *U-Pb concordia diagram for sector-zoned zircon. Error ellipses are shown at the 2σ level, with outlined ellipses representing individual analyses and filled ellipses representing calculated mean ages. The dashed error ellipse in (b) represents analysis G9B and was not used in the concordia or mean-age calculations (see text for discussion).*

the TNB in the Bison–Tullibee lakes area (Figure 1). Similar ages and trace-element signatures suggest that the syenite intrusions at Paint and Max lakes could be related to the FLPS, and the relatively high concentrations of MgO, Ni, and Cr in these intrusions would make them better analogues for the primary, mantle-derived mafic end-member of the FLPS. This would further suggest that the metasomatized mantle that exists beneath the northeastern Kisseynew domain, and is responsible for the FLPS, may continue beneath the TNB at least as far east as Paint Lake.

The strongly negative ε_{Nd} values of the FLPS are interpreted to be inherited from the mantle source rather than reflecting contamination by continental crust (Whalen et al., 2008). This suggests that the subcontinental lithospheric mantle was metasomatized during a subduction event in the Archean, or that it was metasomatized by melts (or volatiles) derived from Archean-sourced sedimentary rocks that were subducted during the Paleoproterozoic. The Archean crust that underlies much of the TNB appears to be equivalent to the Hudson Bay terrane of the Superior craton (Stott et al., 2010). Current models suggest that the Hudson Bay terrane was the underriding plate in the collision with the North Caribou terrane during assembly of the Superior craton (Percival et al., 2006). This suggests that any Archean subduction event that would have affected the Hudson Bay terrane would have predated the assembly of the Superior craton; however, there is growing evidence that the Pikwitonei granulite domain represents an orogenic zone involving the collision of the accreted complex of the Hudson Bay and North Caribou terranes with an unknown tectonic element located to the northwest (present-day configuration; Couëslan, 2014b). If subduction was directed beneath this accreted complex, it could be responsible for the modification/metasomatism of the underlying subcontinental lithospheric mantle during the Neoarchean.

A series of ca. 1890–1870 Ma felsic plutons along the TNB was suggested by Percival et al. (2005) to indicate an arc along the northwestern Superior margin at ca. 1890 Ma, which could also have led to the metasomatism of the mantle wedge beneath the Superior craton margin. However, for this to be the source of metasomatizing melt/fluid, the subducting slab had to carry with it material (sedimentary rocks) derived from an evolved (Archean) source. This is not the preferred model of the author. If the metasomatizing event was contemporaneous with Paleoproterozoic subduction along the Superior craton margin, one might expect the FLPS and Paint Lake melasyenite to be distributed parallel to the craton margin. However, the distribution of these rocks is oblique to what we currently understand as the Superior craton margin (Figures 1, 2). The preferred interpretation is that the metasomatism was related to an Archean subduction event.

An intrusive age of ca. 1883 Ma for the Paint Lake melasyenite is similar to the age of magmatism associated with the Molson dike swarm (1885–1877 Ma; Heaman et al., 2009) and the age of ultramafic magmatism in the TNB (ca. 1881 Ma; Hulbert et al., 2005; Scoates et al., 2010). An age for the Max Lake syenite of 1867 ±10 Ma (Zwanzig, unpublished data, 2005) is within error of this peak period of magmatism; however, this age is based on a two-point linear regression and therefore of dubious reliability (to further this point, a different combination of two points from the same data set yielded an upper intercept age of 1879 ±22 Ma). In addition, geochemically similar syenite at Partridge Crop Lake is crosscut by amphibolitized dikes, which are interpreted as part of the Molson swarm (Couëslan, 2014a).

Heaman et al. (2009) attributed the ca. 1880 Ma mafic–ultramafic magmatism of the Molson dike swarm to passive asthenospheric upwelling along the thinned margin of the Superior craton, while others have attributed the Molson swarm to either continental back-arc rifting or arc-plume interaction (Percival et al., 2005; Whalen et al., 2008; Corrigan et al., 2009). If the magmas that formed the FLPS and the Paint Lake melasyenite were derived from a source similar to that of group I ultrapotassic rocks, it would suggest that the subcontinental lithospheric mantle had a thickness of at least 100 km. This may be difficult to reconcile with models calling for a thinned continental margin or full-scale, continental back-arc rifting. A model involving mild extension associated with a failed rift could still be appropriate; however, this may be challenged by the distribution of known FLPS intrusions oblique to the trend of the Molson swarm, and presumably the trend of a failed rift.

Deposition of the Paint sequence

The dominant (ca. 2670–2645 Ma) $^{207}Pb/^{206}Pb$ age mode of detrital zircon from the Paint sequence wacke (Figure 24a) is similar to the dominant age mode of detrital zircon from the Ospwagan group (Figure 24b). These sedimentary rocks are believed to be sourced from the adjacent Superior craton, which is characterized by similar metamorphic and igneous ages (cf. Figure 24c). The detrital zircon $^{207}Pb/^{206}Pb$ age mode at ca. 2436 Ma for the Paint sequence wacke is more enigmatic, with the closest known potential source of that age being the Sask craton (Ashton et al., 1999; Rayner et al., 2005); however, similar zircon populations (ca. 2.5–2.3 Ga) have been reported for supracrustal rocks and orthogneiss in the Southern Indian domain of the Trans-Hudson orogen (Rayner and Corrigan, 2004; Kremer, 2009), and a unimodal population of ca. 2.45 Ga detrital zircon was reported for a greywacke from Campbell Lake, roughly 120 km north of Paint Lake, within the internides of the Trans-Hudson orogen, which could represent an eastern extension of the Southern Indian domain (Hartlaub et al., 2005). Circa 2.44 Ga metamorphic monazite has also been reported from southwestern Assean Lake, which could suggest active tectonism along the northwestern Superior craton margin at that time (Böhm et al., 2003).

Perhaps just as important as determining the provenance of the zircons is their actual age: ca. 2436 Ma zircon ages would provide a Paleoproterozoic maximum age of deposition for the wacke. However, this interpretation warrants caution. Even minor (<5%) discordancy in the younger zircon analyses theoretically allows these analyses to fall within error of a discordia array anchored at 1797 Ma, the dominant mode of metamorphic zircon, and projected through Neoarchean ages typical for the Pikwitonei granulite domain (ca. 2685 Ma; Figure 21a). In this manner, the detrital grains could all be Archean but with varying degrees of Pb loss. Arguing against this is the discrete clustering of analyses on the concordia diagram, rather

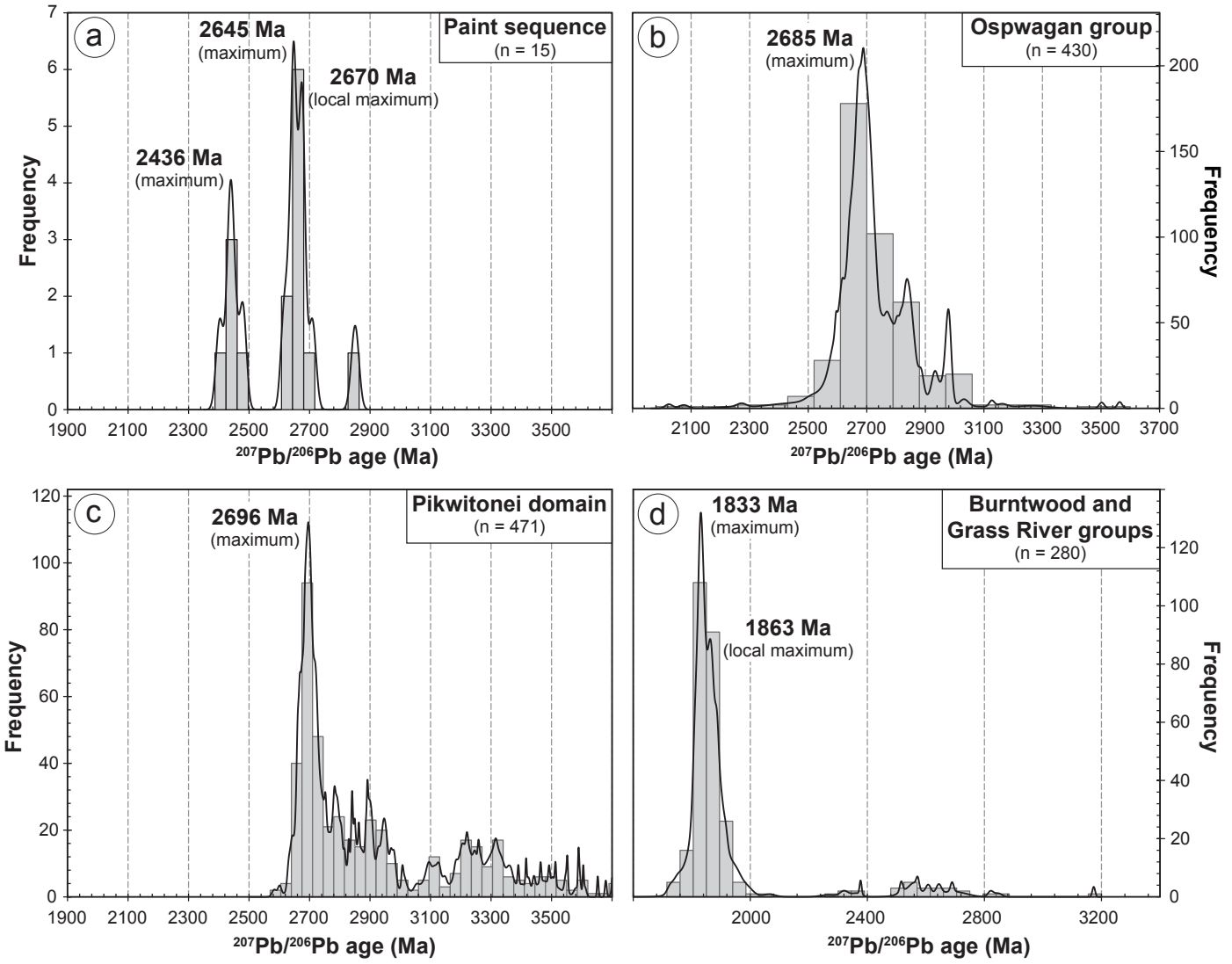

Figure 24: *Frequency histograms and probability curves for $^{207}Pb/^{206}Pb$ ages for zircon:* ***a)*** *detrital zircon from Paint sequence wacke sample 108-08-226;* ***b)*** *detrital zircon composite from Ospwagan group rocks (Rayner et al., 2006; Machado et al., 2011b; Zwanzig, unpublished data, 2008);* ***c)*** *zircon composite from Pikwitonei domain rocks (Böhm et al., 1999; Heaman et al., 2011; Yin et al., 2012; Couëslan, unpublished data, 2013–2015);* ***d)*** *detrital zircon composite from Burntwood group rocks (Percival et al., 2005; Burnham et al., 2009; Couëslan, unpublished data, 2013).*

than a continuous array along a discordia line. Alternatively, the younger zircon ages may result from analyses of multiple age-domains, caused as the laser ablated through an Archean core into a Paleoproterozoic metamorphic growth zone during analysis. If this were the case, however, one would expect a continuous array of ages along the concordia rather than discrete clustering. A Paleoproterozoic age of deposition for the Paint sequence is therefore the favoured interpretation, given this limited dataset of detrital zircon analyses. Deposition likely occurred within the relatively broad time frame of ca. 2440–1880 Ma, as bracketed by the youngest population of robust zircon ages and the intrusion of the Molson dike swarm. The available lithogeochemical, Sm-Nd and U-Pb isotope data suggest that the Paint sequence rocks form a distinct package from the Ospwagan group, with a unique clastic source, and are unlikely to be related as a variation in depositional facies.

Timing of metamorphism for the Paint sequence wacke

Ages calculated for metamorphic zircon have traditionally been assumed to date the peak of metamorphism (e.g., Machado et al., 1991; Rayner et al., 2006; Högdahl et al., 2012); however, a growing body of evidence suggests that this is likely not the case. Metamorphic zircon growth has been attributed to a variety of mechanisms during prograde, peak and retrograde metamorphism. Common metamorphic minerals, such as ilmenite, rutile, garnet and amphibole, are known to contain Zr at the tens to thousands of parts per million level (Fraser et al., 1997; Bingen et al., 2001; Kelsey and Powell, 2011). In extreme cases, both clinopyroxene and amphibole have been documented to contain more than 2000 ppm Zr in association with carbonatitic rocks (Reguir et al., 2012), while oxidized ilmenite from kimberlite has been documented to contain up to 1 wt. % ZrO_2 (Bingen et al., 2001). Metamorphic reaction

involving the breakdown of these minerals could result in the release of Zr and subsequent growth of metamorphic zircon (Fraser et al., 1997; Scoates and Chamberlain, 1997; Bingen et al., 2001; Kelsey and Powell, 2011; Kohn et al., 2015). Dempster et al. (2008) suggested that zircon growth and dissolution under greenschist- to amphibolite-facies conditions is largely controlled by metamorphic-fluid phases. Under this scheme, pre-existing detrital, igneous or metamorphic zircon dissolve into the fluid phase and are later reprecipitated as micro-zircon or new zircon overgrowths as metamorphic/fluid conditions change. Metamorphic reactions involving the liberation of large amounts of fluid, such as chlorite breakdown, could therefore be responsible for significant periods of zircon dissolution and growth.

Anatectic processes have also been suggested to result in zircon growth and dissolution. Melting reactions involving amphibole could potentially liberate Zr, leading to zircon growth (Fraser et al., 1997). Rubatto et al. (2006) suggested that the first appearance of prograde metamorphic zircon in metapelite typically coincides with partial melting, and occurs as overgrowths around inherited cores. These overgrowths could be the result of Ostwald ripening, whereby small differences in interfacial energy between small zircons (large surface area to volume ratio) causes them to dissolve into the melt phase and reprecipitate as overgrowths on large zircons (small surface area to volume ratio; Rubatto et al., 2001; Peck et al., 2010). Thermodynamic models by Kelsey et al. (2008) and Kelsey and Powell (2011) suggest that titanium oxides and silicate melts are likely to have the greatest effects on zircon stability. Titanium oxides are able to incorporate thousands of parts per million Zr at high metamorphic grades and could result in reduced stability of zircon; however, silicate melts are likely to have the largest impact on zircon stability. Models predict the progressive dissolution of zircon along a prograde path under suprasolidus conditions. Precipitation of zircon would then occur along a retrograde path, as the melt cools and crystallizes. The preservation of pre-existing zircon during anatexis suggests either open-system behaviour (melt segregation or escape) or sluggish dissolution kinetics of zircon. The significance of the age results from metamorphic zircon grains from wacke sample 108-08-226A need to be assessed with these considerations in mind.

The presence of homogeneous zircon grains elongated parallel to S_2–S_3 and enclosed by or included in S_2–S_3 biotite suggests that the ca. 1797 Ma zircon grew during D_2–D_3 deformation, prior to or during a period of biotite crystallization. Similar ages of ca. 1792 Ma were obtained for monazite from the same thin sections and a sample of wacke from Phillips Lake (CC-803; Couëslan et al., 2013). The monazite was interpreted as prograde and syn-S_2, and likely predated or was synchronous with orthopyroxene growth. This is in good agreement with the interpretation of the timing of homogeneous zircon growth.

The ca. 1766 Ma, concentrically zoned zircon occurs only as prismatic to equant grains in the leucosome or in schlieric material at the margin of the leucosome. Concentric and oscillatory zoning in zircon indicates crystallization in a dynamic environment influenced by a magma or fluid (Hanchar and Miller, 1993; Roberts and Finger, 1997; Schaltegger et al., 1999; Hoskin and Black, 2000; Corfu et al., 2003; Aleinikoff et al., 2006). The generally prismatic morphology, concentric zoning and close association with the leucosome suggest that the ca. 1766 Ma zircon grew in a magmatic environment as the leucosome attained Zr saturation during cooling and crystallization. Monazite grains dated in the same thin sections and yielding an age of 1748 ±4 Ma are also interpreted to date leucosome crystallization (Couëslan et al., 2013). This apparent discrepancy in age is predicted by the modelling of Kelsey et al. (2008) for typical metapelite under suprasolidus conditions. Zircon is predicted to reach saturation during cooling of a silicate melt at higher temperatures than monazite. As a result, zircon ages are predicted to be older than monazite ages, assuming that cooling and crystallization of the leucosome is not instantaneous.

The ca. 1739 Ma, sector-zoned zircon occurs as a euhedral grain in the leucosome. No distinct textural relationships exist between the sector-zoned zircon and surrounding minerals, making interpretation of the significance of this age difficult. Sector zoning is generally attributed to growth under subsolidus conditions (Schaltegger et al., 1999; Hoskin and Black, 2000; Corfu et al., 2003; Aleinikoff et al., 2006); however, Bingen et al. (2001) attributed sector zoning to magmatic growth. Because this zircon is texturally and chronologically distinct from the oscillatory-zoned zircon, a magmatic/anatectic origin for this grain is considered unlikely. Hoskin and Black (2000) considered weak sector zoning to be characteristic of subsolidus growth and recrystallization. The 1739 ±11 Ma age obtained for the sector-zoned zircon is within error of an $^{40}Ar/^{39}Ar$ hornblende age (1723 ±6 Ma) for a sample collected from the Paint Lake area (Schneider et al., 2007). Based on the relatively young age of this zircon, it is likely that it crystallized, or recrystallized, under retrograde conditions.

Economic considerations

Magmatic nickel

Nickel-sulphide mineralization was discovered in the Thompson nickel belt (TNB) in 1950 and has been continuously mined in the belt since 1961 (Fraser, 1985). Nickel deposits in the TNB are associated with ca. 1880 Ma ultramafic bodies that intruded the Ospwagan group (Bleeker, 1990; Hulbert et al., 2005; Scoates et al., 2010). Sulphide-rich horizons within the Pipe formation of the Ospwagan group acted as sources of sulphur and resulted in sulphur saturation of the ultramafic magmas and precipitation of a sulphide melt. Nickel and copper partitioned into the sulphide melt, leading to a metal-enriched sulphide phase. Because of this association, sulphidic Ospwagan group rocks hosting ultramafic intrusions are the major exploration targets for nickel in the TNB. Similarities between the Ospwagan group and Paint sequence include the presence of siliceous horizons and iron formation, along with local horizons of pelite and calcareous rocks. These similarities allow for easy misidentification of Paint sequence rocks as the more prospective Ospwagan group rocks.

Based on the results of this study, it is important to emphasize that the Paint sequence may also represent a new exploration play in the TNB. Outcrops of Paint sequence wacke

are characterized by variable but ubiquitous gossan staining, suggesting the common presence of sedimentary sulphide. Pyrrhotite-bearing iron formation horizons, although discontinuous, are common. Sedimentary rocks from the Paint sequence could, therefore, have acted as a source of sulphur for intruded ultramafic bodies, similar to Ospwagan group rocks. If the Paint sequence represents a Paleoproterozoic succession, as supported by the current data, it may similarly host ultramafic intrusions. This possibility is supported by the presence of a mineralized body of serpentinized ultramafic rock at Phillips Lake (Assessment File 94497, Manitoba Growth, Enterprise and Trade, Winnipeg), which is roughly 1800 m long and dips steeply west. Four drillholes through this body intersected pyrrhotite-pentlandite mineralization and yielded assays of 1.23% Ni over 1.29 m, 1.19% Ni over 14.3 m, 2.04% Ni over 0.43 m and 1.10% Ni over 8.2 m. Although original core logs describe the ultramafic body as being hosted in mixed Archean gneiss and amphibolite, a re-examination and interpretation of drillcore PL96-22 suggests that it is hosted by the Paint sequence. This is supported by the trace-element geochemistry of wacke (sample PL96-22-11) from this drillhole in comparison to other samples of Paint sequence wacke (Figure 17a), and identification of Paint sequence rocks along the western shoreline of Phillips Lake (Couëslan, 2012). Inco Ltd. diamond-drill cores 15598, 15590 and 16712 from the Phillips Lake area (Assessment Files 92046, 92102, 92122) also contain serpentinized ultramafic rock hosted within the Paint sequence. These examples demonstrate that Paint sequence rocks do host ultramafic bodies, and that some of the bodies are mineralized and may therefore represent a previously unrecognized exploration target for nickel in the TNB.

Volcanogenic massive sulphide

If the amphibolitic gneiss unit does indeed represent metamorphosed and dismembered belts of Archean arc-volcanic rocks, it may have potential to host volcanogenic massive sulphide (VMS) or lode gold deposits, as are found in arc-derived greenstone belts throughout the Superior craton. Normalized REE and multi-element profiles suggest an arc-tholeiite affinity for the amphibolitic gneiss, while the HREE profile suggests relatively shallow-level generation in the mantle, similar to low-Ti tholeiite. These rocks are characteristic of high-heat-flow corridors such as a rifted arc setting, which is a favourable environment for the formation of VMS deposits. The felsic amphibolitic gneiss resembles the FII-type felsic rocks of Hart et al. (2004) that are commonly associated with Archean VMS systems. Possible zones of chlorite alteration (cordierite-bearing rock), comparable to those commonly found in the footwall of VMS deposits, within the amphibolitic gneiss suggest hydrothermal activity prior to high-grade metamorphism and could indicate potential for base-metal mineralization. However, the generally discontinuous nature of the amphibolitic gneiss may not be conducive to the preservation of significant volumes of sulphide mineralization.

Molybdenum

Isolated knots of molybdenite were observed in several outcrops scattered throughout the Paint Lake area. The molybdenite was observed in both the Archean multicomponent gneiss and the Paint sequence wacke and psammite. No discernible alteration is associated with the molybdenite occurrences and the molybdenite was not found to be associated with any discrete structures, such as fractures or quartz veins. Similar occurrences were described by Dawson (1952) in the Wintering Lake area, where minor amounts of molybdenite are present in metasedimentary rocks, and isolated occurrences were described by Charbonneau et al. (1979) in the Paint Lake area.

The origin of the molybdenite is not clear but may relate to variable redox conditions. Under oxidizing conditions, molybdenum is readily soluble in hydrothermal fluids and brines (Seo et al., 2012; Zhang et al., 2012; Hurtig and Williams-Jones, 2014), whereas, under reducing conditions and with increasing sulphur fugacity, molybdenum is quickly deposited as sulphide (MoS_2). It is possible that molybdenum was mobilized in relatively oxidized metamorphic fluids and was deposited as molybdenite when the fluids interacted with more reducing conditions. The Paint sequence wacke contains disseminated pyrrhotite and local graphite, and may have acted as a chemical trap for molybdenum. The isolated nature of the molybdenite occurrences suggests this may have been a relatively local/restricted process.

Rare-earth elements

Post-orogenic–type carbonatite bodies similar to those at Paint Lake are associated with some of the largest rare-earth element (REE) deposits in the world (Chakhmouradian et al., 2009). The carbonatite-associated Maoniuping REE deposit in the Himalayan collisional zone contains a reserve of at least 1.2 million tonnes REE_2O_3 with an average grade of 2.9 wt. % REE_2O_3 (Hou et al., 2009). Although no REE mineralization has yet been identified in association with the carbonatite dikes at Paint Lake, the extensive strike length of the zone of carbonatite diking (at least 23 km; open toward the northeast) suggests that the potential for REE mineralization could be significant.

Pegmatite dikes at Paint Lake locally contain allanite-enriched zones. Radioactive minerals (likely allanite) were also described by Charbonneau et al. (1979) in the Paint Lake area. Two pegmatite dikes containing allanite were found to contain 0.34 and 0.11 wt. % total REE_2O_3. Allanite is not considered a viable ore for REE due to metallurgical difficulties in extracting the REE from the silicate structure; however, future metallurgical advances may one day make it economical.

Acknowledgments

Discussions with S.D. Anderson, C.O. Böhm, A. Camacho, A.R. Chakhmouradian, M.T. Corkery, J.J. Macek, and T. Martins helped to clarify interpretations presented in this report. Inco (now Vale S.A.) and Crowflight Minerals Inc. (now CaNickel Mining Limited) provided access to drillcore and proprietary data. Zircon imaging and analyses were completed by A. Dufrane. B. Coyston, J. Duku, J. Dutka and D. Vessey provided enthusiastic field assistance. E. Anderson and N. Brandson provided logistical support.

References

Aleinikoff, J.N., Schenck, W.S., Plank, M.O., Srogi, L., Fanning, C.M., Kamo, S.L. and Bosbyshell, H. 2006: Deciphering igneous and metamorphic events in high-grade rocks of the Wilmington Complex, Delaware: morphology, cathodoluminescence and backscattered electron zoning, and SHRIMP U-Pb geochronology of zircon and monazite; Geological Society of America Bulletin, v. 118, p. 39–64.

Ansdell, K.M. 2005: Tectonic evolution of the Manitoba–Saskatchewan segment of the Paleoproterozoic Trans-Hudson orogen, Canada; Canadian Journal of Earth Sciences, v. 42, p. 741–759.

Ashton, K.E., Heaman, L.M., Lewry, J.F., Hartlaub, R.P. and Shi, R. 1999: Age and origin of the Jan Lake complex: a glimpse at the buried Archean craton of the Trans-Hudson orogen; Canadian Journal of Earth Sciences, v. 36, no. 2, p. 185–208. doi:10.1139/e98-038

Baragar, W.R.A. and Scoates, R.F.J. 1981: The circum-Superior belt: a Proterozoic plate margin?; Chapter 12 *in* Precambrian Plate Tectonics, A. Kröner (ed.), Developments in Precambrian Geology, v. 4, p. 297–330. doi:10.1016/S0166-2635(08)70017-3

Bell, C.K. 1971: History of the Superior–Churchill boundary in Manitoba; *in* Geoscience Studies in Manitoba, A.C. Turnock (ed.), Geological Association of Canada, Special Paper 9, p. 5–10.

Bingen, B., Austrheim, H. and Whitehorse, M. 2001: Ilmenite as a source for zirconium during high-grade metamorphism: textural evidence from the Caledonides of western Norway and implications for zircon geochronology; Journal of Petrology, v. 42, p. 355–375.

Bleeker, W. 1990: Evolution of the Thompson Nickel Belt and its nickel deposits, Manitoba, Canada; Ph.D. thesis, University of New Brunswick, Fredericton, New Brunswick, 400 p.

Bleeker, W. and Hamilton, M.A. 2001: New SHRIMP U-Pb ages for the Ospwagan Group: implications for the SE margin of the Trans-Hudson orogen (abstract); Geological Association of Canada–Mineralogical Association of Canada, Joint Annual Meeting, St. John's, Newfoundland, May 27–30, 2001, Program with Abstracts, v. 26, p. 15.

Bleeker, W. and Macek, J. 1996: Evolution of the Thompson Nickel Belt, Manitoba: setting of Ni-Cu deposits in the western part of the Circum Superior Boundary Zone; Geological Association of Canada–Mineralogical Association of Canada, Joint Annual Meeting, Winnipeg, Manitoba, May 27–29, 1996, Field Trip Guidebook A1, 44 p.

Böhm, C.O., Heaman, L.M. and Corkery, M.T. 1999: Archean crustal evolution of the northwestern Superior craton margin: U-Pb zircon results from the Split Lake block; Canadian Journal of Earth Sciences, v. 36, p. 1973–1987.

Böhm, C.O., Heaman, L.M., Creaser, R.A. and Corkery, M.T. 2000: Discovery of pre–3.5 Ga exotic crust at the northwestern Superior province margin, Manitoba; Geology, v. 28, p. 75–78.

Böhm, C.O., Heaman, L.M., Stern, R.A., Corkery, M.T. and Creaser, R.A. 2003: The nature of Assean Lake ancient crust, Manitoba: a combined SHRIMP–ID-TIMS U-Pb geochronology and Sm–Nd isotope study; Precambrian Research, v. 126, p. 55–94.

Böhm, C.O., Zwanzig, H.V. and Creaser, R.A. 2007: Sm-Nd isotopic technique as an exploration tool: delineating the northern extension of the Thompson Nickel Belt, Manitoba, Canada; Economic Geology, v. 102, p. 1217–1231.

Bonnet, A.-L. and Corriveau, L. 2007: Alteration vectors to metamorphosed hydrothermal systems in gneissic terranes; *in* Mineral Deposits of Canada: A Synthesis of Major Deposit-Types, District Metallogeny, the Evolution of Geological Provinces, and Exploration Methods, W.D. Goodfellow (ed.), Geological Association of Canada, Mineral Deposits Division, Special Publication 5, p. 409–432.

Bowerman, M.S., Böhm, C.O., Hartlaub, R.P., Heaman, L.M. and Creaser, R.A. 2004: Preliminary geochemical and isotopic results from the Gull Rapids area of the eastern Split Lake block, northwestern Superior Province, Manitoba (parts of NTS 54D5 and 6); *in* Report of Activities 2004, Manitoba Industry, Economic Development and Mines, Manitoba Geological Survey, p. 156–170.

Burnham, O.M., Halden, N., Layton-Matthews, D., Lesher, C.M., Liwanag, J., Heaman, L., Hulbert, L., Machado, N., Michalak, D., Pacey, M., Peck, D.C., Potrel, A., Theyer, P., Toope, K. and Zwanzig, H. 2009: CAMIRO project 97E-02, Thompson Nickel Belt: final report, March 2002, revised and updated 2003; Manitoba Science, Technology, Energy and Mines, Manitoba Geological Survey, Open File OF2008-11, 434 p. plus appendices and GIS shape files for use with ArcInfo®.

Chakhmouradian, A.R., Couëslan, C.G. and Reguir, E.P. 2009: Evidence for carbonatite magmatism at Paint Lake, Manitoba (parts of NTS 63O8, 63P5, 12); *in* Report of Activities 2009, Manitoba Innovation, Energy and Mines, Manitoba Geological Survey, p. 118–126.

Charbonneau, R. and Sutherland S. 1979a: Paint Lake, south part (parts of 63O/9 and 63P/12); Manitoba Department of Mines, Natural Resources and Environment, Mineral Resources Division, Preliminary Map 1979T-1, scale 1:25 000.

Charbonneau, R. and Sutherland S. 1979b: Paint Lake, south part (parts of 63O/8 and 63P/5); Manitoba Department of Mines, Natural Resources and Environment, Mineral Resources Division, Preliminary Map 1979T-2, scale 1:25 000.

Charbonneau, R., Scoates, R.F.J. and Macek, J.J. 1979: Thompson Nickel Belt Project (parts of 63O/8, 9; 63P/5, 12); *in* Report of Field Activities 1979, Manitoba Department of Mines, Natural Resources and Environment, Mineral Resources Division, p. 20–23.

Corfu, F., Hanchar, J.M., Hoskin, P.W.O. and Kinny, P. 2003: Atlas of zircon textures; *in* Zircon, J.M. Hanchar and P.W.O. Hoskin (ed.), Reviews in Mineralogy and Geochemistry, v. 53, p. 469–500.

Corrigan, D., Pehrsson, S., Wodicka, N. and De Kemp, E. 2009: The Paleoproterozoic Trans-Hudson orogen: a prototype of modern accretionary processes; *in* Ancient Orogens and Modern Analogues, J.B. Murphy, J.D. Keppie and A.J. Hynes (ed.), Geological Society of London, Special Publications, v. 327, p. 457–479.

Couëslan, C.G. 2008a: Preliminary results from geological mapping of the west-central Paint Lake area, Manitoba (parts of NTS 63O8, 9, 63P5, 12); *in* Report of Activities 2008, Manitoba Science, Technology, Energy and Mines, Manitoba Geological Survey, p. 99–108.

Couëslan, C.G. 2008b: Geology of the west-central Paint Lake area, Manitoba (parts of NTS 63O8, 9, 63P5, 12); Manitoba Science, Technology, Energy and Mines, Manitoba Geological Survey, Preliminary Map PMAP2008-4, scale 1:20 000.

Couëslan, C.G. 2009a: Progress report of geological mapping at Paint Lake, Manitoba (parts of NTS 63O8, 9, 63P5, 12); *in* Report of Activities 2009, Manitoba Innovation, Energy and Mines, Manitoba Geological Survey, p. 108–117.

Couëslan, C.G. 2009b: Bedrock geology of the Paint Lake area, Manitoba (parts of NTS 63O8, 9, 63P5, 12); Manitoba Innovation, Energy and Mines, Manitoba Geological Survey, Preliminary Map PMAP2009-3, scale 1:20 000.

Couëslan, C.G. 2011: Geological investigations in the Manasan Falls area, Thompson Nickel Belt, Manitoba (parts of NTS 63P12); *in* Report of Activities 2011, Manitoba Innovation, Energy and Mines, Manitoba Geological Survey, p. 86–93.

Couëslan, C.G. 2012: The Grass River Project: geological mapping at Phillips Lake, and new geochronological results from Paint Lake and Manasan Falls, Thompson Nickel Belt, central Manitoba (parts of NTS 63O1, 8, 9, 63P5, 12); *in* Report of Activities 2012, Manitoba Innovation, Energy and Mines, Manitoba Geological Survey, p. 68–78.

Couëslan, C.G. 2013: Preliminary results from bedrock mapping in the Partridge Crop Lake area, eastern margin of the Thompson Nickel Belt, central Manitoba (parts of NTS 63P11, 12); *in* Report of Activities 2013, Manitoba Mineral Resources, Manitoba Geological Survey, p. 34–45.

Couëslan, C.G. 2014a: Preliminary results from bedrock mapping in the Partridge Crop Lake area, eastern margin of the Thompson Nickel Belt, central Manitoba (parts of NTS 63P11, 12) – year two; *in* Report of Activities 2014, Manitoba Mineral Resources, Manitoba Geological Survey, p. 18–31.

Couëslan, C.G. 2014b: Mapping progress in the Pikwitonei granulite domain: tectonic and economic implications; Manitoba Mineral Resources, Manitoba Geological Survey, Manitoba Mining and Minerals Convention 2014, Winnipeg, Manitoba, November 19–21, 2014, oral presentation <http://www.youtube.com/embed/1M-9_jHzjKs>.

Couëslan, C.G. and Martins, T. 2010: Completion of geological mapping at Paint Lake, central Manitoba (parts of NTS 63P5, 12); *in* Report of Activities 2010, Manitoba Innovation, Energy and Mines, Manitoba Geological Survey, p. 129–134.

Couëslan, C.G. and Pattison, D.R.M. 2012: Low-pressure regional amphibolite-facies to granulite-facies metamorphism of the Paleoproterozoic Thompson Nickel Belt, Manitoba; Canadian Journal of Earth Sciences, v. 49, p. 1117–1153.

Couëslan, C.G., Böhm, C.O. and Martins, T. 2012: Preliminary results from geological mapping in the central Sipiwesk Lake area, Pikwitonei granulite domain, central Manitoba (part of NTS 63P4); *in* Report of Activities 2012, Manitoba Innovation, Energy and Mines, Manitoba Geological Survey, p. 79–89.

Couëslan, C.G., Pattison, D.R.M. and Dufrane, S.A. 2013: Paleoproterozoic metamorphic and deformation history of the Thompson Nickel Belt, Superior Boundary Zone, Canada, from in situ U-Pb analysis of monazite; Precambrian Research, v. 237, p. 13–35.

Dawson, A.S. 1952: Geology of the Partridge Crop Lake area, Cross Lake Mining Division, Manitoba; Manitoba Department of Mines and Natural Resources, Mines Branch, Publication 41-1, 26 p. plus 1 map at 1:126 720 scale.

Dempster, T.J., Hay, D.C., Gordon, S.H. and Kelly, N.M. 2008: Microzircon: origin and evolution during metamorphism; Journal of Metamorphic Geology, v. 26, p. 499–507.

Drüppel, K., Elsäßer, L., Sönke, B. and Gerdes, A. 2013: Sveconorwegian mid-crustal ultrahigh-temperature metamorphism in Rogland, Norway: U-Pb LA-ICP-MS geochronology and pseudosections of sapphirine granulites and associated paragenesis; Journal of Petrology, v. 54, p. 305–350.

Feuten, F., Robin, P.-Y. F. and Pickering, M.E. 1986: Deformation in the Thompson Nickel Belt, central Manitoba: a progress report; *in* Current Research, Part B, Geological Survey of Canada, Paper 86-1B, p. 797–809.

Feuten, F. and Robin, P.-Y. F. 1989: Structural petrology along a transect across the Thompson Belt, Manitoba: dip slip at the western Churchill–Superior boundary; Canadian Journal of Earth Sciences, v. 26, p. 1976–1989.

Foley, S.F. 1992: Petrological characterization of the source components of potassic magmas: geochemical and experimental constraints; Lithos, v. 28, p. 187–204.

Foley, S.F., Venturelli, G., Green, D.H. and Toscani, L. 1987: The ultrapotassic rocks: characteristics, classification, and constraints for petrogenic models; Earth-Science Reviews, v. 24, p. 81–134.

Fraser, G., Ellis, D. and Eggins, S. 1997: Zirconium abundance in granulite-facies minerals, with implications for zircon geochronology in high-grade rocks; Geology, v. 25, p. 607–610.

Fraser, H.S. 1985: A journey north, the great Thompson nickel discovery; Inco Ltd., Thompson, Manitoba, 388 p.

Gapais, D., Potrel, A., Machado, N. and Hallot, E. 2005: Kinematics of long-lasting Paleoproterozoic transpression within the Thompson Nickel Belt, Manitoba, Canada; Tectonics, v. 24, TC3002. doi:10.1029/2004TC001700

Goddard, J.D. 1966: Geology of the Hambone Lake area (63O/8); Manitoba Department of Mines and Natural Resources, Mines Branch, Publication 63-1, 44 p. plus 1 map at 1: 60 200 scale.

Goldstein, S.L., O'Nions, R.K. and Hamilton, P.J. 1984: Sm-Nd study of atmospheric dusts and particulates from major river systems; Earth and Planetary Science Letters, v. 70, p. 221–236.

Hanchar, J.M. and Miller, C.F. 1993: Zircon zonation patterns as revealed by cathodoluminescence and backscattered electron images: implications for interpretation of complex crustal histories; Chemical Geology, v. 110, p. 1–13.

Hanson, G.N. 1980: Rare-earth elements in petrogenetic studies of igneous systems; Annual Review of Earth and Planetary Science, v. 8, p. 371–406.

Hart, T.R., Gibson, H.L. and Lesher, C.M. 2004: Trace element geochemistry and petrogenesis of felsic volcanic rocks associated with volcanogenic massive Cu-Zn-Pb sulphide deposits; Economic Geology, v. 99, p. 1003–1013.

Hartlaub, R.P., Böhm, C.O., Heaman, L.M. and Simonetti, A. 2005: Northwestern Superior craton margin, Manitoba: an overview of Archean and Proterozoic episodes of crustal growth, erosion and orogenesis (parts of NTS 54D and 64A); *in* Report of Activities 2005, Manitoba Industry, Economic Development and Mines, Manitoba Geological Survey, p. 54–60.

Heaman, L.M., Böhm, C.O., Machado, N., Krogh, T.E., Weber, W. and Corkery, M.T. 2011: The Pikwitonei Granulite Domain, Manitoba: a giant Neoarchean high-grade terrane in the northwest Superior Province; Canadian Journal of Earth Sciences, v. 48, p. 205–245.

Heaman, L.M., Erdmer, E. and Owen, J.V. 2002: U-Pb geochronologic constraints on the crustal evolution of the Long Range Inlier, Newfoundland; Canadian Journal of Earth Sciences, v. 39, p. 845–865.

Heaman, L.M., Machado, N., Krogh, T.E. and Weber, W. 1986: Precise U-Pb zircon ages for the Molson dike swarm and the Fox River sill: constraints for Early Proterozoic crustal evolution in northeastern Manitoba, Canada; Contributions to Mineralogy and Petrology, v. 94, p. 82–89.

Heaman, L.M., Peck, D. and Toope, K. 2009: Timing and geochemistry of 1.88 Ga Molson Igneous Events, Manitoba: insights into the formation of a craton-scale magmatic and metallogenic province; Precambrian Research, v. 172, p. 143–162. doi:10.1016/j.precamres.2009.03.015

Högdahl, K., Majka, J., Sjöström, H., Nilsson, K.P., Claesson, S. and Konečný, P. 2012: Reactive monazite and robust zircon growth in diatexites and leucogranites from a hot, slowly cooled orogen: implications for the Paleoproterozoic tectonic evolution of the central Fennoscandian Shield, Sweden; Contributions to Mineralogy and Petrology, v. 163, p. 167–188.

Hoskin, P.W.O. and Black, L.P. 2000: Metamorphic zircon formation by solid-state recrystallization of protolith igneous zircon; Journal of Metamorphic Geology, v. 18, p. 423–439.

Hou, Z., Tian, S., Xie, Y., Yang, Z., Yuan, Z., Yin, S., Yi, L., Fei, H., Zou, T., Bai, G. and Li, X. 2009: The Himalayan Mianning-Dechang REE belt associated with carbonatite-alkaline complexes, eastern Indo-Asian collision zone, SW China; Ore Geology Reviews, v. 36, p. 65–89.

Hubregtse, J.J.M.W. 1980: The Archean Pikwitonei granulite domain and its position at the margin of the northwestern Superior Province (central Manitoba); Manitoba Energy and Mines, Manitoba Geological Survey, Geological Paper GP80-3, 16 p.

Hulbert, L.J., Hamilton, M.A., Horan, M.F. and Scoates, R.F.J. 2005: U-Pb zircon and Re-Os isotope geochronology of mineralized ultramafic intrusions and associated nickel ores from the Thompson Nickel Belt, Manitoba, Canada; Economic Geology, v. 100, p. 29–41.

Hurtig, N.C. and Williams-Jones, A.E. 2014: An experimental study of the solubility of MoO_3 in aqueous vapour and low to intermediate density supercritical fluids; Geochimica et Cosmochimica Acta, v. 136, p. 169–193.

Jensen, L.S. and Pyke, D.R. 1982: Komatiites in the Ontario portion of the Abitibi belt; *in* Komatiites, N.T. Arndt and E.G. Nisbet (ed.), George Allen & Unwin, London, United Kingdom, p. 147–157.

Kelsey, D.E. and Powell, R. 2011: Progress in linking accessory mineral growth and breakdown to major mineral evolution in metamorphic rocks: a thermodynamic approach in the Na_2O-CaO-K_2O-FeO-MgO-Al_2O_3-SiO_2-H_2O-TiO_2-ZrO_2 system; Journal of Metamorphic Geology, v. 29, p. 151–166.

Kelsey, D.E., Clark, C. and Hand, M. 2008: Thermobarometric modelling of zircon and monazite growth in melt-bearing systems: examples using model metapelitic and metapsammitic granulites; Journal of Metamorphic Geology, v. 26, p. 199–212.

Kohn, M.J., Corrie, S.L. and Markley, C. 2015: The fall and rise of metamorphic zircon; American Mineralogist, v. 100, p. 897–908.

Kremer, P.D., Rayner, N. and Corkery, M.T. 2009: New results from geological mapping in the west-central and northeastern portions of Southern Indian Lake, Manitoba (parts of NTS 64G1, 2, 8, 64H4, 5); *in* Report of Activities 2009, Manitoba Innovation, Energy and Mines, Manitoba Geological Survey, p. 94–107.

Kuiper, Y.D., Lin, S. and Böhm, C.O. 2011: Himalayan-type escape tectonics along the Superior Boundary Zone in Manitoba, Canada; Precambrian Research, v. 187, p. 248–262.

Layton-Matthews, D., Lesher, C.M., Burnham, O.M., Liwanag, J., Halden, N.M., Hulbert, L. and Peck, D.C. 2007: Magmatic Ni–Cu–platinum-group element deposits of the Thompson Nickel Belt; *in* Mineral Deposits of Canada: A Synthesis of Major Deposit-Types, District Metallogeny, the Evolution of Geological Provinces, and Exploration Methods, W.D. Goodfellow (ed.), Geological Association of Canada, Mineral Deposits Division, Special Publication 5, p. 409–432.

Le Maitre, R.W. 2002: Igneous rocks: a classification and glossary of terms, Cambridge University Press, United Kingdom, 236 p.

Ludwig, K.R. 2003: Isoplot 3.00: a geochronological toolkit for Microsoft® Excel®; Berkeley Geochronological Center, Special Publication 4, 71 p.

Macek, J.J. 1985: Geological investigations in the Phillips Lake area (part of 63O/12); *in* Report of Field Activities 1985, Manitoba Energy and Mines, Geological Services, p. 181–182.

Macek, J.J. and Russell, J.K. 1978: Thompson Nickel Belt Project (parts of 63O-8, 9; 63P-5, 12); *in* Report of Field Activities 1978, Manitoba Department of Mines, Resources and Environmental Management, Mineral Resources Division, p. 43–46.

Macek, J.J., Zwanzig, H.V. and Pacey, J.M. 2006: Thompson nickel belt geological compilation map, Manitoba (parts of NTS 63G, J, O, P and 64A and B); Manitoba Science, Technology, Energy and Mines, Manitoba Geological Survey, Open File Report OF2006-33.

Machado, N., Heaman, L.M., Krogh, T.E., Weber, W. and Corkery, M.T. 2011a: Timing of Paleoproterozoic granitoid magmatism along the northwestern Superior Province margin: implications for the tectonic evolution of the Thompson Nickel Belt; Canadian Journal of Earth Sciences, v. 48, p. 325–346.

Machado, N., Gapais, D., Potrel, A., Gauthier, G. and Hallot, E. 2011b: Chronology of transpression, magmatism, and sedimentation in the Thompson Nickel Belt (Manitoba, Canada) and timing of Trans-Hudson Orogen–Superior Province collision; Canadian Journal of Earth Sciences, v. 48, p. 295–324.

Machado, N., Krogh, T.E. and Weber, W. 1990: U-Pb geochronology of basement gneisses in the Thompson Belt (Manitoba): evidence for pre-Kenoran and Pikwitonei-type crust and Early Proterozoic basement reactivation in the western margin of the Archean Superior Province; Canadian Journal of Earth Sciences, v. 27, p. 794–802.

Machado, N., Lindenmayer, Z., Krogh, T.E. and Lindenmayer, D. 1991: U-Pb geochronology of Archean magmatism and basement reactivation in the Carajás area, Amazon shield, Brazil; Precambrian Research, v. 49, p. 329–354.

Maniar, P.D. and Piccoli, P.M. 1989: Tectonic discrimination of granitoids; Geological Society of America Bulletin, v. 101, p. 635–643.

McDonough, W.F. and Sun, S.-s. 1995: The composition of the Earth; Chemical Geology, v. 120, p. 223–253.

Mehnert K.R. 1968: Migmatites and the origin of granitic rocks; Elsevier, Amsterdam, Netherlands, 393 p.

Mezger, K., Bohlen, S.R. and Hanson, G.N. 1990: Metamorphic history of the Archean Pikwitonei granulite domain and the Cross Lake subprovince, Superior Province, Manitoba, Canada; Journal of Petrology, v. 31, p. 483–517.

Nelson, D.R., McCulloch, M.T. and Sun, S.-s. 1986: The origins of ultrapotassic rocks as inferred from Sr, Nd and Pb isotopes; Geochimica et Cosmochimica Acta, v. 50, p. 231–245.

Pearce, J.A. 1996: A user's guide to basalt discrimination diagrams; *in* Trace-Element Geochemistry of Volcanic Rocks: Applications for Massive Sulphide Exploration, D.A. Wyman (ed.), Geological Association of Canada, Short Course Notes, v. 12, p. 79–113.

Pearce, J.A. 2008: Geochemical fingerprinting of oceanic basalts with applications to ophiolite classification and the search for Archean oceanic crust; Lithos, v. 100, p. 14–48.

Peccerillo, A. 1992: Potassic and ultrapotassic rocks: compositional characteristics, petrogenesis, and geological significance; Episodes, v. 15, p. 243–251.

Peck, W.H. and Smith, M.S. 2005: Cordierite-gedrite rocks from the central metasedimentary belt boundary thrust zone (Grenville Province, Ontario): Mesoproterozoic metavolcanic rocks with affinities to the composite arc belt; Canadian Journal of Earth Sciences, v. 42, p. 1815–1828.

Peck, W.H., Bickford, M.E., McLelland, J.M., Nagle, A.N. and Swarr, G.J. 2010: Mechanism of metamorphic zircon growth in a granulite-facies quartzite, Adirondack Highlands, Grenville Province, New York; American Mineralogist, v. 95, p. 1796–1806.

Percival, J.A., Rayner, N., Growdon, M.L., Whalen, J.B. and Zwanzig, H.V. 2007: New field and geochronological results for the Osik–Atik–Footprint lakes area, Manitoba (NTS 63O13, 14, 15, 64B2, 3); *in* Report of Activities 2007, Manitoba Science, Technology, Energy and Mines, Manitoba Geological Survey, p. 71–81.

Percival, J.A., Sanborn-Barrie, M., Skulski, T., Stott, G.M., Helmstaedt, H. and White, D.J. 2006: Tectonic evolution of the western Superior Province from NATMAP and LITHOPROBE studies; Canadian Journal of Earth Sciences, v. 43, p. 1085–1117.

Percival, J.A., Whalen, J.B. and Rayner, N. 2004: Pikwitonei–Snow Lake, Manitoba transect (parts of NTS 63J, 63O and 63P), Trans-Hudson orogen–Superior Margin Metallotect Project: initial geological, isotopic and SHRIMP U-Pb results; *in* Report of Activities 2004, Manitoba Industry, Economic Development and Mines, Manitoba Geological Survey, p. 120–134.

Percival, J.A., Whalen, J.B. and Rayner, N. 2005: Pikwitonei–Snow Lake Manitoba transect (parts of NTS 63J, 63O and 63P), Trans-Hudson orogen–Superior Margin Metallotect Project: new results and tectonic interpretation; *in* Report of Activities 2005, Manitoba Industry, Economic Development and Mines, Manitoba Geological Survey, p. 69–91.

Piché, M. and Jébrak, M. 2004: Normative minerals and alteration indices developed for mineral exploration; Journal of Geochemical Exploration, v. 82, p. 59–77.

Piercey, S.J. 2011: The setting, style, and role of magmatism in the formation of volcanogenic massive sulphide deposits; Mineralium Deposita, v. 46, p. 449–471.

Rayner, N. and Corrigan, D. 2004: Uranium-lead geochronological results from the Churchill River–Southern Indian Lake transect, northern Manitoba; Geological Survey of Canada, Current Research 2004-F1, 14 p.

Rayner, N., Stern, R.A. and Bickford M.E. 2005: Tectonic implications of new SHRIMP and TIMS U-Pb geochronology of rocks from the Sask Craton, Peter Lake Domain and Hearne margin, Trans-Hudson Orogen, Saskatchewan; Canadian Journal of Earth Sciences, v. 42, p. 635–657.

Rayner, N., Zwanzig, H.V. and Percival, J.A. 2006: Analytical data for sample 7798, Pipe Formation, Pipe II pit and sample 8422, Pipe Formation, Thompson mine, 2500-foot level; Manitoba Science, Technology, Energy and Mines, Manitoba Geological Survey, Data Repository Item DRI2006004, Microsoft® Excel® file.

Reguir, E.P., Chakhmouradian, A.R., Pisiak, L., Halden, N.M., Yang, P., Xu, C., Kynický, J. and Couëslan, C.G. 2012: Trace-element composition and zoning in clinopyroxene- and amphibole-group minerals: implications for element partitioning and evolution of carbonatites; Lithos, v. 128–131, p. 27–45.

Roberts, M.D., Oliver, N.H.S., Fairclough, M.C., Hölttä, P.S. and Lahtinen, R. 2003: Geochemical and oxygen isotope signature of sea-floor alteration associated with polydeformed and highly metamorphosed massive sulphide deposit, Ruostesuo, central Finland; Economic Geology, v. 98, p. 535–556.

Roberts, M.P. and Finger, F. 1997: Do U-Pb zircon ages from granulites reflect peak metamorphic conditions?; Geology, v. 25, p. 319–322.

Rubatto, D., Hermann, J. and Buick, I.S. 2006: Temperature and bulk composition control on the growth of monazite and zircon during low-pressure anatexis (Mount Stafford, central Australia); Journal of Petrology, v. 47, p. 1973–1996.

Rubatto, D., Williams, I.S. and Buick, I.S. 2001: Zircon and monazite response to prograde metamorphism in the Reynolds Range, central Australia; Contributions to Mineralogy and Petrology, v. 140, p. 458–468.

Russell, J.K. 1980: The petrogenesis of the Thompson Nickel Belt gneisses: Paint Lake, Manitoba; M.Sc. thesis, University of Calgary, Calgary, Alberta.

Russell, J.K. 1981: Metamorphism of the Thompson Nickel Belt gneisses: Paint Lake, Manitoba; Canadian Journal of Earth Sciences, v. 18, p. 191–209.

Schaltegger, U., Fanning, C.M., Günther, D., Maurin, J.C., Schulmann, K. and Gebauer, D. 1999: Growth, annealing and recrystallization of zircon and preservation of monazite in high-grade metamorphism: conventional and in situ U-Pb isotope, cathodoluminescence and microchemical evidence; Contributions to Mineralogy and Petrology, v. 134, p. 186–201.

Schmidberger, S.S., Simonetti, A., Heaman, L.M., Creaser, R.A. and Whiteford, S. 2007: Lu-Hf, in-situ Sr and Pb isotope and trace element systematics for mantle eclogites from the Diavik diamond mine: evidence for Paleoproterozoic subduction beneath the Slave craton, Canada; Earth and Planetary Science Letters, v. 245, p. 55–68.

Schneider, D.A., Heizler, M.T., Bickford, M.E., Wortman, G.L., Condie, K.C. and Perilli, S. 2007: Timing constraints of orogeny to cratonization: thermochronology of the Paleoproterozoic Trans-Hudson Orogen, Manitoba and Saskatchewan, Canada; Precambrian Research, v. 153, p. 65–95.

Scoates, J.S. and Chamberlain, K.R. 1997: Orogenic to post-orogenic origin for the 1.76 Ga Horse Creek anorthosite complex, Wyoming, USA; Journal of Geology, v. 105, p. 331–343.

Scoates, J.S., Wall, C.J., Friedman, R.M., Booth, K., Scoates, R.F.J., Couëslan, C. and Macek, J. 2010: Recent progress in determining the precise age of ultramafic sills and mafic dikes associated with mineralization in the Thompson Nickel Belt, Manitoba, Canada; *in* 11th International Platinum Symposium, June 21–24, 2010, Sudbury, Ontario, Canada, Abstracts, G.H. Brown, P.J. Jugo, C.M. Lesher and J.E. Mungall (ed.), Ontario Geological Survey, Miscellaneous Release–Data 269, 4 p.

Scoates, R.F.J. and Macek, J.J. 1978: Molson dyke swarm; Manitoba Mines, Resources and Environmental Management, Manitoba Geological Survey, Geological Paper 78-1, 51 p.

Scoates, R.F.J., Macek, J.J. and Russell, J.K. 1977: Thompson Nickel belt project (parts of 63P-13NE, 63P-14NW, 63P-12SW and 63O-9NE); *in* Report of Field Activities 1977, Manitoba Department of Mines, Resources and Environmental Management, Geological Services, p. 47–53.

Seo, J.H., Guillong, M. and Heinrich, C.A. 2012: Separation of molybdenum and copper in porphyry deposits: the roles of sulfur, redox, and pH in ore mineral deposition at Bingham Canyon; Economic Geology, v. 107, p. 333–356.

Simonetti, A., Heaman, L.M., Chacko, T. and Banerjee, N.R. 2006: In situ petrographic thin section U–Pb dating of zircon, monazite, and titanite using laser ablation–MC–ICP–MS; International Journal of Mass Spectrometry, v. 253, p. 87–97.

Simonetti, A., Heaman, L.M., Hartlaub, R.P., Creaser, R.A., MacHattie, T.G. and Böhm, C. 2005: U-Pb zircon dating by laser ablation–MC–ICP–MS using a new multiple ion counting Faraday collector array; Journal of Analytical Atomic Spectrometry, v. 20, p. 677–686.

Stacey, J.S. and Kramers, J.D. 1975: Approximation of terrestrial lead isotope evolution by a two-stage model; Earth and Planetary Science Letters, v. 26, p. 207–221.

Stern, R.A., Hanson, G.N. and Shirey, S.B. 1989: Petrogenesis of mantle-derived, LILE-enriched Archean monzodiorites and trachyandesites (sanukatoids) in southwestern Superior Province; Canadian Journal of Earth Sciences, v. 26, p. 1688–1712.

Stott, G.M., Corkery, M.T., Percival, J.A., Simard, M. and Goutier, J. 2010: Project units 98-006 and 98-007: a revised terrane subdivision of the Superior province; *in* Summary of Field Work and Other Activities 2010, Ontario Geological Survey, Open File Report 6260, p. 20-1–20-10.

Sun, S.-s. and McDonough, W.F. 1989: Chemical and isotopic systematics of oceanic basalts: implication for mantle composition and processes; *in* Magmatism in the Ocean Basins, A.D. Saunders and M.J. Norry (ed.), Geological Society of London, Special Publications, v. 42, p. 313–345.

Thompson, R.N. 1982: Magmatism of the British Tertiary volcanic province; Scottish Journal of Geology, v. 18, p. 49–107.

Tyrrell, J.B. 1903: Report F: On the northeastern portion of the district of Saskatchewan and adjacent parts of the districts of Athabaska and Keewatin; Geological Survey of Canada, Annual Report, v. 13, p. 5F–37F.

Unterschutz, J.L.E., Creaser, R.A., Erdmer, P., Thompson, R.I. and Daughtry, K.L. 2002: North American margin origin of Quesnel terrane strata in the southern Canadian Cordillera: inferences from geochemical and Nd isotopic characteristics of Triassic metasedimentary rocks; Geological Society of America Bulletin, v. 114, p. 462–475.

Weber, W. 1990: The Churchill-Superior boundary zone, southeast margin of the Trans-Hudson orogen: a review; *in* The Early Proterozoic Trans-Hudson Orogen of North America, J.F. Lewry and M.R. Stauffer (ed.), Geological Association of Canada, Special Paper 37, p. 41–55.

West, D.P., Jr., Tomascak, P.B., Coish, R.A., Yates, M.G. and Reilly, M.J. 2007: Petrogenesis of the ultrapotassic Lincoln syenite, Maine: Late Silurian–Early Devonian melting of a source region modified by subduction driven metasomatism; American Journal of Science, v. 307, p. 265–310.

Whalen, J.B., Zwanzig, H.V., Percival, J.A. and Rayner, N. 2008: Geochemistry of an alkaline, ca. 1885 Ma, K-feldspar–porphyritic, monzonitic to syenogranitic suite, northeastern Kisseynew Domain, Manitoba (parts of NTS 63O); *in* Report of Activities 2008, Manitoba Science, Technology, Energy and Mines, Manitoba Geological Survey, p. 66–78.

White, D.J., Jones, A.G., Lucas, S.B. and Hajnal, Z. 1999: Tectonic evolution of the Superior boundary zone from coincident seismic reflection and magnetotelluric profiles; Tectonics, v. 18, p. 430–451.

White, D.J., Lucas, S.B., Bleeker, W., Hajnal, Z., Lewry, J.F. and Zwanzig, H.V. 2002: Suture-zone geometry along an irregular Paleoproterozoic margin: the Superior boundary zone, Manitoba, Canada; Geology, v. 30, p. 735–738.

Wright, J.F. (1931): Geology and mineral deposits of a part of northwest Manitoba; Geological Survey of Canada, Summary Report, 1930, Part C, p. 1C–124C.

Vale S.A. 2012: Annual report; United States Securities and Exchange Commission, Washington, D.C., 163 p.

Yin, C., Lin, S., Bohm, C. and Couëslan, C. 2012: Ultra-high temperature metamorphism and tectonic implications of sapphirine-bearing granulites in the Pikwitonei granulite domain, Manitoba; Manitoba Innovation, Energy and Mines, Manitoba Geological Survey, Manitoba Mining and Minerals Convention 2012, Winnipeg, Manitoba, November 15–17, 2012, poster presentation.

Zhang, L., Audétat, A. and Dolejš, D. 2012: Solubility of molybdenite (MoS_2) in aqueous fluids at 600–800°C, 200 MPa: a synthetic fluid inclusion study; Geochimica et Cosmochimica Acta, v. 77, p. 175–185.

Zwanzig, H.V. 2005: Geochemistry, Sm-Nd isotope data and age constraints of the Bah Lake assemblage, Thompson Nickel Belt and Kisseynew Domain margin: relation to Thompson-type ultramafic bodies and a tectonic model (NTS 63J, O and P); *in* Report of Activities 2005, Manitoba Industry, Economic Development and Mines, Manitoba Geological Survey, p. 40–53.

Zwanzig, H.V., Macek, J.J. and McGregor, C.R. 2007: Lithostratigraphy and geochemistry of the high-grade metasedimentary rocks in the Thompson Nickel Belt and adjacent Kisseynew Domain, Manitoba: implications for nickel exploration; Economic Geology, v. 102, p. 1197–1216.

Zwanzig, H.V, Macek, J.J. and McGregor, C.R. 2008: Major- and trace-element analyses of the metasedimentary and basement rocks, Thompson Nickel Belt, adjacent Superior Boundary Zone and Kisseynew Domain; Manitoba Science, Technology, Energy and Mines, Manitoba Geological Survey, Data Repository Item DRI2006001, Microsoft® Excel® file.